Chapter 14

Membrane Separations

§14.0 INSTRUCTIONAL OBJECTIVES

After completing this chapter, you should be able to:

- Explain membrane processes in terms of the membrane, feed, sweep, retentate, permeate, and solute-membrane interactions.
- Distinguish effects on membrane mass transfer due to permeability, permeance, solute resistance, selectivity, concentration polarization, fouling, inertial lift, and shear-induced diffusion.
- Explain contributions to mass-transfer coefficients from membrane thickness and tortuosity; solute size, charge, and solubility; and hydrodynamic viscous and shear forces.
- Differentiate between asymmetric and thin-layer composite membranes, and between dense and microporous membranes.
- Distinguish among microfiltration, ultrafiltration, nanofiltration, virus filtration, sterile filtration, filter-aid filtration, and reverse osmosis in terms of average pore size, unique role in a biopurification sequence, and operation in normal flow versus tangential flow.
- Describe four membrane shapes and six membrane modules, and identify the most common types used in bioseparations.
- Distinguish among mass transfer through membranes by bulk flow, molecular diffusion, and solution diffusion.
- Differentiate between predicting flux in normal-flow filtration versus tangential-flow filtration.
- Differentiate among resistances due to cake formation, pore constriction, and pore blockage in both constant-flux and constant-pressure operation, and explain how to distinguish these using data from membrane operation.
- Explain four common idealized flow patterns in membrane modules.
- Differentiate between concentration polarization and membrane fouling, and explain how to minimize effects of each on membrane capacity and throughput.
- Calculate mass-transfer rates for dialysis and electrodialysis, reverse osmosis, gas permeation, pervaporation, normal-flow filtration, and tangential-flow filtration.
- Explain osmosis and how reverse osmosis is achieved.

In a membrane-separation process, a feed consisting of a mixture of two or more components is partially separated by means of a semipermeable barrier (the membrane) through which some species move faster than others. The most general membrane process is shown in Figure 14.1, where the feed mixture is separated into a *retentate* (that part of the feed that does not pass through the membrane) and a *permeate* (that part that does pass through the membrane). Although the feed, retentate, and permeate are usually liquid or gas, in bioprocesses, solid particles may also be present. The barrier is most often a thin, nonporous, polymeric film, but may also be porous polymer, ceramic, or metal material, or even a liquid, gel, or gas. To maintain selectivity, the barrier must not dissolve, disintegrate, or break. The optional sweep, shown in Figure 14.1, is a liquid or gas used to facilitate removal of the permeate. Many of the industrially important membrane-separation operations are listed in Tables 1.2 and Table 14.1.

In membrane separations: (1) the two products are usually miscible, (2) the separating agent is a semipermeable barrier, and (3) a sharp separation is often difficult to achieve. Thus, membrane separations differ in some respects from the more common separation operations of absorption, distillation, and liquid–liquid extraction.

Although membranes as separating agents have been known for more than 100 years [1], large-scale applications have appeared only in the past 60 years. In the 1940s, porous fluorocarbons were used to separate $^{235}UF_6$ from $^{238}UF_6$ [2]. In the mid-1960s, reverse osmosis with cellulose acetate was first used to desalinize seawater to produce potable water (drinkable water with less than 500 ppm by weight of dissolved solids) [3]. Commercial ultrafiltration membranes

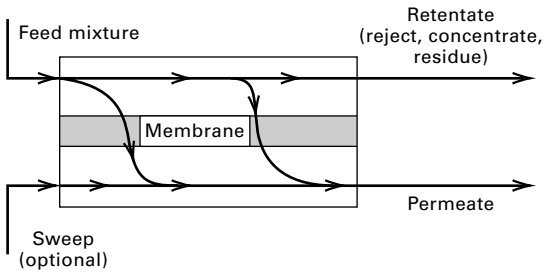

Figure 14.1 General membrane process.

Table 14.1 Industrial Membrane-Separation Processes

1. Reverse osmosis:
   - Desalinization of brackish water
   - Treatment of wastewater to remove a wide variety of impurities
   - Treatment of surface and groundwater
   - Concentration of foodstuffs
   - Removal of alcohol from beer
2. Dialysis:
   - Separation of nickel sulfate from sulfuric acid
   - Hemodialysis (removal of waste metabolites and excess body water, and restoration of electrolyte balance in blood)
3. Electrodialysis:
   - Production of table salt from seawater
   - Concentration of brines from reverse osmosis
   - Treatment of wastewaters from electroplating
   - Demineralization of cheese whey
   - Production of ultra-pure water for the semiconductor industry
4. Microfiltration:
   - Sterilization of liquids, gases, and parenteral drugs
   - Clarification and biological stabilization of beverages
   - Bacterial cell harvest and purification of antibiotics
   - Recovery of mammalian cells from cell culture broth
5. Ultrafiltration:
   - Preconcentration of milk before making cheese
   - Clarification of fruit juice
   - Purification of recombinant proteins and DNA, antigens, and antibiotics from clarified cell broths
   - Color removal from Kraft black liquor in papermaking
6. Pervaporation:
   - Dehydration of ethanol–water azeotrope
   - Removal of water from organic solvents
   - Removal of organics from water
7. Gas permeation:
   - Separation of CO_2 or H_2 from methane
   - Separation of uranium isotopes
   - Adjustment of the H_2/CO ratio in synthesis gas
   - Separation of air into nitrogen- and oxygen-enriched streams
   - Recovery of helium
   - Recovery of methane from biogas
8. Liquid membranes:
   - Recovery of zinc from wastewater in the viscose fiber industry
   - Recovery of nickel from electroplating solutions

followed in the 1960s. In 1979, Monsanto Chemical Company introduced a hollow-fiber membrane of polysulfone to separate certain gas mixtures—for example, to enrich hydrogen- and carbon-dioxide-containing streams [4]. Commercialization of alcohol dehydration by pervaporation began in the late 1980s, as did the large-scale application of emulsion liquid membranes for removal of metals and organics from wastewater. Also in the 1980s, the application of membrane separations to bioprocesses began to emerge, particularly ultrafiltration to separate proteins and microfiltration to separate bacteria and yeast. A recent industrial membrane catalog, Filmtec Inc., a subsidiary of the Dow Chemical Company, lists 76 membrane products.

Replacement of more-common separation operations with membrane separations has the potential to save energy and lower costs. It requires the production of high-mass-transfer-flux, defect-free, long-life membranes on a large scale and the fabrication of the membrane into compact, economical modules of high surface area per unit volume. It also requires considerable clean-up of process feeds and careful control of operating conditions to prevent membrane deterioration and to avoid degradation of membrane functionality due to caking, plugging, and fouling.

Industrial Example

A large-scale membrane process, currently uneconomical because its viability depends on the price of toluene compared to that of benzene, is the manufacture of benzene from toluene, which requires the separation of hydrogen from methane. After World War II, during which large amounts of toluene were required to produce TNT (trinitrotoluene) explosives, petroleum refiners sought other markets for toluene. One was the use of toluene for manufacturing benzene, xylenes, and a number of other chemicals, including polyesters. Toluene can be catalytically disproportionated to benzene and xylenes in an adiabatic reactor with the feed entering at 950°F at a pressure above 500 psia. The main reaction is

$$2C_7H_8 \rightarrow C_6H_6 + C_8H_{10}\text{ isomers}$$

To suppress coke formation, which fouls the catalyst, the reactor feed must contain a large fraction of hydrogen at a partial pressure of at least 215 psia. Unfortunately, the hydrogen takes part in a side reaction, the hydrodealkylation of toluene to benzene and methane:

$$C_7H_8 + H_2 \rightarrow C_6H_6 + CH_4$$

Makeup hydrogen is usually not pure, but contains perhaps 15 mol% methane and 5 mol% ethane. Thus, typically, the reactor effluent contains H_2, CH_4, C_2H_6, C_6H_6, unreacted C_7H_8, and C_8H_{10} isomers. As shown in Figure 14.2a for the reactor section of the process, this effluent is cooled and partially condensed to 100°F at a pressure of 465 psia. At these conditions, a good separation between C_2H_6 and C_6H_6 is achieved in the flash drum. The vapor leaving the flash contains most of the H_2, CH_4, and C_2H_6, with the aromatic

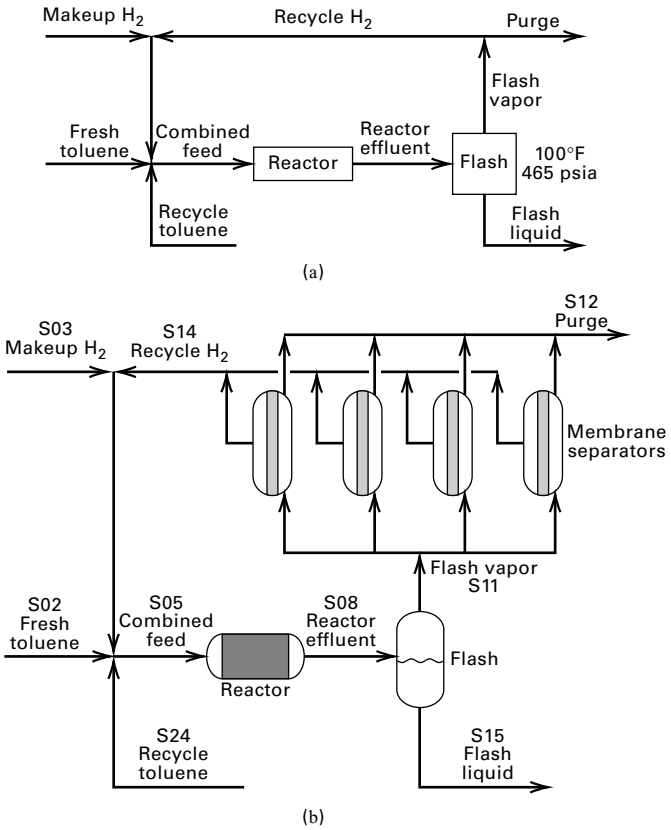

Figure 14.2 Reactor section of process to disproportionate toluene into benzene and xylene isomers. (a) Without a vapor-separation step. (b) With a membrane-separation step. Note: Heat exchangers, compressors, pump not shown.

chemicals leaving in the liquid. The large amount of hydrogen in the flash-drum vapor should be recycled to the reactor, rather than sending it to a flare or using it as a fuel. However, if all of the vapor were recycled, methane and ethane would build up in the recycle loop, since no other exit is provided. Before the development of acceptable membranes for the separation of H_2 from CH_4 by permeation, part of the vapor stream was purged from the process, as shown in Figure 14.2a, to provide an exit for CH_4 and C_2H_6. With the introduction of a suitable membrane in 1979, it became possible to install membrane separators, as shown in Figure 14.2b.

Table 14.2 is the material balance of Figure 14.2b for a plant processing 7,750 barrels (42 gal/bbl) per day of toluene feed. The permeation membranes separate the flash vapor (stream S11) into an H_2-enriched permeate (S14, the recycled hydrogen), and a methane-enriched retentate (S12, the purge). The feed to the membrane system is 89.74 mol% H_2 and 9.26 mol% CH_4. No sweep gas is necessary. The permeate is enriched to 94.5 mol% H_2, and the retentate is 31.2 mol % CH_4. The recovery of H_2 in the permeate is 90%, leaving only 10% of the H_2 lost to the purge.

Before entering the membrane-separator system, the vapor is heated to at least 200°F (the dew-point temperature of the retentate) at a pressure of 450 psia (heater not shown). Because the hydrogen in the feed is reduced in passing through the separator, the retentate becomes more concentrated in the heavier components and, without the heater, undesirable condensation would occur. The retentate leaves the separator at about the same temperature and pressure as that of heated flash vapor. Permeate leaves at a pressure of 50 psia and a temperature lower than 200°F because of gas expansion.

The membrane is an aromatic polyamide polymer, 0.3-μm thick, with the nonporous layer in contact with the feed, and a much-thicker porous support backing to give the membrane strength to withstand the pressure differential of $450 - 50 = 400$ psi. This large pressure difference is needed to force the hydrogen through the membrane, which is in the form of a spiral-wound module made from flat membrane sheets. The average flux of hydrogen through the membrane is 40 scfh (standard ft^3/h at 60°F and 1 atm) per ft^2 of membrane surface area. From the material balance in Table 14.2, the H_2 transported through the membrane is

$$(1{,}685.1 \text{ lbmol/h})(379 \text{ scf/lbmol}) = 639{,}000 \text{ scfh}$$

The total membrane surface area required is $639{,}000/40 = 16{,}000$ ft^2. The membrane is packaged in pressure-vessel modules of 4,000 ft^2 each. Thus, four modules in parallel are used. A disadvantage of the membrane process is the need to recompress the recycle hydrogen to the reactor inlet pressure.

Membrane separations are well developed for the applications listed in Table 14.1. Important progress is being made in developing new membrane applications, efficient membrane materials, and the modularization thereof. Applications covering wider ranges of temperature and types of membrane materials are being found. Membrane-separation processes have found wide application in the diverse industries listed in Table 14.1 and Table 1.2. Often, compared to other separation equipment, membrane separators are more compact, less capital intensive, and more easily operated, controlled, and maintained. However, membrane units are modular in

Table 14.2 Material Balance for Toluene Disproportionation Plant; Flow Rates in lbmol/h for Streams in Reactor Section of Figure 14.2b

Component	S02	S03	S24	S14	S05	S08	S15	S11	S12
Hydrogen		269.0		1,685.1	1,954.1	1,890.6	18.3	1,872.3	187.2
Methane		50.5		98.8	149.3	212.8	19.7	193.1	94.3
Ethane		16.8			16.8	16.8	5.4	11.4	11.4
Benzene			13.1		13.1	576.6	571.8	4.8	4.8
Toluene	1,069.4		1,333.0		2,402.4	1,338.9	1,334.7	4.2	4.2
p-Xylene			8.0		8.0	508.0	507.4	0.6	0.6
Total	1,069.4	336.3	1,354.1	1,783.9	4,543.7	4,543.7	2,457.4	2,086.3	302.4

construction, with many parallel units required for large-scale applications, in contrast to common separation techniques, where larger pieces of equipment are designed as plant size increases.

A key to an efficient and economical membrane-separation process is the membrane and how it is packaged to withstand large pressure differences. Research and development of membrane processes deals mainly with the discovery of suitably thin, selective membrane materials and their fabrication.

This chapter discusses membrane materials and modules, the theory of transport through membranes, and the scale-up of separators from experimental data. Emphasis is on dialysis, electrodialysis, reverse osmosis, gas permeation, pervaporation, ultrafiltration, and microfiltration. Many of the theoretical principles apply as well to emerging but less-commercialized membrane processes such as membrane distillation, membrane gas absorption, membrane stripping, membrane solvent extraction, perstraction, and facilitated transport, which are not covered here. The status of industrial membrane systems and directions in research to improve existing applications and make possible new applications are considered in detail by Baker et al. [5] and by contributors to a handbook edited by Ho and Sirkar [6], which includes emerging processes. Baker [49] treats theory and technology.

§14.1 MEMBRANE MATERIALS

Originally, membranes were made from processed natural polymers such as cellulose and rubber, but now many are custom-made synthetically, a wide variety of them having been developed and commercialized since 1930. Synthetic polymers are produced by condensation reactions, or from monomers by free-radical or ionic-catalyzed addition (chain) reactions. The resulting polymer is categorized as having (1) a long linear chain, such as linear polyethylene; (2) a branched chain, such as polybutadiene; (3) a three-dimensional, highly cross-linked structure, such as a condensation polymer like phenol–formaldehyde; or (4) a moderately cross-linked structure, such as butyl rubber or a partially cross-linked polyethylene. The linear-chain polymers soften with an increase in temperature, are soluble in organic solvents, and are referred to as *thermoplastic* polymers. At the other extreme, highly cross-linked polymers decompose at high temperature, are not soluble in organic solvents, and are referred to as *thermosetting* polymers. Of more interest in the application of polymers to membranes is a classification based on the arrangement or conformation of the polymer molecules.

Polymers can be classified as *amorphous* or *crystalline.* The former refers to a polymer that is glassy in appearance and lacks crystalline structure, whereas the latter refers to a polymer that is opaque and has a crystalline structure. If the temperature of a glassy polymer is increased, a point called the *glass-transition temperature*, T_g, may be reached where the polymer becomes *rubbery*. If the temperature of a crystalline polymer is increased, a point called the *melting temperature*, T_m, is reached where the polymer becomes a melt. However, a thermosetting polymer never melts. Most polymers have both amorphous and crystalline regions—that is, a certain degree of crystallinity that varies from 5 to 90%, making it possible for some polymers to have both a T_g and a T_m. Membranes made of glassy polymers can operate below or above T_g; membranes of crystalline polymers must operate below T_m.

Table 14.3 lists *repeat units* and values of T_g and/or T_m for some of the many natural and synthetic polymers from which membranes have been fabricated. Included are crystalline, glassy, and rubbery polymers. Cellulose triacetate is the reaction product of cellulose and acetic anhydride. The repeat unit of cellulose is identical to that shown for cellulose triacetate, except that the acetyl, Ac (CH_3CO), groups are replaced by H. The repeat units (*degree of polymerization*) in cellulose triacetate number ~300. Triacetate is highly crystalline, of uniformly high quality, and hydrophobic.

Polyisoprene (natural rubber) is obtained from at least 200 different plants, with many of the rubber-producing countries located in the Far East. Polyisoprene has a very low glass-transition temperature. Natural rubber has a degree of polymerization of from about 3,000 to 40,000 and is hard and rigid when cold, but soft, easily deformed, and sticky when hot. Depending on the temperature, it slowly crystallizes. To increase strength, elasticity, and stability of rubber, it is vulcanized with sulfur, a process that introduces cross-links.

Aromatic polyamides (also called aramids) are high-melting, crystalline polymers that have better long-term thermal stability and higher resistance to solvents than do aliphatic polyamides such as nylon. Some aromatic polyamides are easily fabricated into fibers, films, and sheets. The polyamide structure shown in Table 14.3 is that of Kevlar, a trade name of DuPont.

Polycarbonates, characterized by the presence of the –OCOO– group in the chain, are mainly amorphous. The polycarbonate shown in Table 14.3 is an aromatic form, but aliphatic forms also exist. Polycarbonates differ from most other amorphous polymers in that they possess ductility and toughness below T_g. Because polycarbonates are thermoplastic, they can be extruded into various shapes, including films and sheets.

Polyimides are characterized by the presence of aromatic rings and heterocyclic rings containing nitrogen and attached oxygen. The structure shown in Table 14.3 is only one of a number available. Polyimides are tough, amorphous polymers with high resistance to heat and excellent wear resistance. They can be fabricated into a wide variety of forms, including fibers, sheets, and films.

Polystyrene is a linear, amorphous, highly pure polymer of about 1,000 units of the structure shown in Table 14.3. Above a low T_g, which depends on molecular weight, polystyrene becomes a viscous liquid that is easily fabricated by extrusion or injection molding. Polystyrene can be annealed

Table 14.3 Common Polymers Used in Membranes

Polymer	Type	Representative Repeat Unit	Glass-Transition Temp., °C	Melting Temp., °C
Cellulose triacetate	Crystalline	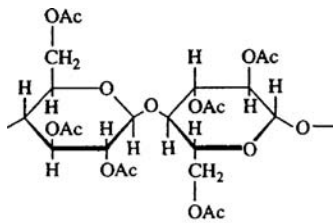		300
Polyisoprene (natural rubber)	Rubbery	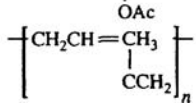	−70	
Aromatic polyamide	Crystalline	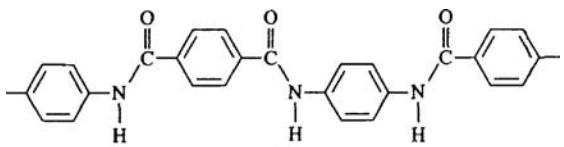		275
Polycarbonate	Glassy	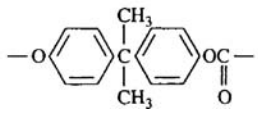	150	
Polyimide	Glassy	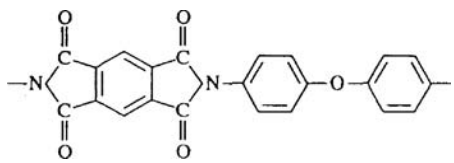	310–365	
Polystyrene	Glassy	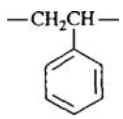	74–110	
Polysulfone	Glassy	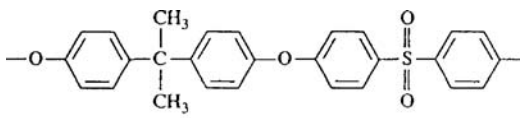	190	
Polytetrafluoroethylene (Teflon)	Crystalline			327

(heated and then cooled slowly) to convert it to a crystalline polymer with a melting point of 240°C. Styrene monomer can be copolymerized with a number of other organic monomers, including acrylonitrile and butadiene to form ABS copolymers.

Polysulfones are synthetic polymers first introduced in 1966. The structure in Table 14.3 is just one of many, all of which contain the SO_2 group, which gives the polymers high strength. Polysulfones are easily spun into hollow fibers. Membranes of closely related polyethersulfone have also been commercialized.

Polytetrafluoroethylene is a straight-chain, highly crystalline polymer with a high degree of polymerization of the order of 100,000, giving it considerable strength. It possesses exceptional thermal stability and can be formed into films and tubing, as can polyvinylidenefluoride.

To be effective for separating a mixture of chemical components, a polymer membrane must possess high *permeance* and a high permeance ratio for the two species being separated by the membrane. The permeance for a given species diffusing through a membrane of given thickness is analogous to a mass-transfer coefficient, i.e., the flow rate of that species per unit cross-sectional area of membrane per unit driving force (concentration, partial pressure, etc.) across the membrane thickness. The molar transmembrane flux of species i is

$$N_i = \left(\frac{P_{M_i}}{l_M}\right)(\text{driving force}) = \bar{P}_{M_i}(\text{driving force}) \tag{14-1}$$

where $\bar{P}_{M_i}$ is the permeance, which is defined as the ratio of P_{M_i}, the *permeability*, to l_M, the membrane thickness.

Polymer membranes can be characterized as dense or microporous. For dense, amorphous membranes, pores of microscopic dimensions may be present, but they are generally less than a few Å in diameter, such that most, if not all, diffusing species must dissolve into the polymer and then diffuse through the polymer between the segments of the macromolecular chains. Diffusion can be difficult, but highly selective, for glassy polymers. If the polymer is partly crystalline, diffusion will occur almost exclusively through the amorphous regions, with the crystalline regions decreasing the diffusion area and increasing the diffusion path.

Microporous membranes contain interconnected pores and are categorized by their use in microfiltration (MF), ultrafiltration (UF), and nanofiltration (NF). The MF membranes, which have pore sizes of 200–100,000 Å, are used primarily to filter bacteria and yeast and provide cell-free suspensions. UF membranes have pore sizes of 10–200 Å and are used to separate low-molecular-weight solutes such as enzymes from higher-molecular-weight solutes like viruses. NF membranes have pore sizes from 1 to 10 Å and can retain even smaller molecules. NF membranes are used in osmosis and pervaporation processes to purify liquids. The pores are formed by a variety of proprietary techniques, some of which are described by Baker et al. [5]. Such techniques are valuable for producing symmetric, microporous, crystalline membranes. Permeability for microporous membranes is high, but selectivity is low for small molecules. However, when there are molecules smaller and larger than the pore size, they may be separated almost perfectly by size.

The separation of small molecules presents a dilemma. A high permeability is not compatible with a high separation factor. The beginning of the resolution of this dilemma occurred in 1963 with the fabrication by Loeb and Sourirajan [7] of an asymmetric membrane of cellulose acetate by a novel casting procedure. As shown in Figure 14.3a, the resulting membrane consists of a thin dense skin about 0.1–1.0 μm in. thick, called the *permselective* layer, formed over a much thicker microporous layer that provides support for the skin.

The flux rate of a species is controlled by the permeance of the very thin permselective skin. From (14-1), the permeance of species i can be high because of the very small value of l_M even though the permeability, P_{M_i}, is low because of the absence of pores. When large differences of P_{M_i} exist among molecules, both high permeance and high selectivity can be achieved with asymmetric membranes.

A very thin, asymmetric membrane is subject to formation of minute holes in the permselective skin, which can render the membrane useless. A solution to the defect problem for an asymmetric polysulfone membrane was patented by Henis and Tripodi [8] of the Monsanto Company in 1980. They pulled silicone rubber, from a coating on the skin surface, into the defects by applying a vacuum. The resulting membrane, referred to as a *caulked membrane*, is shown in Figure 14.3b.

Wrasidlo [9] in 1977 introduced the thin-film composite membrane as an alternative to the asymmetric membrane. In the first application, shown in Figure 14.3c, a thin, dense film of polyamide polymer, 250 to 500 Å in thickness, was formed on a thicker microporous polysulfone support. Today, both asymmetric and thin-film composites are fabricated from polymers by a variety of techniques.

Application of polymer membranes is often limited to temperatures below 200°C and to mixtures that are chemically inert. Operation at high temperatures and with chemically active mixtures requires membranes made of inorganic materials. These include mainly microporous ceramics, metals, and carbon; and dense metals, such as palladium, that allow the selective diffusion of small molecules such as hydrogen and helium.

Examples of inorganic membranes are (1) asymmetric, microporous α-alumina tubes with 40–100 Å pores at the inside surface and 100,000 Å pores at the outside; (2) microporous glass tubes, the pores of which may be filled with other oxides or the polymerization–pyrolysis product of trichloromethylsilane; (3) silica hollow fibers with extremely fine pores of 3–5 Å; (4) porous ceramic, glass, or polymer materials coated with a thin, dense film of palladium metal that is just a few μm thick; (5) sintered metal; (6) pyrolyzed carbon; and (7) zirconia on sintered carbon. Extremely fine pores (<10 Å) are necessary to separate gas mixtures. Larger pores (>50 Å) are satisfactory for the separation of large molecules or solid particles from solutions containing small molecules.

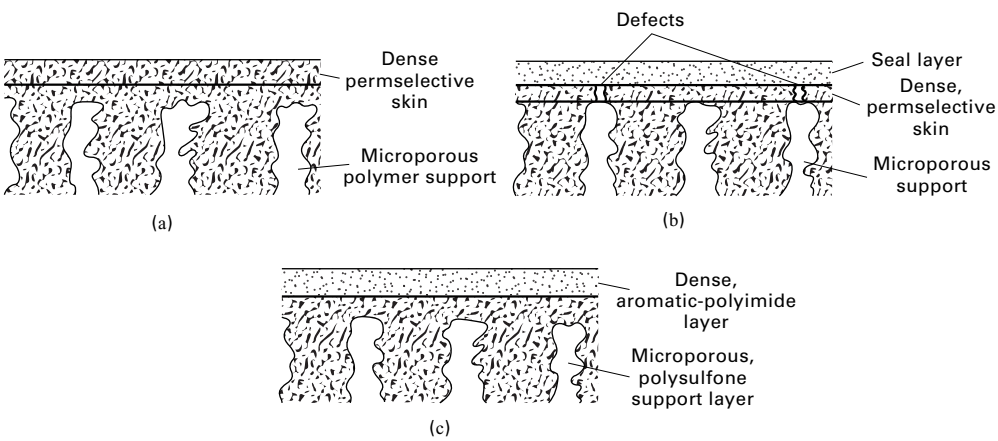

Figure 14.3 Polymer membranes: (a) asymmetric, (b) caulked asymmetric, and (c) typical thin-film composite.

EXAMPLE 14.1 Membrane Flux from Permeability.

A silica-glass membrane, 2-μm thick with pores <10 Å in diameter, has been developed for separating H_2 from CO at a temperature of 500°F. From laboratory data, the membrane permeabilities for H_2 and CO, respectively, are 200,000 and 700 barrer, where the barrer, a common unit for gas permeation, is defined by:

$$1 \text{ barrer} = 10^{-10} \text{ cm}^3 \text{ (STP)-cm/(cm}^2\text{-s-cmHg)}$$

where cm^3 (STP)/(cm^2-s) refers to the volumetric transmembrane flux of the diffusing species in terms of standard conditions of 0°C and 1 atm; cm refers to the membrane thickness; and cmHg refers to the transmembrane partial-pressure driving force for the diffusing species.

The barrer unit is named for R. M. Barrer, who published an early article [10] on diffusion in a membrane, followed by a widely referenced monograph on diffusion in and through solids [11].

If the transmembrane, partial-pressure driving forces for H_2 and CO, respectively, are 240 psi and 80 psi, calculate the transmembrane fluxes in kmol/m^2-s. Compare the H_2 flux to that for H_2 in the industrial application described at the beginning of this chapter.

Solution

At 0°C and 1 atm, 1 kmol of gas occupies 22.42×10^6 cm^3. Also, 2 μm thickness $= 2 \times 10^{-4}$ cm, and 1 cmHg $\Delta P = 0.1934$ psi. Therefore, using (14.1):

$$N_{H_2} = \frac{(200{,}000)(10^{-10})(240/0.1934)(10^4)}{(22.42 \times 10^6)(2 \times 10^{-4})} = 0.0554 \frac{\text{kmol}}{\text{m}^2\text{-s}}$$

$$N_{CO} = \frac{(700)(10^{-10})(80/0.1934)(10^4)}{(22.42 \times 10^6)(2 \times 10^{-4})} = 0.000065 \frac{\text{kmol}}{\text{m}^2\text{-s}}$$

In the application discussed at the beginning of this chapter, the flux of H_2 for the polymer membrane is

$$\frac{(1685.1)(1/2.205)}{(16{,}000)(0.3048)^2(3600)} = 0.000143 \frac{\text{kmol}}{\text{m}^2\text{-s}}$$

Thus, the flux of H_2 through the ultra-microporous-glass membrane is more than 100 times higher than the flux through the dense-polymer membrane. Large differences in molar fluxes through different membranes are common.

The following are useful factors for converting barrer to SI and American Engineering units:

Multiply barrer by 3.348×10^{-19} to obtain units of $(\text{kmol} \times \text{m})/(\text{m}^2 \times \text{s} \times \text{Pa})$.

Multiply barrer by 5.584×10^{-12} to obtain units of $(\text{lbmol} \times \text{ft})/(\text{ft}^2 \times \text{h} \times \text{psi})$.

§14.2 MEMBRANE MODULES

The asymmetric and thin-film, composite, polymer-membrane materials in the previous section are available in one or more of the three shapes shown in Figures 14.4a, b, and c. Flat sheets have typical dimensions of 1 m × 1 m × 200 μm thick, with a dense skin or thin, dense layer 500 to 5,000 Å in thickness. Tubular membranes are typically 0.5 to 5.0 cm in diameter and up to 6 m long. The thin, dense layer is on the inside, as seen in Figure 14.4b, or on the outside tube surface. The porous tube support is fiberglass, perforated metal, or other suitable material. Very small-diameter hollow fibers, first reported by Mahon [12, 13] in the 1960s, are typically 42 μm i.d. × 85 μm o.d. × 1.2 m long with a 0.1- to 1.0-μm-thick dense skin. The hollow fibers shown in Figure 14.4c provide a large membrane surface area per unit volume. A honeycomb, monolithic element for inorganic oxide membranes is included in Figure 14.4d. Elements of hexagonal and circular cross section are available [14]. The circular flow channels are 0.3 to 0.6 cm in diameter, with a 20- to

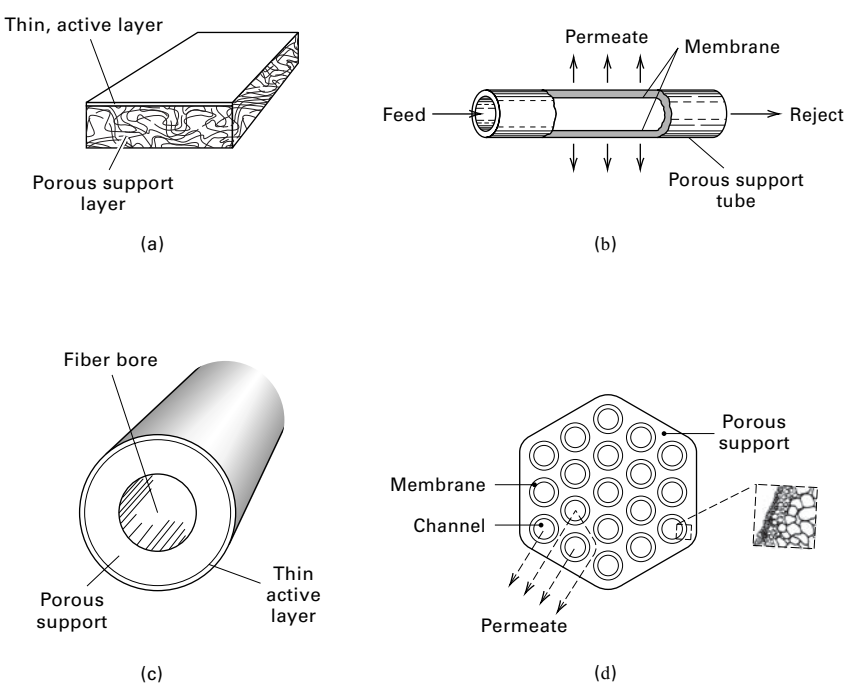

Figure 14.4 Common membrane shapes: (a) flat, asymmetric or thin-film composite sheet; (b) tubular; (c) hollow-fiber; (d) monolithic.

40-mm-thick membrane layer. The hexagonal element in Figure 14.4d has 19 channels and is 0.85 m long. Both the bulk support and the thin membrane layer are porous, but the pores of the latter can be as small as 40 Å.

The shapes in Figure 14.4 are incorporated into modules and cartridges, some of which are shown in Figure 14.5. Flat sheets used in plate-and-frame modules are circular, square, or rectangular in cross section. The sheets are separated by support plates that channel the permeate. In Figure 14.5a, a feed of brackish water flows across the surface of each sheet in the stack. Pure water is the permeate, while brine is the retentate.

Flat sheets are also fabricated into spiral-wound modules, as in Figure 14.5b. A laminate, consisting of two membrane sheets separated by spacers for the flow of the feed and permeate, is wound around a central, perforated collection tube

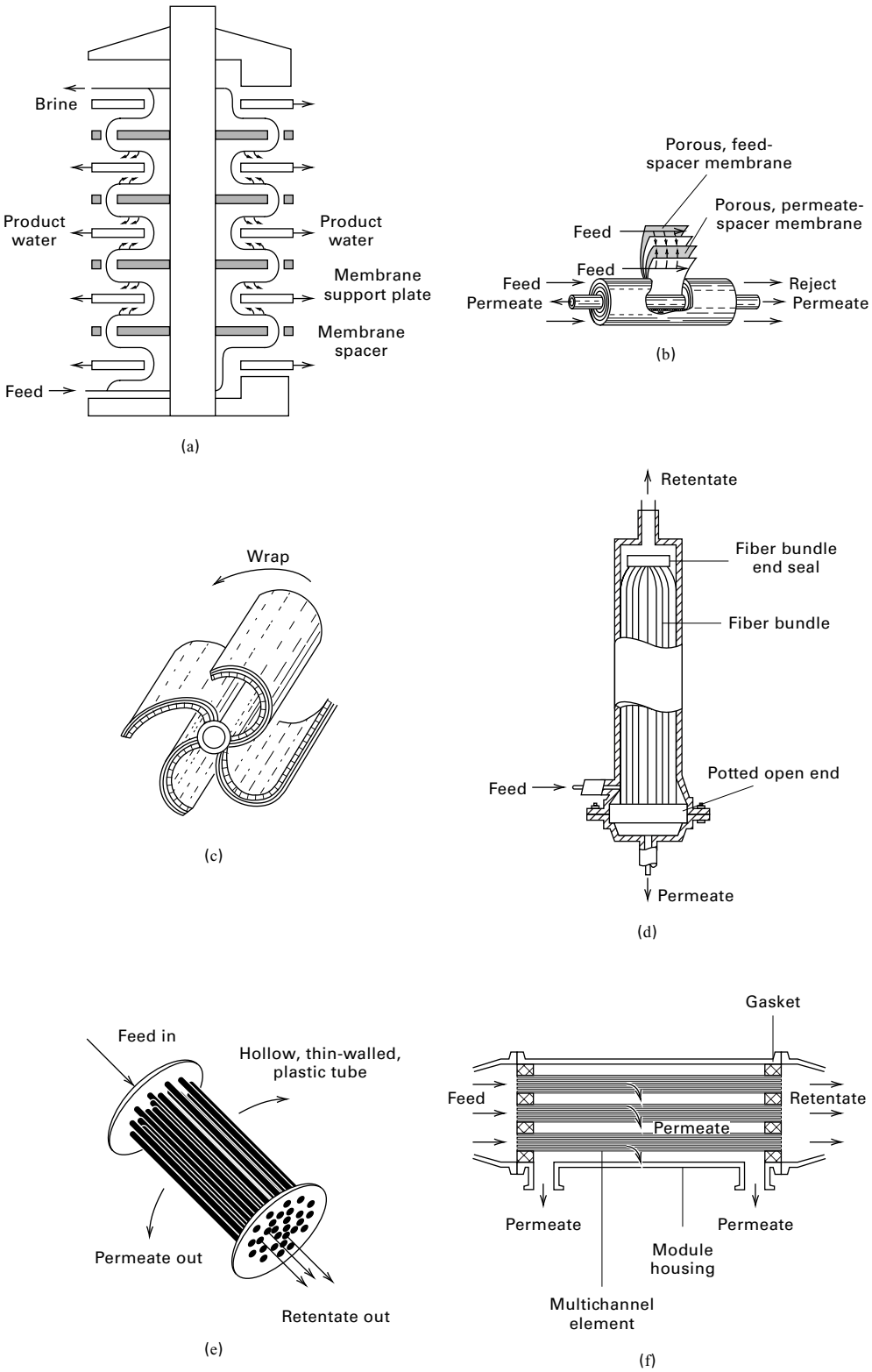

Figure 14.5 Common membrane modules: (a) plate-and-frame, (b) spiral-wound, (c) four-leaf spiral-wound, (d) hollow-fiber, (e) tubular, (f) monolithic.

Table 14.4 Typical Characteristics of Membrane Modules

	Plate-and-Frame	Spiral-Wound	Tubular	Hollow-Fiber
Packing density, m^2/m^3	30 to 500	200 to 800	30 to 200	500 to 9,000
Resistance to fouling	Good	Moderate	Very good	Poor
Ease of cleaning	Good	Fair	Excellent	Poor
Relative cost	High	Low	High	Low
Main applications	D, RO, PV, UF, MF	D, RO, GP, UF, MF	RO, UF	D, RO, GP, UF

Note: D, dialysis; RO, reverse osmosis; GP, gas permeation; PV, pervaporation; UF, ultrafiltration; MF, microfiltration.

to form a module that is inserted into a pressure vessel. Feed flows axially in the channels created between the membranes by porous spacers. Permeate passes through the membrane, traveling inward in a spiral path to the central collection tube. From there, the permeate flows in either axial direction through and out of the tube. A typical spiral-wound module is 0.1–0.3 m in diameter and 3 m long. The four-leaf modification in Figure 14.5c minimizes the permeate pressure drop because the permeate travel is less for the same membrane area.

The hollow-fiber module in Figure 14.5d, for a gas-permeation application, resembles a shell-and-tube heat exchanger. The pressurized feed enters the shell side at one end. While flowing over the fibers toward the other end, permeate passes through the fiber walls into the central fiber channels. Typically, the fibers are sealed at one end and embedded into a tube sheet with epoxy resin at the other end. A module might be 1 m long $\times$ 0.1 to 0.25 m in diameter, and contain more than 1 million hollow fibers.

The tubular module in Figure 14.5e also resembles a heat exchanger, but the feed flows through the tubes. Permeate passes through the tube wall into the shell side of the module. Tubular modules contain up to 30 tubes.

The monolithic module in Figure 14.5f contains from 1 to 37 elements in a housing. Feed flows through the circular channels, and permeate passes through the membrane and porous support and into the open region between elements.

Table 14.4 is a comparison of the characteristics of four of the modules shown in Figure 14.5. The packing density is the membrane surface area per unit volume of module, for which hollow-fiber membrane modules are clearly superior.

Although the plate-and-frame module has a high cost and a moderate packing density, it finds use in all membrane applications except gas permeation. It is the only module widely used for pervaporation. The spiral-wound module is very popular for most applications because of its low cost and reasonable resistance to fouling. Tubular modules are used only for low-flow applications or when resistance to fouling and/or ease of cleaning is essential. Hollow-fiber modules, with their very high packing density and low cost, are popular where fouling does not occur and cleaning is not necessary.

§14.3 TRANSPORT IN MEMBRANES

Calculation of membrane surface area for a new application must be based on laboratory data for the selected membrane system. Nevertheless, because both the driving force and the permeability (or permeance) depend markedly on the mechanism of transport, it is important to understand the nature of transport in membranes so that an appropriate membrane process is selected. This section deals with the theoretical aspects of the transport processes that lead to proper choice of membrane. Applications to dialysis, reverse osmosis, gas permeation, pervaporation, ultrafiltration, and microfiltration are presented in subsequent sections.

Membranes can be macroporous, microporous, or dense (nonporous). Only microporous or dense membranes are permselective. Macroporous membranes are used to support thin microporous and dense membranes when significant pressure differences across the membrane are necessary to achieve high flux. The theoretical basis for transport through microporous membranes is more highly developed than that for dense membranes, so porous-membrane transport is discussed first, with respect to bulk flow, liquid diffusion, and then gas diffusion. This is followed by nonporous (dense)-membrane solution-diffusion transport, first for liquid mixtures and second for gas mixtures. External mass-transfer resistances in the fluid films on either side of the membrane are treated where appropriate. It is important to note that, because of the range of pore sizes in membranes, the distinction between porous and nonporous membranes is not always obvious. The distinction can be made based only on the relative permeabilities for diffusion through the pores of the membrane and diffusion through the solid, amorphous regions of the membrane, respectively.

§14.3.1 Transport Through Porous Membranes

Mechanisms for transport of liquid and gas molecules through a porous membrane are depicted in Figures 14.6a, b, and c. If the pore diameter is large compared to the molecular diameter and a pressure difference exists, bulk, convective flow through the pores occurs, as in Figure 14.6a. This flow is generally undesirable because it is not permselective and, therefore, no separation between feed components occurs. If fugacity, activity, chemical-potential, concentration, or partial-pressure differences exist across the membrane for the various components, but the pressure is the same on both sides of the membrane so as not to cause a bulk flow, permselective diffusion of the components through the pores takes place, effecting a separation as shown in Figure 14.6b. If the pores are of the order of molecular size for at least some of the components in the feed mixture, the diffusion of those components will be

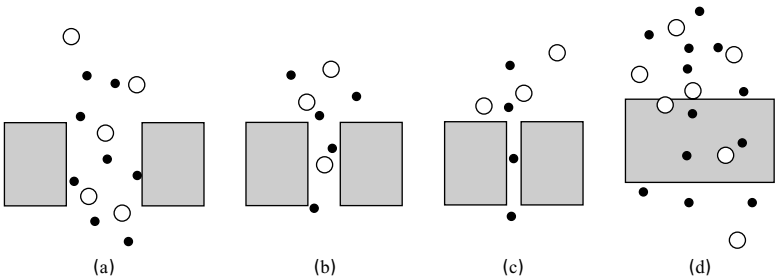

Figure 14.6 Mechanisms of transport in membranes. (Flow is downward.) (a) Bulk flow through pores; (b) diffusion through pores; (c) restricted diffusion through pores; (d) solution diffusion through dense membranes.

restricted (hindered) as shown in Figure 14.6c, resulting in an enhanced separation. Molecules of size larger than the pores will be prevented altogether from diffusing through the pores. This special case is highly desirable and is referred to as *size exclusion* or *sieving*. Another special case exists for gas diffusion in which the pore size and/or pressure (typically a vacuum) is such that the mean free path of the molecules is greater than the pore diameter, resulting in so-called *Knudsen diffusion*, which is dependent on molecular weight.

Bulk Flow

Bulk flow is pressure-driven flow of fluid through a semipermeable barrier (e.g., a membrane used for microfiltration and ultrafiltration), which results in accumulation of retained (sieved) solutes in suspension at the upstream face of the membrane, referred to as a cake. In 1855, Darcy found that the flow rate of water through sand is proportional to pressure drop. Darcy's law, which originally lacked a term for viscosity (as Wakeman and others have observed), has become the basis for describing bulk flow in applications including normal-flow (dead-end) filtration (DEF) modes like continuous rotary filtration using filter aids or sterile filtration; filtration through the cake where Reynolds numbers are <1 (laminar flow) and inertial effects are negligible; and local membrane flux in crossflow (tangential flow, TFF) modes like ultrafiltration. In Darcy's law, the instantaneous rate of filtration, $dV\{t\}/dt$, and the flux of permeate, J (dm^3/m^2-h or LMH), of viscosity μ through a medium of permeability k and cross-sectional area A_M are proportional to a constant-pressure (or vacuum) differential pressure drop dP through thickness dz:

$$J = \frac{1}{A_M}\frac{dV\{t\}}{dt} = -\frac{k}{\mu}\frac{dP}{dz} \tag{14-2}$$

where the flux, J, corresponds to the superficial fluid velocity, $u = J$ (volume flow rate per unit filter area). Bulk flow through a series of media—each with characteristic resistance $R_i = \Delta z_i/k_i$, such as a filter cake (R_c) and filter medium (R_m), which can be as porous as a canvas cloth, is illustrated in Figure 14.7. The series resistances have a common superficial velocity given by

$$u = (P - P_i)/\mu R_c = (P_i - P_o)/\mu R_m \tag{14-3}$$

For total pressure drop across cake and medium equal to $\Delta P = P - P_o$,

$$\boxed{J = \frac{1}{A_M}\frac{dV\{t\}}{dt} = \frac{\Delta P}{\mu(R_m + R_c)}} \tag{14-4}$$

where bulk flow varies inversely with viscosity; with resistance due to filter medium, R_m; and with accumulated cake, R_c, which have dimensions of reciprocal length. Cake resistance often dominates filter resistance as filtration proceeds and cake accumulates, provided that the cake collects on something like a porous cloth.

Expressions for the resistance terms, R_i, in (14-4), which arise from various hydrodynamic and phenomenological descriptions specific to particular filter media and cakes, allow Darcy's law in (14-4) to be used to select process equipment, identify operating conditions, and troubleshoot filtration processes. Resistance varies inversely with hydraulic membrane permeability, L_p, given by

$$L_p = \frac{J}{\Delta P} \tag{14-5}$$

which is a function of pore-size distribution, porosity, and thickness of barrier or cake, as well as solvent properties.

Pore Resistance to Flow

Consider bulk flow of a fluid due to a pressure difference through an idealized straight, cylindrical pore. If the flow is laminar ($N_{Re} = D\upsilon\rho/\mu < 2{,}100$), which is almost always true for small-diameter pores, flow velocity, υ, given by the Hagen–Poiseuille law [15], is directly proportional to the transmembrane pressure drop:

$$\upsilon = \frac{D^2}{32\mu L}(P_0 - P_L) \tag{14-6}$$

where D is the pore diameter, large enough to pass all molecules; μ is the fluid viscosity; and L is the length of the pore. This assumes a parabolic velocity profile, a Newtonian fluid, and, if a gas, that the mean free path of the molecules is small compared to the pore diameter. If the membrane contains n such pores per unit cross section

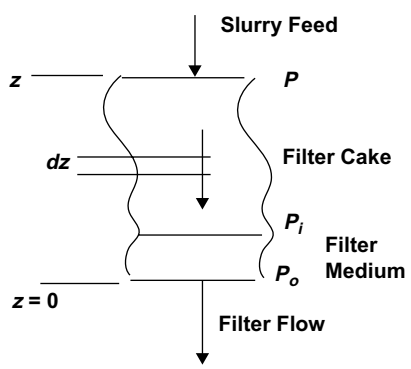

Figure 14.7 Profile of composite filtration.

of membrane surface area normal to flow, the porosity (void fraction) of the membrane is

$$\epsilon = n\pi D^2/4 \tag{14-7}$$

Then the superficial bulk-flow flux (mass velocity), N, through the membrane is

$$N = \upsilon\rho\epsilon = \frac{\epsilon\rho D^2}{32\mu l_M}(P_0 - P_L) = \frac{n\pi\rho D^4}{128\mu l_M}(P_0 - P_L) \tag{14-8}$$

where l_M is the membrane thickness and ρ and μ are fluid properties.

In real porous membranes, pores may not be cylindrical and straight, making it necessary to modify (14-8). Kozeny, in 1927, and Carman, in 1938, replaced cylindrical pores by a bundle of capillary tubes oriented at 45° to the surface. Ergun [16] extended this model by replacing, as a rough approximation, the pore diameter in (14-6) by the hydraulic diameter

$$\begin{aligned} d_H &= 4\left(\frac{\text{Volume available for flow}}{\text{Total pore surface area}}\right) \\ &= \frac{4\left(\dfrac{\text{Total pore volume}}{\text{Membrane volume}}\right)}{\left(\dfrac{\text{Total pore surface area}}{\text{Membrane volume}}\right)} = \frac{4\epsilon}{a} \end{aligned} \tag{14-9}$$

where the membrane volume includes the volume of the pores. The specific surface area, a_υ, which is the total pore surface area per unit volume of just the membrane material (not including the pores), is

$$a_\upsilon = a/(1-\epsilon) \tag{14-10}$$

Pore length is longer than the membrane thickness and can be represented by $l_M\tau$, where τ is a tortuosity factor >1. Substituting (14-9), (14-10), and the tortuosity factor into (14-8) gives

$$N = \frac{\rho\epsilon^2(P_0 - P_L)}{2(1-\epsilon)^2\tau a_\upsilon^2\mu l_M} \tag{14-11}$$

In terms of a bulk-flow permeability, (14-11) becomes

$$N = \frac{P_M}{l_M}(P_0 - P_L) \tag{14-12}$$

where

$$P_M = \frac{\rho\epsilon^3}{2(1-\epsilon)^2\tau a_\upsilon^2\mu} \tag{14-13}$$

Typically, τ is 2.5, whereas a_υ is inversely proportional to the average pore diameter, giving it a wide range of values.

Particulate Resistance to Flow

Equation (14-11) may be compared to the semitheoretical Ergun equation [16], which represents the best fit of data for flow of a fluid through a packed bed:

$$\frac{P_0 - P_L}{l_M} = \frac{150\mu\upsilon_0(1-\epsilon)^2}{D_P^2\epsilon^3} + \frac{1.75\rho\upsilon_0^2(1-\epsilon)}{D_P\epsilon^3} \tag{14-14}$$

where D_P is the mean particle diameter, υ_0 is the superficial fluid velocity through the bed, and υ_0/ϵ is the average velocity in the void space outside the particles. The first term on the RHS of (14-14) applies to the laminar-flow region, and together with the LHS is the Kozeny–Carman equation. It may be included in Darcy's law as shown in (14-17) to estimate cake resistance. The second term applies to the turbulent region. For a spherical particle, the specific surface area is

$$\begin{aligned} a_\upsilon &= \pi D_P^2/\pi\left(\pi D_P^3/6\right) \quad \text{or} \\ D_P &= 6/a_\upsilon \end{aligned} \tag{14-15}$$

Substitution of (14-15) into (14-14) for laminar flow, and rearrangement into the bulk-flow flux form gives

$$N = \frac{\rho\epsilon^3(P_0 - P_L)}{(150/36)(1-\epsilon)^2 a_\upsilon^2\mu l_M} \tag{14-16}$$

Comparing (14-16) to (14-11), it is seen that the term (150/36) in (14-16) corresponds to the term 2τ in (14-11), giving $\tau = 2.08$, which seems reasonable. Accordingly, (14-16) can be used as a first approximation to the pressure drop for flow through a porous membrane when the pores are not straight cylinders.

For gas flow, the density is taken as the average of the densities at the two membrane faces. Bulk transport through porous membranes in constant-pressure and constant-flux operation is considered in detail below. In cake filtration, described in Chapter 19, porosity has a slightly different meaning, usually defined being as the volume fraction of the cake occupied by occluded liquid.

EXAMPLE 14.2 Pressure Drop Through a Membrane.

It is desired to pass water at 70°F through a supported polypropylene membrane, with a skin of 0.003-cm thickness and 35% porosity, at the rate of 200 m^3/m^2 membrane surface area/day. The pores can be considered straight cylinders of uniform diameter equal to 0.2 μm. If the pressure on the downstream side of the membrane is 150 kPa, estimate the required pressure on the upstream side of the membrane. The pressure drop through the support is negligible.

Solution

Equation (8) applies, where in SI units:

$N/\rho = 200/(24)(3600) = 0.00232\ m^3/m^2\text{-s}$,
$\epsilon = 0.35$, $D_P = 0.2 \times 10^{-6}$ m, $l_M = 0.00003$ m, $P_L = 150$ kPa = 150,000 Pa, $\mu = 0.001$ Pa-s

From a rearrangement of (8),

$$\begin{aligned} P_0 &= P_L + \frac{32\mu l_M(N/\rho)}{\epsilon D_P^2} \\ &= 150{,}000 + \frac{(32)(0.001)(0.00003)(0.00232)}{(0.35)\left(0.2\times10^{-6}\right)^2} \\ &= 309{,}000\ \text{Pa} \quad \text{or} \quad 309\ \text{kPa} \end{aligned}$$

Cake Resistance to Flow

Resistance from a cake, R_c, of incompressible, close-packed, colloidal ($1–10^3$ nm) particulates at low Reynolds numbers (laminar flow) may be described using the first term on the

RHS of the Ergun equation (14-14), which is the Kozeny–Carman term:

$$R_c = \frac{150 l_c (1-\epsilon_c)^2}{D_P^2 \epsilon_c^3} = K_1 \frac{l_c (1-\epsilon_c)^2}{\epsilon_c^3} \tag{14-17}$$

where l_c = cake thickness, which increases with time; ϵ_c = cake porosity; D_P = effective diameter of the matter in the cake; and K_1 = constant for a particular filtration system.

The solid matter in the feed, m_c, retained in the cake as a function of filtration time, t, is

$$m_c\{t\} = c_F V\{t\} = \rho_c (1-\epsilon_c) A_c l_c\{t\} \tag{14-18}$$

where c_F = solid matter per unit volume of liquid in the feed, and A_c = area of the cake when it is very thin relative to the membrane radius of curvature. Equation (14-18) is often rewritten in terms of the mass of dry filter cake per unit filter area, $W = m_c\{t\}/A_c$, and thus the differential change in mass, dW, is related to the differential change in cake thickness, dz, by

$$dW = \rho_c (1-\epsilon_c) dz \tag{14-19}$$

where ϵ_c is the fraction of voids in the filter cake and, thus, is a measure of the volume of flow paths through the medium.

Substituting (14-18) into (14-17) to eliminate l_c shows that cake resistance increases during filtration in proportion to the volume filtered,

$$R_c\{t\} = K_1 \frac{(1-\epsilon_c)}{\epsilon_c^3} \frac{c_F V\{t\}}{\rho_c A_c} = \alpha \frac{c_F V\{t\}}{A_c} \tag{14-20}$$

where α is the average specific resistance of the cake, which can be measured experimentally. Unfortunately, the complex structure of a compressible filter cake and its dependence on pressure, preclude direct calculation of ϵ_c or α from scanning electron micrographs or other means.

As filtration progresses, cake thickness, filtrate volume, and resistance to flow pressure drop increase, but R_m is assumed to remain constant. W, the weight of the dry cake, is related to V and c_F by $W = c_F V$. However, care must be exercised when applying this formula because the cake is wet, and then dried, so c_F will have different values depending on whether wet or dry cake masses are used.

It is useful to replace R_c by α, which replaces k in the Darcy equation (14-4), where, now, $R_c = \alpha W/A_c = \alpha c_F (V/A_c)$. Thus, if length is in ft, R_c has units of ft^{-1} and α has units of ft/lb_m because ΔP must be multiplied by g_c for dimensional consistency if AE units are used [15, 19]. For SI units, α has dimensions of m/kg. Substituting the definition of α into (14-4) gives an alternative Darcy equation, where $A_c = A_M$:

$$\frac{d(V/A_c)}{dt} = \frac{\Delta P}{\mu [R_m + \alpha c_F (V/A_c)]} \tag{14-21}$$

For membranes like capillary or hollow fibers with small inner and outer radii, r_i and r_o, respectively, in which cake thickness is not negligible relative to radius of curvature, the resistance is

$$R_c\{t\} = \alpha r_j \ln\left\{ \left[\left(r_j + (-1)^a \delta_c\{t\} \right) / r_j \right]^{(-1)^a} \right\} \tag{14-22}$$

where cake thickness is $\delta_c\{t\} = c_F V\{t\}/\rho_c A_c$, with ρ_c being the cake density. For operation in which permeate exits the cylinder, subscript $j = i$ and superscript $a = 1$, while for permeate entering the cylinder, subscript $j = 0$ and $a = 0$.

Summary of Resistance Models

Other resistances neglected in Darcy's law (14-21) arise from matter blocking or constricting the pores and from osmotic pressure. These resistances can be negligible in microfiltration of high-molecular-weight solutes. Table 14.5 from [69] summarizes the four general mechanisms for pore blockage, intermediate pore blockage, pore constriction, and cake formation. Expressions are given for each mechanism for two common regimes of operations: decline of filtrate flow rate, Q, at constant trans-membrane pressure drop, ΔP; and change in pressure drop at constant filtrate rate. Linearized forms of each

Table 14.5 Models for Corresponding Flux and Pressure [69]

Constant Pressure	Flux	Linearized Form
Pore blockage	$\frac{Q}{Q_o} = \exp(-\beta t)$	$\ln(Q) = at + b$
Intermediate blockage	$\frac{Q}{Q_o} = (1+\beta t)^{-1}$	$\frac{1}{Q} = at + b$
Pore constriction	$\frac{Q}{Q_o} = (1+\beta t)^{-2}$	$\frac{t}{V} = at + b$
Cake formation	$\frac{Q}{Q_o} = (1+\beta t)^{-1/2}$	$\frac{t}{V} = aV + b$
Constant Flux	**Pressure**	**Linearized Form**
Pore blockage	$\frac{P}{P_o} = (1-\beta t)^{-1/2}$	$\frac{1}{P^2} = a - bV$
Intermediate blockage	$\frac{P}{P_o} = (1-\beta t)^{-1}$	$\frac{1}{P} = a - bV$
Pore constriction	$\frac{P}{P_o} = (1-\beta t)^{-2}$	$\frac{1}{P^{1/2}} = a - bV$
Cake formation	$\frac{P}{P_o} = 1 + \beta t$	$P = a + bV$

expression (usually in terms of cumulative filtrate volume, V, at filtration time, t) allow model identification, parameter estimation, and data analysis. As described above, fouling due to *cake formation* occurs as foulant deposits on the external membrane surface, producing an additional resistance in series with the membrane resistance. The remaining models assume that parallel arrays of uniform, right-cylindrical pores permeate a membrane barrier. *Pore constriction* occurs as foulant deposits on internal pore surfaces, reducing the effective pore size. Standard and intermediate *pore blockage* occurs when foulant occludes flow through individual pores. Intermediate pore blockage allows for superposition of foulant on the external membrane surface.

A combined pore-blockage, cake-filtration model describes experimental data for fouling by protein aggregates, which exhibits an initial flux decline attributable to pore occlusion leaving the membrane partially permeable to flow, followed by cake formation [70]. It has been extended to account for asymmetric membrane structures [71] and pore interconnectivity [72], which significantly reduce flux-decline rates relative to parallel pore arrays.

Consider application of the cake-formation model in (14-21) and its two forms in Table 14.5 to two regimes of filtration: constant-pressure, and constant-flow rate.

Constant-Pressure Filtration

Operating with constant-pressure drop produces a permeate flow rate and flux that decrease with time as cake thickness increases.

Assuming the filtration area is constant, (14-21) can be integrated from $V = 0$ to $V = V$ for $t = 0$ to $t = t$ to obtain the time-dependent permeate volume $V\{t\}$ and flux $J\{t\}$:

$$\int_0^V \left(R_m + \alpha \frac{c_F V}{A_c}\right) dV = \frac{A_c \Delta P}{\mu} \int_0^t dt \tag{14-23}$$

This yields the constant-pressure-drop form of the Ruth equation for sieve (i.e., surface) retention developed in 1933 [20, 68]:

$$V^2\{t\} + 2V\{t\} \frac{R_m A_c}{\alpha c_F} = 2 \frac{A_c^2 \Delta P}{\alpha c_F \mu} t \tag{14-24}$$

or

$$V^2\{t\} + 2V\{t\} V_o = Kt \tag{14-25}$$

where $V_o = R_m A_c / \alpha c_F$ and $K = 2A_c^2 \Delta P / \alpha c_F \mu$

In Exercise 14.27, the quadratic Ruth equation (14-25) is solved to obtain the positive root for $V\{t\}$. That result is then differentiated with respect to time to yield the permeate flux, $J\{t\}$. The following straight-line form of the Ruth equation shows that filtration time per unit volume, $t/V\{t\}$, increases with filtrate volume in proportion to c_F and α for a given filtration area at constant-pressure drop:

$$\frac{t}{V\{t\}} = \frac{1}{K}(V\{t\} + 2V_o) \tag{14-26}$$

Fitting (14-26) to experimental data for $t/V\{t\}$ versus $V\{t\}$ yields slope K^{-1} (to estimate α and determine cake resistance) and intercept $2V_o/K$ (to estimate R_m).

Constant-Flux Cake Filtration

In a plate-and-frame filter or a pressure leaf filter, where centrifugal pumps are used, the early stages of filtration are frequently at a reasonably constant rate; then, as the cake builds up, the ability of the pump to develop pressure becomes the limiting factor and the process continues at a constant pressure and a falling rate. Operating so that permeate flux, J, remains constant corresponds to a constant permeate flow rate, $dV/dt = V/t$, in (14-4) with $V = 0$ at $t = 0$. After the early filtration stages, this requires increasing the pressure differential across the membrane as cake thickness increases. For constant dV/dt, (14-4) becomes

$$J = \frac{V/A_c}{t} = \frac{\Delta P\{t\}}{\mu[R_m + \alpha c_F (V/A_c)]} \tag{14-27}$$

The expected value for $\Delta P\{t\}$ is obtained by rearranging (14-27) using an initial pressure drop of $\Delta P_o = J\mu R_m$ to yield

$$\frac{\Delta P\{t\}}{\Delta P_o} = 1 + \alpha \frac{c_F}{R_m} t \tag{14-28}$$

The ΔP increase is linear with time, in proportion to specific cake resistance and solid content in the feed. Rewriting (14-28) after substituting $u = V/t$, the superficial velocity of the filtrate through the cake, yields a similar linear equation for the variation of the ΔP with time:

$$\Delta P = au^2 t + bu \tag{14-29}$$

where

$$a = \alpha c_F \mu / A_c^2 \tag{14-30}$$

$$b = R_m \mu / A_c \tag{14-31}$$

Since u must be constant for a constant rate of filtration, (14-29) defines a straight line on a plot of ΔP versus t, as shown below in Example 14.3.

Combined Operation

Yield is improved in a combined operation in which: (1) constant-flux operation is employed in Stage 1 up to a limiting pressure drop, followed by (2) constant-pressure operation in Stage 2 until a minimum flux is reached. Let V_{CF} = volume of permeate obtained during Stage 1 for time period t_{CF}. For constant-permeate flux, with A_c replaced by A_M,

$$V_{CF} = JA_M t_{CF} \tag{14-32}$$

Let ΔP_{UL} = the upper limit of the pressure drop across the cake and membrane. Substituting ΔP_{UL} for ΔP into (14-23), using V_{CF} and t_{CF} for the lower limits of volumetric and time integration, respectively; and letting $K_2 = \alpha$, yields a quadratic equation for V. Solving the resulting quadratic equation for the positive root of V,

$$V = -\frac{R_m A_M}{K_2 c_F} + \left[A_M^2 R_m^2 + \frac{2A_M}{K_2 c_F} \times \left(R_m V_{CF} + \frac{K_2 c_F V_{CF}^2}{2A_M} + \frac{A_M \Delta P_{UL}(t - t_{CF})}{\mu}\right)\right]^{\frac{1}{2}} \tag{14-33}$$

where $V - V_{CF}$ = volume of permeate obtained during the Stage 2 time period $t - t_{CF}$. During Stage 2, the permeate flux decreases with time, according to an equation obtained by applying the definition of the permeate flux

from (14-2) to (14-33).

$$J = \frac{A_M \Delta P_{UL}}{K_2 c_F \mu}\left[\frac{A_M^2 R_m^2}{K_2^2 c_F^2} + \frac{2A_M}{K_2 c_F} \times \left(R_m V_{CF} + \frac{K_2 c_F V_{CF}^2}{2A_M} + \frac{A_M \Delta P_{UL}(t - t_{CF})}{\mu}\right)\right]^{-\frac{1}{2}} \tag{14-34}$$

Application of the above equations for a combined operation is illustrated in the following microfiltration example.

EXAMPLE 14.3 Microfiltration of Skim Milk.

Diluted skim milk with a protein concentration of 4.3 g/L is to undergo DEF microfiltration. Experiments have been performed using a cellulose-acetate membrane with an average pore diameter of 0.45 μm and $A_M = 17.3$ cm^2. For Stage 1 operation at a constant-permeate rate of 15 mL/minute, pressure drop across the cake and membrane increases from 0.3 psi to an upper limit of 20 psi in 400 seconds. The permeate viscosity is 1 cP. If continued in a second stage at constant ΔP at the upper limit until the permeate rate drops to 5 mL/minute, estimate the additional time of operation. Also, prepare plots of permeate volume in mL and permeate flux in mL/cm^2-minute as functions of time.

Solution

In SI units, $c_F = 4.3$ kg/m^3, $A_M = 0.00173$ m^2, volumetric flow rate in Stage 1 $= 0.25 \times 10^{-6}$ m^3/s, ΔP at zero time = 2,068 Pa, ΔP at 400 s = 137,900 Pa, and $\mu = 0.001$ Pa-s. Based on the experimental results for Stage 1, calculate values of R_m and $K_2 = \alpha$ as follows. From (14-27),

$$R_m = \frac{(\Delta P \text{ at } t = 0)}{J\mu} = \frac{2068}{\left(\frac{0.25 \times 10^{-6}}{0.00173}\right)(0.001)} = 1.43 \times 10^{10} \text{ m}^{-1}$$

For $t = 400$ s,

$$K_2 = \frac{\Delta P - J\mu R_m}{J^2 \mu c_F t} = \frac{\Delta P - (\Delta P \text{ at } t = 0)}{J^2 \mu c_F t} = \frac{6895(20 - 0.3)}{\left(\frac{0.25 \times 10^{-6}}{0.00173}\right)^2 (0.001)(4.3)(400)} = 3.78 \times 10^{12} \text{ m/kg}$$

Assume that these values of R_m and K_2 are valid during Stage 2. At the end of Stage 2, the permeate flux $= J =$ (5 mL/minute)/(17.3 cm^2) = 0.289 mL/minute-cm^2 $= 4.82 \times 10^{-5}$ m/s.

Solving (14-34) for t gives 2,025 s. Plots of permeate volume and flux versus time, in Figures 14.8 and 14.9, respectively, are obtained by solving, in time, (14-33) and (14-34) with a spreadsheet.

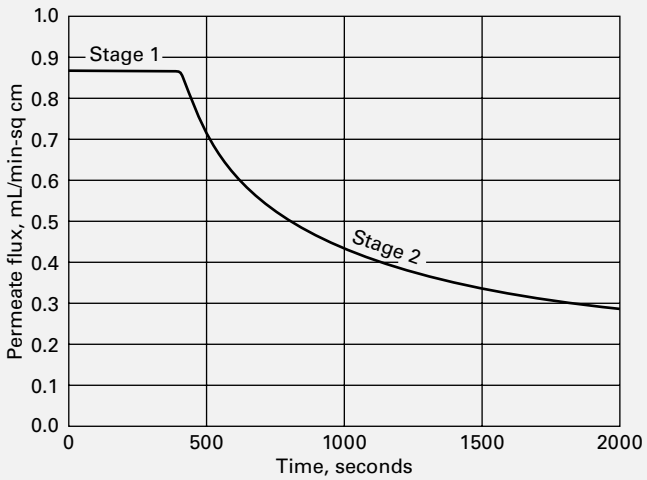

Figure 14.9 Instantaneous permeate flux for Example 14.3.

Compressibility

Filtration of cells or flocculated clays produces cakes that exhibit decreased void volume and increased specific cake resistance, α, as filtration proceeds. This indicates cake compressibility, which may be expressed by [66, 67]

$$\alpha = \alpha'(\Delta P)^s \tag{14-35}$$

where s is an empirical compressibility factor that ranges from zero for incompressible filter-aid cakes to near unity for highly compressible cakes, and α' is an empirical constant related to the size and shape of cake-forming particles.

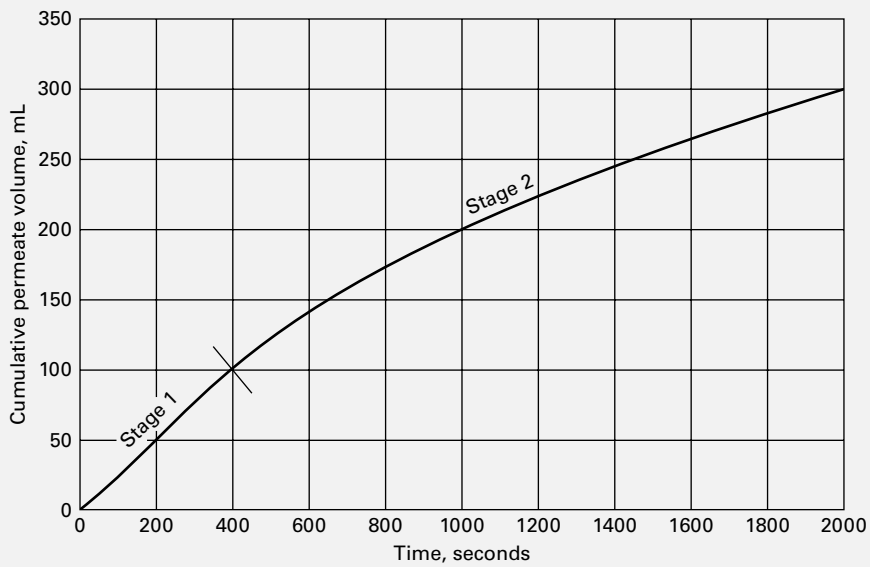

Figure 14.8 Cumulative permeate volume for Example 14.3.

§14.3.2 Liquid Diffusion Through Pores

Consider diffusion through the pores of a membrane from a fluid feed to a sweep fluid when identical total pressures but different component concentrations exist on both sides of the membrane. Bulk flow through the membrane due to a pressure difference does not occur, but if species diffuse at different rates, a separation can be achieved. If the feed mixture is a liquid of solvent and solutes i, the transmembrane flux for each solute is given by a modified form of Fick's law (§3.1.1):

$$N_i = \frac{D_{e_i}}{l_M}(c_{i_0} - c_{i_L}) \tag{14-36}$$

where D_{e_i} is the effective diffusivity, and c_i is the concentration of i in the liquid in the pores at the two faces of the membrane. The effective diffusivity is

$$D_{e_i} = \frac{\epsilon D_i}{\tau} K_{r_i} \tag{14-37}$$

where D_i is the molecular diffusion coefficient (diffusivity) of solute i in the solution, ϵ is the volume fraction of pores in the membrane, τ is tortuosity, and K_r is a restrictive factor that accounts for pore diameter, d_p, causing interfering collisions of the diffusing solutes with the pore wall, when the ratio of molecular diameter, d_m, to pore diameter exceeds about 0.01. The restrictive factor, according to Beck and Schultz [17], is:

$$K_r = \left[1 - \frac{d_m}{d_p}\right]^4, \quad (d_m/d_p) \le 1 \tag{14-38}$$

From (14-38), when $(d_m/d_p) = 0.01$, $K_r = 0.96$, but when $(d_m/d_p) = 0.3$, $K_r = 0.24$. When $d_m > d_p$, $K_r = 0$, and the solute cannot diffuse through the pore. This is the sieving or size-exclusion effect illustrated in Figure 14.6c. As illustrated in the next example, transmembrane fluxes for liquids through microporous membranes are very small because effective diffusivities are low.

For solute molecules not subject to size exclusion, a useful selectivity ratio is defined as

$$S_{ij} = \frac{D_i K_{r_i}}{D_j K_{r_j}} \tag{14-39}$$

This ratio is greatly enhanced by the effect of restrictive diffusion when the solutes differ widely in molecular weight and one or more molecular diameters approach the pore diameter. This is shown in the following example.

EXAMPLE 14.4 Solute Diffusion Through Membrane Pores.

Beck and Schultz [18] measured effective diffusivities of urea and different sugars, in aqueous solutions, through microporous mica membranes especially prepared to give almost straight, elliptical pores of almost uniform size. Based on the following data for a membrane and two solutes, estimate transmembrane fluxes for the two solutes in g/cm^2-s at 25°C. Assume the aqueous solutions on either side of the membrane are sufficiently dilute that no multicomponent diffusional effects are present.

Membrane:

Material	Microporous mica
Thickness, μm	4.24
Average pore diameter, Angstroms	88.8
Tortuosity, τ	1.1
Porosity, ϵ	0.0233

Solutes (in aqueous solution at 25°C):

Solute	MW	$D_i \times 10^6$ cm^2/s	molecular diameter, d_m, Å	g/cm^3 c_{i_0}	g/cm^3 c_{i_L}
1 Urea	60	13.8	5.28	0.0005	0.0001
2 β-Dextrin	1135	3.22	17.96	0.0003	0.00001

Solution

Calculate the restrictive factor and effective diffusivity from (14-38) and (14-37), respectively. For urea (1):

$$K_{r_1} = \left[1 - \left(\frac{5.28}{88.8}\right)\right]^4 = 0.783$$

$$D_{e_1} = \frac{(0.0233)(13.8 \times 10^{-6})(0.783)}{1.1} = 2.29 \times 10^{-7} \text{ cm}^2/\text{s}$$

For β-dextrin (2):

$$K_{r_2} = \left[1 - \left(\frac{17.96}{88.8}\right)\right]^4 = 0.405$$

$$D_{e_2} = \frac{(0.0233)(3.22 \times 10^{-6})(0.405)}{1.1} = 2.78 \times 10^{-8} \text{ cm}^2/\text{s}$$

Because of differences in molecular size, effective diffusivities differ by an order of magnitude. From (14-39), selectivity is

$$S_{1,2} = \frac{(13.8 \times 10^{-6})(0.783)}{(3.22 \times 10^{-6})(0.405)} = 8.3$$

Next, calculate transmembrane fluxes from (36), noting that the given concentrations are at the two faces of the membrane. Concentrations in the bulk solutions on either side of the membrane may differ from concentrations at the faces, depending upon the magnitudes of external mass-transfer resistances in boundary layers or films adjacent to the two faces of the membrane.

For urea:

$$N_1 = \frac{(2.29 \times 10^{-7})(0.0005 - 0.0001)}{4.24 \times 10^{-4}}$$

$$= 2.16 \times 10^{-7} \text{ g/cm}^2\text{-s}$$

For β-dextrin:

$$N_2 = \frac{(2.768 \times 10^{-8})(0.0003 - 0.00001)}{(4.24 \times 10^{-4})}$$

$$= 1.90 \times 10^{-8} \text{ g/cm}^2\text{-s}$$

Note that these fluxes are extremely low.

§14.3.3 Gas Diffusion Through Porous Membranes

When the mixture on either side of a microporous membrane is a gas, rates of diffusion can be expressed in terms of Fick's law (§3.1.1). If pressure and temperature on either side of the membrane are equal and the ideal-gas law holds, (14-36) in terms of a partial-pressure driving force is:

$$N_i = \frac{D_{e_i} c_M}{P l_M}\left(p_{i_0} - p_{i_L}\right) = \frac{D_{e_i}}{RT l_M}\left(p_{i_0} - p_{i_L}\right) \qquad (14\text{-}40)$$

where c_M is the total gas-mixture concentration given as P/RT by the ideal-gas law.

For a gas, diffusion through a pore occurs by ordinary diffusion, as with a liquid, and/or in series with Knudsen diffusion when pore diameter is very small and/or total pressure is low. In the Knudsen-flow regime, collisions occur primarily between gas molecules and the pore wall, rather than between gas molecules. In the absence of a bulk-flow effect or restrictive diffusion, (14-14) is modified to account for both mechanisms of diffusion:

$$D_{e_i} = \frac{\epsilon}{\tau}\left[\frac{1}{(1/D_i) + (1/D_{K_i})}\right] \qquad (14\text{-}41)$$

where $D_{K_i}$is the Knudsen diffusivity, which from the kinetic theory of gases as applied to a straight, cylindrical pore of diameter d_p is

$$D_{K_i} = \frac{d_p \bar{v}_i}{3} \qquad (14\text{-}42)$$

where $\bar{v}_i$ is the average molecule velocity given by

$$\bar{v}_i = (8RT/\pi M_i)^{1/2} \qquad (14\text{-}43)$$

where M is molecular weight. Combining (14-42) and (14-43):

$$D_{K_i} = 4{,}850 d_p (T/M_i)^{1/2} \qquad (14\text{-}44)$$

where D_K is cm^2/s, d_p is cm, and T is K. When Knudsen flow predominates, as it often does for micropores, a selectivity based on the permeability ratio for species A and B is given from a combination of (14-1), (14-40), (14-41), and (14-44):

$$\frac{P_{M_A}}{P_{M_B}} = \left(\frac{M_B}{M_A}\right)^{1/2} \qquad (14\text{-}45)$$

Except for gaseous species of widely differing molecular weights, the permeability ratio from (14-45) is not large, and the separation of gases by microporous membranes at low to moderate pressures that are equal on both sides of the membrane to minimize bulk flow is almost always impractical, as illustrated in the following example. However, the separation of the two isotopes of UF_6 by the U.S. government was accomplished by Knudsen diffusion, with a permeability ratio of only 1.0043, at Oak Ridge, Tennessee, using thousands of stages and acres of membrane surface.

EXAMPLE 14.5 Knudsen Diffusion.

A gas mixture of hydrogen (H) and ethane (E) is to be partially separated with a composite membrane having a 1-μm-thick porous skin with an average pore size of 20 Å and a porosity of 30%. Assume $\tau = 1.5$. The pressure on either side of the membrane is 10 atm and the temperature is 100°C. Estimate permeabilities of the components in barrer.

Solution

From (14-1), (14-40), and (14-41), the permeability can be expressed in mol-cm/cm^2-s-atm:

$$P_{M_i} = \frac{\epsilon}{RT\tau}\left[\frac{1}{(1/D_i) + (1/D_{K_i})}\right]$$

where $\epsilon = 0.30$, $R = 82.06$ cm^3-atm/mol-K, $T = 373$ K, and $\tau = 1.5$.

At 100°C, the ordinary diffusivity is given by $D_H = D_E = D_{H,E} = 0.86/P$ in cm^2/s with total pressure P in atm. Thus, at 10 atm, $D_H = D_E = 0.086$ cm^2/s. Knudsen diffusivities are given by (44), with $d_p = 20 \times 10^{-8}$ cm.

$$D_{K_H} = 4{,}850(20 \times 10^{-8})(373/2.016)^{1/2} = 0.0132 \text{ cm}^2/\text{s}$$

$$D_{K_E} = 4{,}850(20 \times 10^{-8})(373/30.07)^{1/2} = 0.00342 \text{ cm}^2/\text{s}$$

For both components, diffusion is controlled mainly by Knudsen diffusion.

For hydrogen: $\frac{1}{(1/D_H)+(1/D_{K_H})} = 0.0114$ cm^2/s.
For ethane: $\frac{1}{(1/D_E)+(1/D_{K_E})} = 0.00329$ cm^2/s.

$$P_{M_H} = \frac{0.30(0.0114)}{(82.06)(373)(1.5)} = 7.45 \times 10^{-8} \frac{\text{mol-cm}}{\text{cm}^2\text{-s-atm}}$$

$$P_{M_E} = \frac{0.30(0.00329)}{(82.06)(373)(1.5)} = 2.15 \times 10^{-8} \frac{\text{mol-cm}}{\text{cm}^2\text{-s-atm}}$$

To convert to barrer as defined in Example 14.1, note that

$$76 \text{ cmHg} = 1 \text{ atm and } 22{,}400 \text{ cm}^3 \text{ (STP)} = 1 \text{ mol}$$

$$P_{M_H} = \frac{7.45 \times 10^{-8}(22{,}400)}{(10^{-10})(76)} = 220{,}000 \text{ barrer}$$

$$P_{M_E} = \frac{2.15 \times 10^{-8}(22{,}400)}{(10^{-10})(76)} = 63{,}400 \text{ barrer}$$

§14.3.4 Transport Through Nonporous Membranes

Transport through nonporous (dense) solid membranes is the predominant mechanism of membrane separators for reverse osmosis, gas permeation, and pervaporation (liquid and vapor). As indicated in Figure 14.6d, gas or liquid species absorb at the upstream face of the membrane, diffuse through the membrane, and desorb at the downstream face.

Liquid diffusivities are several orders of magnitude less than gas diffusivities, and diffusivities of solutes in solids are a few orders of magnitude less than diffusivities in liquids. Thus, differences between diffusivities in gases and solids are enormous. For example, at 1 atm and 25°C, diffusivities in cm^2/s for water are as follows:

Water vapor in air	0.25
Water in ethanol liquid	1.2×10^{-5}
Dissolved water in cellulose-acetate solid	1×10^{-8}

As might be expected, small molecules fare better than large molecules for diffusivities in solids. From the *Polymer Handbook* [19], diffusivities in cm^2/s for several species in low-density polyethylene at 25°C are

Helium	6.8×10^{-6}
Hydrogen	0.474×10^{-6}
Nitrogen	0.320×10^{-6}
Propane	0.0322×10^{-6}

Regardless of whether a nonporous membrane is used to separate a gas or a liquid mixture, the *solution-diffusion model* of Lonsdale, Merten, and Riley [20] is used with experimental permeability data to design nonporous membrane separators. This model is based on Fick's law for diffusion through solid, nonporous membranes based on the driving force, $c_{i_0} - c_{i_L}$ shown in Figure 14.10b, where concentrations are those for solute dissolved in the membrane.

Concentrations in the membrane are related to the concentrations or partial pressures in the fluid adjacent to the membrane faces by assuming thermodynamic equilibrium for the solute at the fluid–membrane interfaces. This assumption has been validated by Motanedian et al. [21] for permeation of light gases through dense cellulose acetate at up to 90 atm.

Solution-Diffusion for Liquid Mixtures

Figures 14.10a and b show typical solute-concentration profiles for liquid mixtures with porous and nonporous (dense) membranes. Included is the drop in concentration across the membrane, and also possible drops due to resistances in the fluid boundary layers or films on either side of the membrane.

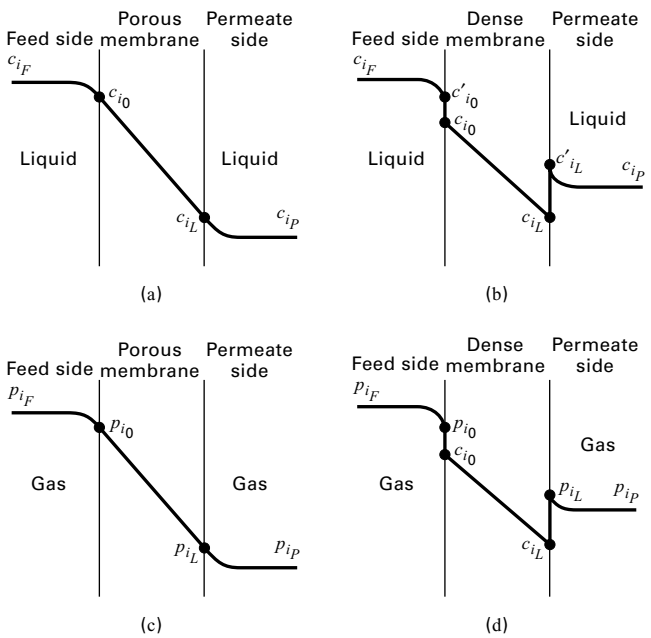

Figure 14.10 Concentration and partial-pressure profiles for solute transport through membranes. Liquid mixture with (a) a porous and (b) a nonporous membrane; gas mixture with (c) a porous and (d) a nonporous membrane.

For porous membranes considered above, the concentration profile is continuous from the bulk-feed liquid to the bulk-permeate liquid because liquid is present continuously from one side to the other. The concentration c_{i_0} is the same in the liquid feed just adjacent to the membrane surface and in the liquid just within the pore entrance. This is not the case for the nonporous membrane in Figure 14.10b. Solute concentration c'_{i_0} is that in the feed liquid just adjacent to the upstream membrane surface, whereas c_{i_0} is that in the membrane just adjacent to the upstream membrane surface. In general, c_{i_0} is considerably smaller than c'_{i_0}, but the two are related by a thermodynamic equilibrium partition coefficient K_i, defined by

$$K_{i_0} = c_{i_0}/c'_{i_0} \tag{14-46}$$

Similarly, at the other face:

$$K_{i_L} = c_{i_L}/c'_{i_L} \tag{14-47}$$

Fick's law for the dense membrane of Figure 14.10b is:

$$N_i = \frac{D_i}{l_M}(c_{i_0} - c_{i_L}) \tag{14-48}$$

where D_i is the diffusivity of the solute in the membrane. If (14-46) and (14-47) are combined with (14-48), and the partition coefficient is assumed independent of concentration, such that $K_{i_0} = K_{i_L} = K_i$, the flux is

$$\boxed{N_i = \frac{K_i D_i}{l_M}\left(c'_{i_0} - c'_{i_L}\right)} \tag{14-49}$$

If the mass-transfer resistances in the two fluid boundary layers or films are negligible:

$$N_i = \frac{K_i D_i}{l_M}(c_{i_F} - c_{i_P}) \tag{14-50}$$

In (14-49) and (14-50), $P_{M_i} = K_i D_i$ is the permeability for the solution-diffusion model, where K_i accounts for the solute solubility in the membrane and D_i accounts for diffusion through the membrane. Because D_i is generally very small, it is important that the membrane material have a large value for K_i and/or a small membrane thickness.

D_i and K_i, and therefore P_{M_i}, depend on the solute and the membrane. When solutes dissolve in a polymer membrane, it will swell, causing both D_i and K_i to increase. Other polymer-membrane factors that influence D_i, K_i, and P_{M_i} are listed in Table 14.6. However, the largest single factor is the chemical

Table 14.6 Factors That Influence Permeability of Solutes in Dense Polymers

Factor	Value Favoring High Permeability
Polymer density	low
Degree of crystallinity	low
Degree of cross-linking	low
Degree of vulcanization	low
Amount of plasticizers	high
Amount of fillers	low
Chemical affinity of solute for polymer (solubility)	high

structure of the membrane polymer. Because of the many factors involved, it is important to obtain experimental permeability data for the membrane and feed mixture of interest. The effect of external mass-transfer resistances is considered later in this section.

Solution-Diffusion for Gas Mixtures

Figures 14.10c and d show typical solute profiles for gas mixtures with porous and nonporous membranes, including the effect of the external-fluid boundary layer. For the porous membrane, a continuous partial-pressure profile is shown. For the nonporous membrane, a concentration profile is shown within the membrane, where the solute is dissolved. Fick's law holds for transport through the membrane. Assuming that thermodynamic equilibrium exists at the fluid–membrane interfaces, concentrations in Fick's law are related to partial pressures adjacent to the membrane faces by Henry's law as

$$H_{i_0} = c_{i_0}/p_{i_0} \tag{14-51}$$

and

$$H_{i_L} = c_{i_L}/p_{i_L} \tag{14-52}$$

If it is assumed that H_i is independent of total pressure and that the temperature is the same at both membrane faces:

$$H_{i_0} = H_{i_L} = H_i \tag{14-53}$$

Combining (14-48), (14-51), (14-52), and (14-53), the flux is

$$\boxed{N_i = \frac{H_i D_i}{l_M}\left(p_{i_0} - p_{i_L}\right)} \tag{14-54}$$

If the external mass-transfer resistances are neglected, $p_{i_F} = p_{i_0}$ and $p_{i_L} = p_{i_P}$, giving

$$N_i = \frac{H_i D_i}{l_M}\left(p_{i_F} - p_{i_P}\right) = \frac{P_{M_i}}{l_M}\left(p_{i_F} - p_{i_P}\right) \tag{14-55}$$

where

$$P_{M_i} = H_i D_i \tag{14-56}$$

Thus, permeability depends on both solubility of the gas component in the membrane and its diffusivity when dissolved in the membrane. An acceptable rate of transport can be achieved only by using a very thin membrane and a high pressure on the feed side. The permeability of a gas through a polymer membrane is subject to factors listed in Table 14.6. Light gases do not interact with the polymer or cause it to swell. Thus, a light-gas–permeant–polymer combination is readily characterized experimentally. Often both solubility and diffusivity are measured. An extensive tabulation is given in the *Polymer Handbook* [19]. Representative data at 25°C are given in Table 14.7. In general, diffusivity decreases and solubility increases with increasing molecular weight of the gas species, making it difficult to achieve a high selectivity. The effect of temperature over a modest range of about 50°C can be represented for both solubility and diffusivity by Arrhenius equations. For example,

$$D = D_0 e^{-E_D/RT} \tag{14-57}$$

The modest effect of temperature on solubility may act in either direction; however, an increase in temperature can cause an increase in diffusivity, and a corresponding increase in permeability. Typical activation energies of diffusion in polymers, E_D, range from 15 to 60 kJ/mol.

Application of Henry's law to rubbery polymers is well accepted, particularly for low-molecular-weight penetrants, but is less accurate for glassy polymers, for which alternative theories have been proposed. Foremost is the dual-mode model first proposed by Barrer and co-workers [22–24] as the result of a comprehensive study of sorption and diffusion in ethyl cellulose. In this model, sorption of penetrant occurs by ordinary dissolution in polymer chains, as described by Henry's law, and by Langmuir sorption into holes or sites

Table 14.7 Coefficients for Gas Permeation in Polymers

	Gas Species					
	H_2	O_2	N_2	CO	CO_2	CH_4
Low-Density Polyethylene:						
$D \times 10^6$	0.474	0.46	0.32	0.332	0.372	0.193
$H \times 10^6$	1.58	0.472	0.228	0.336	2.54	1.13
$P_M \times 10^{13}$	7.4	2.2	0.73	1.1	9.5	2.2
Polyethylmethacrylate:						
$D \times 10^6$	—	0.106	0.0301	—	0.0336	—
$H \times 10^6$	—	0.839	0.565	—	11.3	—
$P_M \times 10^{13}$	—	0.889	0.170	—	3.79	—
Polyvinylchloride:						
$D \times 10^6$	0.5	0.012	0.0038	—	0.0025	0.0013
$H \times 10^6$	0.26	0.29	0.23	—	4.7	1.7
$P_M \times 10^{13}$	1.3	0.034	0.0089	—	0.12	0.021
Butyl Rubber:						
$D \times 10^6$	1.52	0.081	0.045	—	0.0578	—
$H \times 10^6$	0.355	1.20	0.543	—	6.71	—
$P_M \times 10^{13}$	5.43	0.977	0.243	—	3.89	—

Note: Units: D in cm^2/s; H in cm^3 (STP)/cm^3-Pa; P_M in cm^3 (STP)-cm/cm^2-s-Pa.

between chains of glassy polymers. When downstream pressure is negligible compared to upstream pressure, the permeability for Fick's law is given by

$$P_{M_i} = H_i D_i + \frac{D_{L_i} ab}{1 + bP} \tag{14-58}$$

where the second term refers to Langmuir sorption, with D_{L_i} = diffusivity of Langmuir sorbed species, P = penetrant pressure, and ab = Langmuir constants for sorption-site capacity and site affinity, respectively.

Koros and Paul [25] found that the dual-mode theory accurately represents data for CO_2 sorption in polyethylene terephthalate below its glass-transition temperature of 85°C. Above that temperature, the rubbery polymer obeys Henry's law. Mechanisms of diffusion for the Langmuir mode have been suggested by Barrer [26].

The ideal dense-polymer membrane has a high permeance, P_{M_i}/l_M, for the penetrant molecules and a high separation factor between components. The separation factor is defined similarly to relative volatility in distillation:

$$\alpha_{A,B} = \frac{(y_A/x_A)}{(y_B/x_B)} \tag{14-59}$$

where y_i is the mole fraction in the permeate leaving the membrane, corresponding to partial pressure p_{i_P} in Figure 14.10d, while x_i is the mole fraction in the retentate on the feed side of the membrane, corresponding to partial pressure p_{i_F} in Figure 14.10d. Unlike distillation, y_i and x_i are not in equilibrium.

For the separation of a binary gas mixture of A and B in the absence of external boundary layer or film mass-transfer resistances, transport fluxes are given by (14-55):

$$N_A = \frac{H_A D_A}{l_M}\left(p_{A_F} - p_{A_P}\right) = \frac{H_A D_A}{l_M}\left(x_A P_F - y_A P_P\right) \tag{14-60}$$

$$N_B = \frac{H_B D_B}{l_M}\left(p_{B_F} - p_{B_P}\right) = \frac{H_B D_B}{l_M}\left(x_B P_F - y_B P_P\right) \tag{14-61}$$

When no sweep gas is used, the ratio of N_A to N_B fixes the composition of the permeate so that it is simply the ratio of y_A to y_B in the permeate gas. Thus,

$$\boxed{\frac{N_A}{N_B} = \frac{y_A}{y_B} = \frac{H_A D_A (x_A P_F - y_A P_P)}{H_B D_B (x_B P_F - y_B P_P)}} \tag{14-62}$$

If the downstream (permeate) pressure, P_P, is negligible compared to the upstream pressure, P_F, such that $y_A P_P \ll x_A P_F$ and $y_B P_P \ll x_B P_F$, (14-62) can be rearranged and combined with (14-59) to give an *ideal separation factor*:

$$\boxed{\alpha^*_{A,B} = \frac{H_A D_A}{H_B D_B} = \frac{P_{M_A}}{P_{M_B}}} \tag{14-63}$$

Thus, a high separation factor results from a high solubility ratio, a high diffusivity ratio, or both. The factor depends on both transport phenomena and thermodynamic equilibria.

When the downstream pressure is not negligible, (14-62) can be rearranged to obtain an expression for $\alpha_{A,B}$ in terms of the pressure ratio, $r = P_P/P_F$, and the mole fraction of A on the retentate side of the membrane. Combining (14-59), (14-63), and the definition of r with (14-62):

$$\alpha_{A,B} = \alpha^*_{A,B}\left[\frac{(x_B/y_B) - r\alpha_{A,B}}{(x_B/y_B) - r}\right] \tag{14-64}$$

Because $y_A + y_B = 1$, it is possible to substitute into (14-64) for x_B, the identity:

$$x_B = x_B y_A + x_B y_B$$

to give

$$\alpha_{A,B} = \alpha^*_{A,B}\left[\frac{x_B\left(\frac{y_A}{y_B} + 1\right) - r\alpha_{A,B}}{x_B\left(\frac{y_A}{y_B} + 1\right) - r}\right] \tag{14-65}$$

Combining (14-59) and (14-65) and replacing x_B with $1 - x_A$, the separation factor becomes:

$$\alpha_{A,B} = \alpha^*_{A,B}\left[\frac{x_A(\alpha_{A,B} - 1) + 1 - r\alpha_{A,B}}{x_A(\alpha_{A,B} - 1) + 1 - r}\right] \tag{14-66}$$

Equation (14-66) is an implicit equation for $\alpha_{A,B}$ in terms of the pressure ratio, r, and x_A, which is readily solved for $\alpha_{A,B}$ by rearranging the equation into a quadratic form. In the limit when $r = 0$, (14-66) reduces to (14-63), where $\alpha_{A,B} = \alpha^*_{A,B} = (P_{M_A}/P_{M_B})$. Many investigators report values of $\alpha^*_{A,B}$. Table 14.8, taken from the *Membrane Handbook* [6], gives data at 35°C for various binary pairs with polydimethyl siloxane (PDMS), a rubbery polymer, and bisphenol-A-polycarbonate (PC), a glassy polymer. For the rubbery polymer, permeabilities are high, but separation factors are low. The opposite is true for a glassy polymer. For a given feed composition, the separation factor places a limit on the achievable degree of separation.

Table 14.8 Ideal Membrane-Separation Factors of Binary Pairs for Two Membrane Materials

	PDMS, Silicon Rubbery Polymer Membrane	PC, Polycarbonate Glassy Polymer Membrane
$P_{M_{He}}$, barrer	561	14
$\alpha^*_{He,\,CH_4}$	0.41	50
$\alpha^*_{He,\,C_2H_4}$	0.15	33.7
$p_{M_{CO_2}}$, barrer	4,550	6.5
$\alpha^*_{CO_2,\,CH_4}$	3.37	23.2
$\alpha^*_{CO_2,\,C_2H_4}$	1.19	14.6
$p_{M_{O_2}}$, barrer	933	1.48
$\alpha^*_{O_2,\,N_2}$	2.12	5.12

EXAMPLE 14.6 Air Separation by Permeation

Air can be separated by gas permeation using different dense-polymer membranes. In all cases, the membrane is more permeable to oxygen. A total of 20,000 scfm of air is compressed, cooled, and treated to remove moisture and compressor oil prior to being sent to a membrane separator at 150 psia and 78°F. Assume the composition of the air is 79 mol% N_2 and 21 mol% O_2. A low-density, thin-film, composite polyethylene membrane with solubilities and diffusivities given in Table 14.7 is being considered.

If the membrane skin is 0.2 μm thick, calculate the material balance and membrane area in ft^2 as a function of the cut, which is defined as

$$\theta = \text{cut} = \text{fraction of feed permeated} = \frac{n_P}{n_F} \tag{14-67}$$

where n = flow rate in lbmol/h and subscripts F and P refer, respectively, to the feed and permeate. Assume 15 psia on the permeate side with perfect mixing on both sides of the membrane, such that compositions on both sides are uniform and equal to exit compositions. Neglect pressure drop and mass-transfer resistances external to the membrane. Comment on the practicality of the membrane for making a reasonable separation.

Solution

Assume that standard conditions are 0°C and 1 atm (359 ft^3/lbmol).

$$n_F = \text{Feed flow rate} = \frac{20{,}000}{359}(60) = 3{,}343 \text{ lbmol/h}$$

For the low-density polyethylene membrane, from Table 14.7, and applying (14-56), letting A = O_2 and B = N_2:

$$P_{M_B} = H_B D_B = \left(0.228 \times 10^{-6}\right)\left(0.32 \times 10^{-6}\right)$$
$$= 0.073 \times 10^{-12} \text{ cm}^3\text{(STP)-cm/cm}^2\text{-s-Pa}$$

or, in AE units,

$$P_{M_B} = \frac{\left(0.073 \times 10^{-12}\right)(2.54 \times 12)(3600)(101{,}300)}{(22{,}400)(454)(14.7)}$$
$$= 5.43 \times 10^{-12} \frac{\text{lbmol-ft}}{\text{ft}^2\text{-h-psia}}$$

Similarly, for oxygen:

$$P_{M_A} = 16.2 \times 10^{-12} \frac{\text{lbmol-ft}}{\text{ft}^2\text{-h-psia}}$$

Permeance values are based on a 0.2-μm-thick membrane skin (0.66×10^{-6} ft).

From (14-1),

$$\bar{P}_{M_i} = P_{M_i}/l_M$$
$$\bar{P}_{M_B} = 5.43 \times 10^{-12}/0.66 \times 10^{-6}$$
$$= 8.23 \times 10^{-6} \text{ lbmol/ft}^2\text{-h-psia}$$
$$\bar{P}_{M_A} = 16.2 \times 10^{-12}/0.66 \times 10^{-6}$$
$$= 24.55 \times 10^{-6} \text{ lbmol/ft}^2\text{-h-psia}$$

Material-balance equations:

For N_2,
$$x_{F_B} n_F = y_{P_B} n_P + x_{R_B} n_R \tag{1}$$

where n = flow rate in lbmol/h and subscripts F, P, and R refer, respectively, to the feed, permeate, and retentate. Since θ = cut = n_P/n_F, $(1-\theta) = n_R/n_F$.

Note that if all components of the feed have a finite permeability, the cut, θ, can vary from 0 to 1. For a cut of 1, all of the feed becomes permeate and no separation is achieved. Substituting (14-67) into (1) gives

$$x_{R_B} = \frac{x_{F_B} - y_{P_B}\theta}{1-\theta} = \frac{0.79 - y_{P_B}\theta}{1-\theta} \tag{2}$$

Similarly, for O_2,
$$x_{R_A} = \frac{0.21 - y_{P_A}\theta}{1-\theta} \tag{3}$$

Separation factor:
From the definition of the separation factor, (14-59), with well-mixed fluids, compositions are those of the retentate and permeate,

$$\alpha_{A,B} = \frac{y_{P_A}/x_{R_A}}{\left(1-y_{P_A}\right)/\left(1-x_{R_A}\right)} \tag{4}$$

Transport equations:
The transport of A and B through the membrane of area A_M, with partial pressures at exit conditions, can be written as

$$N_B = y_{P_B} n_P = A_M \bar{P}_{M_B}\left(x_{R_B} P_R - y_{P_B} P_P\right) \tag{5}$$

$$N_A = y_{P_A} n_P = A_M \bar{P}_{M_A}\left(x_{R_A} P_R - y_{P_A} P_P\right) \tag{6}$$

where A_M is the membrane area normal to flow, n_P, through the membrane. The ratio of (6) to (7) is y_{P_A}/y_{P_B}, and subsequent manipulations lead to (14-66),

where

$$r = P_P/P_R = 15/150 = 0.1 \text{ and } \alpha^*_{A,B} = \alpha_{O_2,N_2} = \bar{P}_{M_{O_2}}/\bar{P}_{M_{N_2}}$$
$$= \left(24.55 \times 10^{-6}\right)/\left(8.23 \times 10^{-6}\right) = 2.98$$

From (66):

$$\alpha_{A,B} = \alpha = 2.98\left[\frac{x_{R_A}(\alpha-1)+1-0.1\alpha}{x_{R_A}(\alpha-1)+1-0.1}\right] \tag{7}$$

Equations (3), (4), and (7) contain four unknowns: x_{R_A}, y_{P_A}, θ, and $\alpha_{A,B} = \alpha$. The variable θ is bounded between 0 and 1, so values of θ are selected in that range. The other three variables are computed in the following manner. Combine (3), (4), and (7) to eliminate α and x_{R_A}. Solve the resulting nonlinear equation for y_{P_A}. Then solve (3) for x_{R_A} and (4) for α. Solve (6) for the membrane area, A_M. The following results are obtained:

θ	x_{R_A}	y_{P_A}	$\alpha_{A,B}$	A_M, ft^2
0.01	0.208	0.406	2.602	22,000
0.2	0.174	0.353	2.587	462,000
0.4	0.146	0.306	2.574	961,000
0.6	0.124	0.267	2.563	1,488,000
0.8	0.108	0.236	2.555	2,035,000
0.99	0.095	0.211	2.548	2,567,000

Note that the separation factor remains almost constant, varying by only 2% with a value of about 86% of the ideal. The maximum permeate O_2 content (40.6 mol%) occurs with the smallest amount of permeate (θ = 0.01). The maximum N_2 retentate content (90.5 mol%) occurs with the largest amount of permeate (θ = 0.99). With a retentate equal to 60 mol% of the feed (θ = 0.4), the N_2 retentate content has increased only from 79 to 85.4 mol%. Furthermore, the membrane area requirements are very large. The low-density polyethylene membrane is thus not a practical membrane for this separation. To achieve a reasonable separation, say, with θ = 0.6 and a retentate of 95 mol% N_2, it is necessary to use a membrane with an ideal separation factor of 5, in a membrane module that approximates crossflow or countercurrent flow of permeate and retentate with no mixing and a higher O_2 permeance. For higher purities, a cascade of two or more stages is needed. These alternatives are developed in the next two subsections.

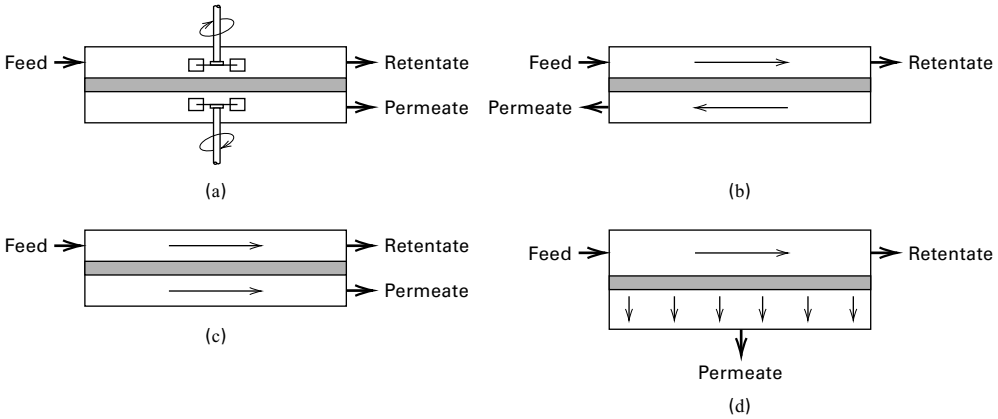

Figure 14.11 Idealized flow patterns in membrane modules: (a) perfect mixing; countercurrent flow; (b) cocurrent flow; (c) crossflow.

§14.3.5 Module Flow Patterns

In Example 14.6, perfect mixing, as shown in Figure 14.11a, was assumed. The three other idealized flow patterns shown, which have no mixing, have received considerable attention and are comparable to the idealized flow patterns used to design heat exchangers. These patterns are (b) countercurrent flow; (c) cocurrent flow; and (d) crossflow. For a given θ (14-67), the flow pattern can significantly affect the degree of separation and the membrane area. For flow patterns (b) to (d), fluid on the feed or retentate side of the membrane flows along and parallel to the upstream side of the membrane. For countercurrent and cocurrent flow, permeate fluid at a given location on the downstream side of the membrane consists of fluid that has just passed through the membrane at that location plus the permeate fluid flowing to that location. For the crossflow case, there is no flow of permeate fluid along the membrane surface. The permeate fluid that has just passed through the membrane at a given location is the only fluid there.

For a given module geometry, it is not obvious which idealized flow pattern to assume. This is particularly true for the spiral-wound module of Figure 14.5b. If the permeation rate is high, the fluid issuing from the downstream side of the membrane may continue to flow perpendicularly to the membrane surface until it finally mixes with the bulk permeate fluid flowing past the surface. In that case, the idealized crossflow pattern might be appropriate. Hollow-fiber modules are designed to approximate idealized countercurrent, cocurrent, or crossflow patterns. The hollow-fiber module in Figure 14.5d is approximated by a countercurrent-flow pattern.

Walawender and Stern [27] present methods for solving all four flow patterns of Figure 14.11, under assumptions of a binary feed with constant-pressure ratio, r, and constant ideal separation factor, $\alpha^*_{A,B}$. Exact analytical solutions are possible for perfect mixing (as in Example 14.6) and for crossflow, but numerical solutions are necessary for countercurrent and cocurrent flow. A reasonably simple, but approximate, analytical solution for the crossflow case, derived by Naylor and Backer [28], is presented here.

Consider a module with the crossflow pattern shown in Figure 14.12. Feed passes across the upstream membrane surface in plug flow with no longitudinal mixing. The pressure ratio, $r = P_P/P_F$, and the ideal separation factor, $\alpha^*_{A,B}$, are assumed constant. Boundary-layer (or film) mass-transfer resistances external to the membrane are assumed negligible. At the differential element, local mole fractions in the retentate and permeate are x_i and y_i, and the penetrant molar flux is dn/dA_M. Also, the local separation factor is given by (14-66) in terms of the local x_A, r, and $\alpha^*_{A,B}$. An alternative expression for the local permeate composition in terms of y_A, x_A, and r is obtained by combining (14-59) and (14-64):

$$\frac{y_A}{1-y_A} = \alpha^*_{A,B}\left[\frac{x_A - r y_A}{(1-x_A) - r(1-y_A)}\right] \tag{14-68}$$

A material balance for A around the differential-volume element gives

$$y_A dn = d(n x_A) = x_A dn + n dx_A \quad \text{or} \quad \frac{dn}{n} = \frac{dx_A}{y_A - x_A} \tag{14-69}$$

which is identical in form to the Rayleigh equation (13-2) for batch differential distillation. If (14-59) is combined with (14-69) to eliminate y_A,

$$\frac{dn}{n} = \left[\frac{1 + (\alpha - 1)x_A}{x_A(\alpha - 1)(1 - x_A)}\right] dx_A \tag{14-70}$$

where $\alpha = \alpha_{A,B}$.

In the solution to Example 14.6, it was noted that $\alpha = \alpha_{A,B}$ is relatively constant over the entire range of cut, θ. Such is generally the case when the pressure ratio, r, is small. If the assumption of constant $\alpha = \alpha_{A,B}$ is made in (14-70) and integration is carried out from the intermediate location of the

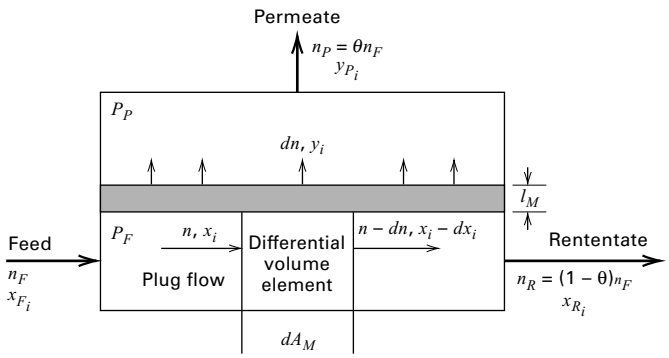

Figure 14.12 Crossflow model for membrane module.

differential element to the final retentate, that is, from n to n_R and from x_A to x_{R_A}, the result is

$$n = n_R \left[\left(\frac{x_A}{x_{R_A}} \right)^{\left(\frac{1}{\alpha-1}\right)} \left(\frac{1 - x_{R_A}}{1 - x_A} \right)^{\left(\frac{1}{\alpha-1}\right)} \right] \tag{14-71}$$

The mole fraction of A in the final permeate and the total membrane surface area are obtained by integrating the values obtained from solving (14-68) to (14-70):

$$y_{P_A} = \int_{x_{F_A}}^{x_{R_A}} y_A dn / \theta n_F \tag{14-72}$$

By combining (14-72) with (14-70), (14-71), and the definition of α, the integral in n can be transformed to an integral in x_A, which when integrated gives

$$y_{P_A} = x_{R_A}^{\left(\frac{1}{1-\alpha}\right)} \left(\frac{1-\theta}{\theta} \right) \times \left[(1 - x_{R_A})^{\left(\frac{\alpha}{\alpha-1}\right)} \left(\frac{x_{F_A}}{1 - x_{F_A}} \right)^{\left(\frac{\alpha}{\alpha-1}\right)} - x_{R_A}^{\left(\frac{\alpha}{1-\alpha}\right)} \right] \tag{14-73}$$

where $\alpha = \alpha_{A,B}$ can be estimated from (14-70) by using $x_A = x_{F_A}$.

The differential rate of mass transfer of A across the membrane is given by

$$y_A dn = \frac{P_{M_A} d A_M}{l_M} [x_A P_F - y_A P_P] \tag{14-74}$$

from which the total membrane surface area can be obtained by integration:

$$A_M = \int_{x_{R_A}}^{x_{F_A}} \frac{l_M y_A dn}{P_{M_A}(x_A P_F - y_A P_P)} \tag{14-75}$$

The crossflow model is illustrated in the next example.

EXAMPLE 14.7 Gas Permeation in a Crossflow Module.

For the conditions of Example 14.6, compute exit compositions for a spiral-wound module that approximates crossflow.

Solution

From Example 14.6: $\alpha^*_{A,B} = 2.98$; $r = 0.1$; $x_{F_A} = 0.21$

From (14-66), using $x_A = x_{F_A}$: $\alpha_{A,B} = 2.60$

An overall module material balance for O_2 (A) gives

$$x_{F_A} n_F = x_{R_A}(1-\theta) n_F + y_{P_A} \theta n_F \quad \text{or} \quad x_{R_A} = \frac{(x_{F_A} - y_{P_A}\theta)}{(1-\theta)} \tag{1}$$

Solving (1) and (14-73) simultaneously with a program such as Mathcad, Matlab, or Polymath gives the following results:

θ	x_{R_A}	x_{P_A}	Stage α_S
0.01	0.208	0.407	2.61
0.2	0.168	0.378	3.01
0.4	0.122	0.342	3.74
0.6	0.0733	0.301	5.44
0.8	0.0274	0.256	12.2
0.99	0.000241	0.212	1,120.

Comparing these results to those of Example 14.6, it is seen that for crossflow, the permeate is richer in O_2 and the retentate is richer in N_2. Thus, for a given cut, θ, crossflow is more efficient than perfect mixing, as might be expected.

Also included in the preceding table is the calculated degree of separation for the stage, α_S, defined on the basis of the mole fractions in the permeate and retentate exiting the stage by

$$(\alpha_{A,B})_S = \alpha_S = \frac{(y_{P_A}/x_{R_A})}{(1 - y_{P_A})/(1 - x_{R_A})} \tag{2}$$

The ideal separation factor, $\alpha^*_{A,B}$, is 2.98. Also, if (2) is applied to the perfect mixing case of Example 14.6, α_S is 2.603 for $\theta = 0.01$ and decreases slowly with increasing θ until at $\theta = 0.99$, $\alpha_S = 2.548$. Thus, for perfect mixing, $\alpha_S < \alpha^*$ for all θ. Such is not the case for crossflow. In the above table, $\alpha_S < \alpha^*$ for $\theta > 0.2$, and α_S increases with increasing θ. For $\theta = 0.6$, α_S is almost twice α^*.

Calculating the degree of separation of a binary mixture in a membrane module utilizing cocurrent- or countercurrent-flow patterns involves numerical solution of ODEs. These and computer codes for their solution are given by Walawender and Stern [27]. A representative solution is shown in Figure 14.13 for the separation of air (20.9 mol% O_2) for conditions of $\alpha^* = 5$ and $r = 0.2$. For a given cut, θ, it is seen that the best separation is with countercurrent flow. The curve for cocurrent flow lies between crossflow and perfect mixing. The computed crossflow case is considered to be a conservative estimate of membrane module performance. The perfect mixing case for binary mixtures is extended to multicomponent mixtures by Stern et al. [29]. As with crossflow, countercurrent flow also offers the possibility of a separation

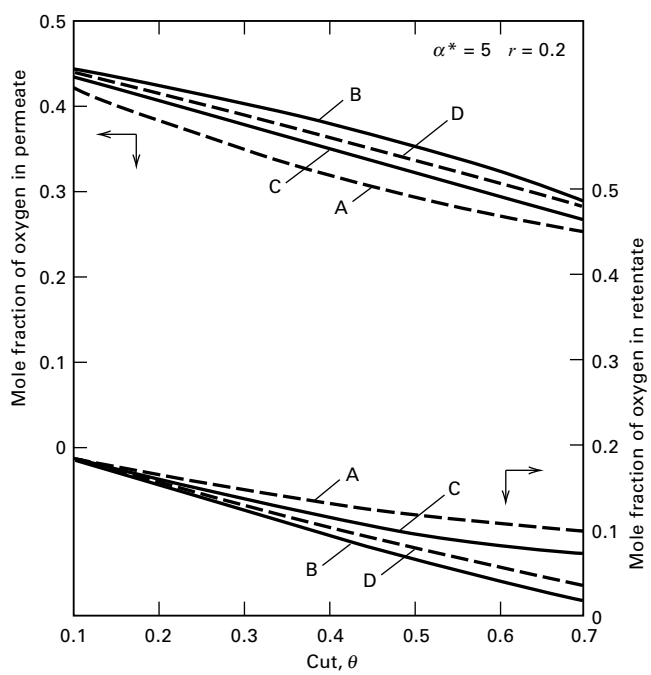

Figure 14.13 Effect of membrane module flow pattern on degree of separation of air. A, perfect mixing; B, countercurrent flow; C, cocurrent flow; D, crossflow.

factor for the stage, α_S, defined by (2) in Example 14.6, that is considerably greater than α^*.

§14.3.6 Cascades

A single membrane module or a number of such modules arranged in parallel or in series without recycle constitutes a single-stage membrane-separation process. The extent to which a feed mixture can be separated in a single stage is limited and determined by the separation factor, α. This factor depends, in turn, on module flow patterns; the permeability ratio (ideal separation factor); the cut, θ; and the driving force for membrane mass transfer. To achieve a higher degree of separation than is possible with a single stage, a countercurrent cascade of membrane stages—such as used in distillation, absorption, stripping, and liquid–liquid extraction—or a hybrid process that couples a membrane separator with another type of separator can be devised. Membrane cascades were presented briefly in §5.5. They are now discussed in detail and illustrated with an example.

A countercurrent recycle cascade of membrane separators, similar to a distillation column, is depicted in Figure 14.14a. The feed enters at stage F, somewhere near the middle of the column. Permeate is enriched in components of high permeability in an enriching section, while the retentate is enriched in components of low permeability in a stripping section. The final permeate is withdrawn from stage 1, while the final retentate is withdrawn from stage N. For a cascade, additional factors that affect the degree of separation are the number of stages and the recycle ratio (permeate recycle rate/permeate product rate). As discussed by Hwang and Kammermeyer [30], it is best to manipulate the cut and reflux rate at each stage so as to force compositions of the two streams entering each stage to be identical. For example, the composition of retentate leaving stage 1 and entering stage 2 would be identical to the composition of permeate flowing from stage 3 to stage 2. This corresponds to the least amount of entropy production for the cascade and, thus, the highest second-law efficiency. Such a cascade is referred to as "ideal".

Calculation methods for cascades are discussed by Hwang and Kammermeyer [30] and utilize single-stage methods that depend upon the module flow pattern, as discussed in the previous section. The calculations are best carried out on a computer, but results for a binary mixture can be conveniently displayed on a McCabe–Thiele-type diagram (§7.2) in terms of the mole fraction in the permeate leaving each stage, y_i, versus the mole fraction in the retentate leaving each stage, x_i. For a cascade, the equilibrium curve becomes the selectivity curve in terms of the separation factor for the stage, a_S.

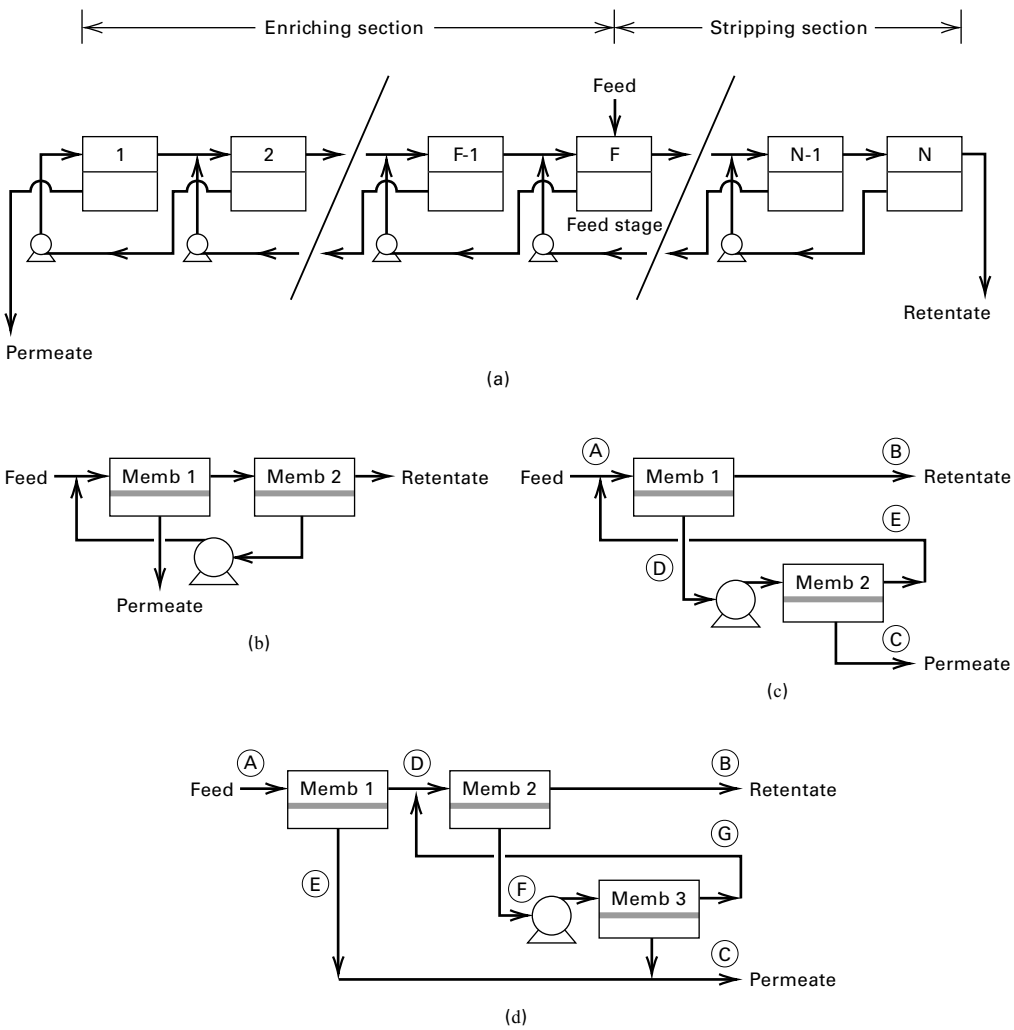

Figure 14.14 Countercurrent recycle cascades of membrane separators. (a) Multiple-stage unit. (b) Two-stage stripping cascade. (c) Two-stage enriching cascade. (d) Two-stage enriching cascade with additional premembrane stage.

In Figure 14.14, it is assumed that pressure drop on the feed or upstream side of the membrane is negligible. Thus, only the permeate must be pumped to the next stage if a liquid, or compressed if a gas. In the case of gas, compression costs are high. Thus, membrane cascades for gas permeation are often limited to just two or three stages, with the most common configurations shown in Figures 14.14b, c, and d.

Compared to one stage, the two-stage stripping cascade is designed to obtain a purer retentate, whereas a purer permeate is the goal of the two-stage enriching cascade. Addition of a premembrane stage, shown in Figure 14.14d, may be attractive when feed concentration is low in the component to be passed preferentially through the membrane, desired permeate purity is high, separation factor is low, and/or a high recovery of the more permeable component is desired. An example of the application of enrichment cascades is given by Spillman [31] for the removal of carbon dioxide from natural gas (simulated by methane) using cellulose-acetate membranes in spiral-wound modules that approximate crossflow. The ideal separation factor, $\alpha^*_{CO_2,CH_4}$, is 21. Results of calculations are given in Table 14.9 for a single stage (not shown in Figure 14.14), a two-stage enriching cascade (Figure 14.14c), and a two-stage enriching cascade with an additional premembrane stage (Figure 14.14d). Carbon dioxide flows through the membrane faster than methane. In all three cases, the feed is 20 million (MM) scfd of 7 mol% CO_2 in methane at 850 psig (865 psia) and the retentate is 98 mol% in methane. For each stage, the downstream (permeate-side) membrane pressure is 10 psig (25 psia). In Table 14.9, for all three cases, stream A is the feed, stream B is the final retentate, and stream C is the final permeate. Case 1 achieves a 90.2% recovery of methane. Case 2 increases that recovery to 98.7%. Case 3 achieves an intermediate recovery of 94.6%. The following degrees of separation are computed from data given in Table 14.9:

	α_s for Membrane Stage		
Case	1	2	3
1	28	—	—
2	28	57	—
3	20	19	44

Table 14.9 Separation of CO_2 and CH_4 with Membrane Cascades

Case 1: Single Membrane Stage:

	Stream		
	A Feed	B Retentate	C Permeate
Composition (mole%)			
CH_4	93.0	98.0	63.4
CO_2	7.0	2.0	36.6
Flow rate (MM SCFD)	20.0	17.11	2.89
Pressure (psig)	850	835	10

Case 2: Two-Stage Enriching Cascade (Figure 14.14c):

	Stream				
	A	B	C	D	E
Composition (mole%)					
CH_4	93.0	98.0	18.9	63.4	93.0
CO_2	7.0	2.0	81.1	36.6	7.0
Flow rate (MM SCFD)	20.00	18.74	1.26	3.16	1.90
Pressure (psig)	850	835	10	10	850

Case 3: Two-Stage Enriching Cascade with Premembrane Stage (Figure 14.14d):

	Stream						
	A	B	C	D	E	F	G
Composition (mole%)							
CH_4	93.0	98.0	49.2	96.1	56.1	72.1	93.0
CO_2	7.0	2.0	50.8	3.9	43.9	27.9	7.0
Flow rate (MM SCFD)	20.00	17.95	2.05	19.39	1.62	1.44	1.01
Pressure (psig)	850	835	10	840	10	10	850

Note: MM = million.

It is also possible to compute overall degrees of separation for the cascades, α_C, for cases 2 and 3, giving values of 210 and 51, respectively.

§14.3.7 External Mass-Transfer Resistances

Thus far, resistance to mass transfer has been associated only with the membrane. Thus, concentrations in the fluid at the upstream and downstream faces of the membrane have been assumed equal to the respective bulk-fluid concentrations. When mass-transfer resistances external to the membrane are not negligible, gradients exist in the boundary layers (or films) adjacent to the membrane surfaces, as is illustrated for four cases in Figure 14.10. For given bulk-fluid concentrations, the presence of these resistances reduces the driving force for mass transfer across the membrane and, therefore, the flux of penetrant.

Gas permeation by solution-diffusion (14-54) is slow compared to diffusion in gas boundary layers or films, so external mass-transfer resistances are negligible and $P_{i_F} = P_{i_0}$ and $P_{i_P} = P_{i_L}$ in Figure 14.10d. Because diffusion in liquid boundary layers and films is slow, concentration polarization, which is the accumulation of non-permeable species on the upstream surface of the membrane, cannot be neglected in membrane processes that involve liquids, such as dialysis, reverse osmosis, and pervaporation. The need to consider the effect of concentration polarization is of particular importance in reverse osmosis, where the effect can reduce the water flux and increase the salt flux, making it more difficult to obtain potable water.

Consider a membrane process of the type in Figure 14.10a, involving liquids with a porous membrane. At steady state, the rate of mass transfer of a penetrating species, i, through the three resistances is as follows, assuming no change in area for mass transfer across the membrane:

$$N_i = k_{i_F}(c_{i_F} - c_{i_0}) = \frac{D_{e_i}}{l_M}(c_{i_0} - c_{i_L}) = k_{i_P}(c_{i_L} - c_{i_P})$$

where D_{e_i} is given by (14-38). If these three equations are combined to eliminate the intermediate concentrations, c_{i_0} and c_{i_L},

$$N_i = \frac{c_{i_F} - c_{i_P}}{\dfrac{1}{k_{i_F}} + \dfrac{l_M}{D_{e_i}} + \dfrac{1}{k_{i_P}}} \qquad (14\text{-}76)$$

Now consider the membrane process in Figure 14.10b, involving liquids with a nonporous membrane, for which the solution-diffusion mechanism, (14-49), applies for mass transfer through the membrane. At steady state, for constant mass-transfer area, the rate of mass transfer through the three resistances is:

$$N_i = k_{i_F}\left(c_{i_F} - c'_{i_0}\right) = \frac{K_i D_i}{l_M}\left(c'_{i_0} - c'_{i_L}\right) = k_{i_P}\left(c'_{i_L} - c_{i_P}\right)$$

If these three equations are combined to eliminate the intermediate concentrations, c'_{i_0} and c'_{i_L},

$$N_i = \frac{c_{i_F} - c_{i_P}}{\dfrac{1}{k_{i_F}} + \dfrac{l_M}{K_i D_i} + \dfrac{1}{k_{i_P}}} \qquad (14\text{-}77)$$

where in (14-76) and (14-77), k_{i_F} and k_{i_P} are mass-transfer coefficients for the feed-side and permeate-side boundary layers (or films). The three terms in the RHS denominator are the resistances to the mass flux. Mass-transfer coefficients depend on fluid properties, flow-channel geometry, and flow regime. In the laminar-flow regime, a long entry region may exist where the mass-transfer coefficient changes with distance, L, from the entry of the membrane channel. Estimation of coefficients is complicated by fluid velocities that change because of mass exchange between the two fluids. In (14-76) and (14-77), the membrane resistances, l_M/D_{e_i} and l_M/K_iD_i, respectively, can be replaced by l_M/P_{M_i} or $\bar{P}_{M_i}$.

Mass-transfer coefficients for channel flow can be obtained from the general empirical film-model correlation [32]:

$$N_{Sh} = k_i d_H / D_i = a N_{Re}^b N_{Sc}^{0.33} (d_H/L)^d \qquad (14\text{-}78)$$

where $N_{Re} = d_H \upsilon \rho/\mu$, $N_{Sc} = \mu/\rho D_i$, d_H = hydraulic diameter, and υ = velocity.

Values for constants a, b, and d are as follows:

Flow Regime	Flow Channel Geometry	d_H	a	b	d
Turbulent, ($N_{Re} > 10{,}000$)	Circular tube	D	0.023	0.8	0
	Rectangular channel	$2hw/(h+w)$	0.023	0.8	0
Laminar, ($N_{Re} < 2{,}100$)	Circular tube	D	1.86	0.33	0.33
	Rectangular channel	$2hw/(h+w)$	1.62	0.33	0.33

where w = width of channel, h = height of channel, and L = length of channel.

EXAMPLE 14.8 Solute Flux Through a Membrane.

A dilute solution of solute A in solvent B is passed through a tubular-membrane separator, where the feed flows through the tubes. At a certain location, solute concentrations on the feed and permeate sides are 5.0×10^{-2} kmol/m^3 and 1.5×10^{-2} kmol/m^3, respectively. The permeance of the membrane for solute A is given by the membrane vendor as 7.3×10^{-5} m/s. If the tube-side Reynolds number is 15,000, the feed-side solute Schmidt number is 500, the diffusivity of the feed-side solute is 6.5×10^{-5} cm^2/s, and the inside diameter of the tube is 0.5 cm, estimate the solute flux through the membrane if the mass-transfer resistance on the permeate side of the membrane is negligible.

Solution

Flux of the solute is from the permeance form of (14-76) or (14-77):

$$N_A = \frac{c_{A_F} - c_{A_P}}{\dfrac{1}{k_{A_F}} + \dfrac{1}{\bar{P}_{M_A}} + 0}$$

$$c_{A_F} - c_{A_P} = 5 \times 10^{-2} - 1.5 \times 10^{-2} = 3.5 \times 10^{-2} \text{ kmol/m}^3 \qquad (1)$$

$$\bar{P}_{M_A} = 7.3 \times 10^{-5} \text{ m/s}$$

From (14-78), for turbulent flow in a tube, since $N_{Re} > 10{,}000$:

$$k_{A_F} = 0.023\frac{D_A}{D}N_{Re}^{0.8}N_{Sc}^{0.33}$$

$$= 0.023\left(\frac{6.5\times10^{-5}}{0.5}\right)(15{,}000)^{0.8}(500)^{0.33}$$

$$= 0.051 \text{ cm/s or } 5.1\times10^{-4} \text{ m/s}$$

From (1),

$$N_A = \frac{3.5\times10^{-2}}{\frac{1}{5.1\times10^{-4}}+\frac{1}{7.3\times10^{-5}}} = 2.24\times10^{-6} \text{ kmol/s-m}^2$$

The fraction of the total resistance due to the membrane is

$$\frac{\frac{1}{7.3\times10^{-5}}}{\frac{1}{5.1\times10^{-4}}+\frac{1}{7.3\times10^{-5}}} = 0.875 \text{ or } 87.5\%$$

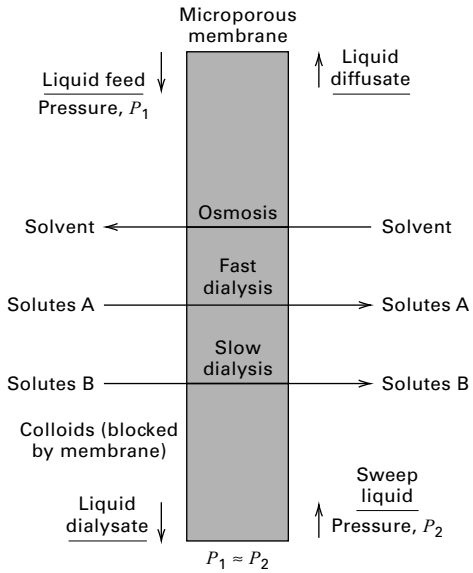

Figure 14.15 Dialysis.

§14.3.8 Concentration Polarization and Fouling

When gases are produced during electrolysis, they accumulate on and around the electrodes of the electrolytic cell, reducing the flow of electric current. This is referred to as polarization. A similar phenomenon, *concentration polarization*, occurs in membrane separators when the membrane is permeable to A, but relatively impermeable to B. Thus, molecules of B are carried by bulk flow to the upstream surface of the membrane, where they accumulate, causing their concentration at the surface of the membrane to increase in a "polarization layer." The equilibrium concentration of B in this layer is reached when its back-diffusion to the bulk fluid on the feed-retentate side equals its bulk flow toward the membrane.

Concentration polarization is most common in pressure-driven membrane separations involving liquids, such as reverse osmosis and ultrafiltration, where it reduces the flux of A. The polarization effect can be serious if the concentration of B reaches its solubility limit on the membrane surface. Then, a precipitate of gel may form, the result being fouling on the membrane surface or within membrane pores, with a further reduction in the flux of A. Concentration polarization and fouling are most severe at high values of the flux of A. Theory and examples of concentration polarization and fouling are given in §14.6 and §14.8 on reverse osmosis and ultrafiltration.

§14.4 DIALYSIS

In the dialysis membrane-separation process, shown in Figure 14.15, the feed is liquid at pressure P_1 and contains solvent, solutes of type A, and solutes of type B and insoluble, but dispersed, colloidal matter. A sweep liquid or wash of the same solvent is fed at pressure P_2 to the other side of the membrane. The membrane is thin, with micropores of a size such that solutes of type A can pass through by a concentration-driving force. Solutes of type B are larger in molecular size than those of type A and pass through the membrane only with difficulty or not at all. This transport of solutes through the membrane is called dialysis. Colloids do not pass through the membrane. With pressure $P_1 = P_2$, the solvent may also pass through the membrane, but by a concentration-driving force acting in the opposite direction. The transport of the solvent is called osmosis. By elevating P_1 above P_2, solvent osmosis can be reduced or eliminated if the difference is higher than the osmotic pressure. The products of a dialysis unit (dialyzer) are a liquid *diffusate* (permeate) containing solvent, solutes of type A, and little or none of type B solutes; and a *dialysate* (retentate) of solvent, type B solutes, remaining type A solutes, and colloidal matter. Ideally, the dialysis unit would enable a perfect separation between solutes of type A and solutes of type B and any colloidal matter. However, at best only a fraction of solutes of type A are recovered in the diffusate, even when solutes of type B do not pass through the membrane.

For example, when dialysis is used to recover sulfuric acid (type A solute) from an aqueous stream containing sulfate salts (type B solutes), the following results are obtained, as reported by Chamberlin and Vromen [33]:

	Streams in		Streams out	
	Feed	Wash	Dialysate	Diffusate
Flow rate, gph	400	400	420	380
H_2SO_4, g/L	350	0	125	235
$CuSO_4$, g/L as Cu	30	0	26	2
$NiSO_4$, g/L as Ni	45	0	43	0

Thus, about 64% of the H_2SO_4 is recovered in the diffusate, accompanied by only 6% of the $CuSO_4$, and no $NiSO_4$.

Dialysis is closely related to other membrane processes that use other driving forces for separating liquid mixtures, including (1) reverse osmosis, which depends

upon a transmembrane pressure difference for solute and/or solvent transport; (2) electrodialysis and electro-osmosis, which depend upon a transmembrane electrical-potential difference for solute and solvent transport, respectively; and (3) thermal osmosis, which depends upon a transmembrane temperature difference for solute and solvent transport.

Dialysis is attractive when concentration differences for the main diffusing solutes are large and permeability differences between those solutes and the other solute(s) and/or colloids are large. Although dialysis has been known since the work of Graham in 1861 [34], commercial applications of dialysis do not rival reverse osmosis and gas permeation. Nevertheless, dialysis has been used in separations, including: (1) recovery of sodium hydroxide from a 17–20 wt% caustic viscose liquor contaminated with hemicellulose to produce a diffusate of 9–10 wt% caustic; (2) recovery of chromic, hydrochloric, and hydrofluoric acids from contaminating metal ions; (3) recovery of sulfuric acid from aqueous solutions containing nickel sulfate; (4) removal of alcohol from beer to produce a low-alcohol beer; (5) recovery of nitric and hydrofluoric acids from spent stainless steel pickle liquor; (6) removal of mineral acids from organic compounds; (7) removal of low-molecular-weight contaminants from polymers; and (8) purification of pharmaceuticals. Also of great importance is hemodialysis, in which urea, creatine, uric acid, phosphates, and chlorides are removed from blood without removing essential higher-molecular-weight compounds and blood cells in a device called an artificial kidney. Dialysis centers servicing those suffering from incipient kidney failure are common in shopping centers.

Typical microporous-membrane materials used in dialysis are hydrophilic, including cellulose, cellulose acetate, various acid-resistant polyvinyl copolymers, polysulfones, and polymethylmethacrylate, typically less than 50 μm thick and with pore diameters of 15 to 100 Å. The most common membrane modules are plate-and-frame and hollow-fiber. Compact hollow-fiber hemodialyzers, such as the one shown in Figure 14.16, which are widely used, typically contain several thousand 200-μm-diameter fibers with a wall thickness of 20–30 μm and a length of 10–30 cm. Dialysis membranes can be thin because pressures on either side of the membrane are essentially equal. The differential rate of solute mass transfer across the membrane is

$$dn_i = K_i(c_{i_F} - c_{i_P})d A_M \tag{14-79}$$

where K_i is the overall mass-transfer coefficient, in terms of the three coefficients from the permeability form of (14-76):

$$\frac{1}{K_i} = \frac{1}{k_{i_F}} + \frac{l_M}{P_{M_i}} + \frac{1}{k_{i_P}} \tag{14-80}$$

Membrane area is determined by integrating (14-79), taking into account module flow patterns, bulk-concentration gradients, and individual mass-transfer coefficients in (14-80).

One of the oldest membrane materials used with aqueous solutions is porous cellophane, for which solute permeability is given by (14-37) with $P_{M_i} = D_{e_i}$ and $\bar{P}_{M_i} l_M$. If immersed, cellophane swells to about twice its dry thickness. The wet thickness should be used for l_M. Typical values of parameters in (14-36) to (14-38) for commercial cellophane are as follows: Wet thickness $= l_M = 0.004$ to 0.008 cm; porosity $= \epsilon = 0.45$ to 0.60; tortuosity $= \tau = 3$ to 5; pore diameter $= D = 30$ to 50 Å.

If a solute does not interact with the membrane material, diffusivity, D_{e_i}, in (14-37) is the ordinary molecular-diffusion coefficient, which depends only on solute and solvent properties. In practice, the membrane may have a profound effect on solute diffusivity if membrane–solute interactions such as covalent, ionic, and hydrogen bonding; physical adsorption and chemisorption; and increases in membrane polymer flexibility occur. Thus, it is best to measure $\bar{P}_{M_i}$ experimentally using process fluids.

Although transport of solvents such as water, usually in a direction opposite to the solute, can be described in terms of Fick's law, it is common to measure the solvent flux and report a so-called *water-transport number*, which is the ratio of the water flux to the solute flux, with a negative value indicating transport of solvent in the solute direction. The membrane can also interact with solvent and curtail solvent transport. Ideally, the water-transport number should be a small value, less than +1.0. Design parameters for dialyzers are best measured in the laboratory using a batch cell with a variable-speed stirring mechanism on both sides of the membrane so that external mass-transfer resistances, $1/k_{i_F}$ and $1/k_{i_P}$ in (14-80), are made negligible. Stirrer speeds >2,000 rpm may be required.

A common dialyzer is the plate-and-frame type of Figure 14.5a. For dialysis, the frames are vertical and a unit might contain 100 square frames, each 0.75 m × 0.75 m on 0.6-cm spacing, equivalent to 56 m^2 of membrane surface. A typical dialysis rate for sulfuric acid is 5 lb/day-ft^2. Recent dialysis units utilize hollow fibers of 200-μm inside diameter, 16-μm

Figure 14.16 Artificial kidney.

wall thickness, and 28-cm length, packed into a heat-exchanger-like module to give 22.5 m^2 of membrane area in a volume that might be one-tenth of the volume of an equivalent plate-and-frame unit.

In a plate-and-frame dialyzer, the flow pattern is nearly countercurrent. Because total flow rates change little and solute concentrations are small, it is common to estimate solute transport rate by assuming a constant overall mass-transfer coefficient with a log-mean concentration-driving force. Thus, from (14-79):

$$n_i = K_i A_M (\Delta c_i)_{\text{LM}} \qquad (14\text{-}81)$$

where K_i is from (14-80). This design method is used in the following example.

EXAMPLE 14.9 Recovery of H_2SO_4 by Dialysis.

A countercurrent-flow, plate-and-frame dialyzer is to be sized to process 0.78 m^3/h of an aqueous solution containing 300 kg/m^3 of H_2SO_4 and smaller amounts of copper and nickel sulfates, using a wash water sweep of 1.0 m^3/h. It is desired to recover 30% of the acid at 25°C. From batch experiments with an acid-resistant vinyl membrane, in the absence of external mass-transfer resistances, a permeance of 0.025 cm/min for the acid and a water-transport number of +1.5 are measured. Membrane transport of copper and nickel sulfates is negligible. Experience with plate-and-frame dialyzers indicates that flow will be laminar and the combined external liquid-film mass-transfer coefficients will be 0.020 cm/min. Determine the membrane area required in m^2.

Solution

$m_{H_2SO_4}$ in feed $= 0.78(300) = 234$ kg/h;

$m_{H_2SO_4}$ transferred $= 0.3(234) = 70$ kg/h;

m_{H_2O} transferred to dialysate $= 1.5(70) = 105$ kg/h;

m_{H_2O} in entering wash $= 1.0(1{,}000) = 1{,}000$ kg/h;

m_P leaving $= 1{,}000 - 105 + 70 = 965$ kg/h

For mixture densities, assume aqueous sulfuric acid solutions and use the appropriate table in *Perry's Chemical Engineers' Handbook*:

$\rho_F = 1{,}175$ kg/m^3; $\rho_R = 1{,}114$ kg/m^3; $\rho_P = 1{,}045$ kg/m^3;

$m_F = 0.78(1{,}175) = 917$ kg/h; m_R leaving $= 917 + 105 - 70 = 952$ kg/h

Sulfuric acid concentrations:

$$c_F = 300 \text{ kg/m}^3;\ c_{\text{wash}} = 0 \text{ kg/m}^3$$

$$c_R = \frac{(234 - 70)}{952}(1{,}114) = 192 \text{ kg/m}^3$$

$$c_P = \frac{70}{965}(1{,}045) = 76 \text{ kg/m}^3$$

The log-mean driving force for H_2SO_4 with countercurrent flow of feed and wash:

$$(\Delta c)_{\text{LM}} = \frac{(c_F - c_P) - (c_R - c_{\text{wash}})}{\ln\left(\dfrac{c_F - c_P}{c_R - c_{\text{wash}}}\right)} = \frac{(300 - 76) - (192 - 0)}{\ln\left(\dfrac{300 - 76}{192 - 0}\right)} = 208 \text{ kg/m}^3$$

The driving force is almost constant in the membrane module, varying only from 224 to 192 kg/m^3.

From (14-80), $$K_{H_2SO_4} = \frac{1}{\dfrac{1}{P_M} + \left(\dfrac{1}{k}\right)_{\text{combined}}} = \frac{1}{\dfrac{1}{0.025} + \dfrac{1}{0.020}} = (0.0111 \text{ cm/min or } 0.0067 \text{ m/h})$$

From (14-81), using mass units instead of molar units:

$$A_M = \frac{m_{H_2SO_4}}{K_{H_2SO_4}(\Delta c_{H_2SO_4})_{\text{LM}}} = \frac{70}{0.0067(208)} = 50 \text{ m}^2$$

§14.5 ELECTRODIALYSIS

Electrodialysis dates back to the early 1900s, when electrodes and a direct current were used to increase the rate of dialysis. Since the 1940s, electrodialysis has become a process that differs from dialysis in many ways. Today, electrodialysis refers to an electrolytic process for separating an aqueous, electrolyte feed into concentrate and dilute or desalted water diluate by an electric field and ion-selective membranes. An electrodialysis process is shown in Figure 14.17, where the four ion-selective membranes are of two types arranged in an alternating-series pattern. The cation-selective membranes (C) carry a negative charge, and thus attract and pass positively charged ions (cations), while retarding negative ions (anions). The anion-selective membranes (A) carry a positive charge that attracts and permits passage of anions. Both types of membranes are impervious to water. The net result is that both anions and cations are concentrated in compartments 2 and 4, from which concentrate is withdrawn, and ions are depleted in compartment 3, from which the diluate is withdrawn. Compartment pressures are essentially equal. Compartments 1 and 5 contain the anode and cathode, respectively. A direct-current voltage causes current to flow through the cell by ionic conduction from the cathode to the anode. Both electrodes are chemically neutral metals, with the anode being typically stainless steel and the cathode platinum-coated tantalum, niobium, or titanium. Thus, the electrodes are neither oxidized nor reduced.

The most easily oxidized species is oxidized at the anode and the most easily reduced species is reduced at the cathode. With inert electrodes, the result at the cathode is the reduction of water by the half reaction

$$2H_2O + 2e^- \rightarrow 2OH^- + H_{2_{(g)}},\ E^0 = -0.828 \text{ V}$$

The oxidation half reaction at the anode is

$$H_2O \rightarrow 2e^- + \tfrac{1}{2}O_{2_{(g)}} + 2H^+,\ E^0 = -1.23 \text{ V}$$

or, if chloride ions are present:

$$2Cl^- \rightarrow 2e^- + Cl_{2_{(g)}},\ E^0 = -1.360 \text{ V}$$

where the electrode potentials are the standard values at 25°C for 1-M solution of ions, and partial pressures of 1 atmosphere for the gaseous products. Values of E^0 can be corrected for nonstandard conditions by the Nernst equation

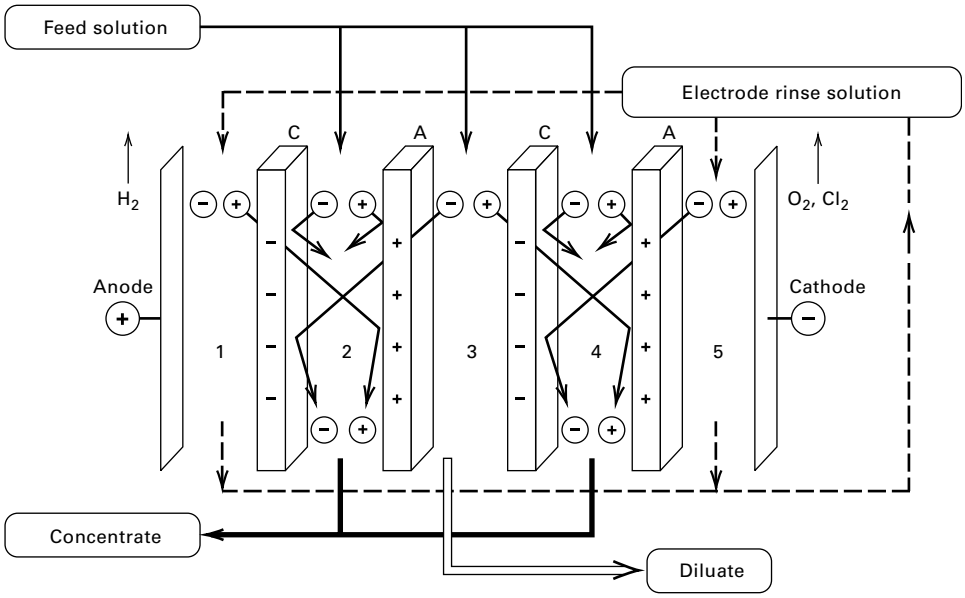

Figure 14.17 Schematic diagram of the electrodialysis process. C, cation-transfer membrane; A, anion-transfer membrane.

[Adapted from W.S.W. Ho and K.K. Sirkar, Eds., *Membrane Handbook*, Van Nostrand Reinhold, New York (1992).]

[92]. The corresponding overall cell reactions are:

$$3H_2O \rightarrow H_{2_{(g)}} + \tfrac{1}{2}O_{2_{(g)}} + 2H^+ + 2OH^-$$

or

$$2H_2O + 2Cl^- \rightarrow 2OH^- + H_{2_{(g)}} + Cl_{2_{(g)}}, E^0_{\text{cell}} = -2.058\ \text{V}$$

The net reaction for the first case is

$$H_2O \rightarrow H_{2_{(g)}} + \frac{1}{2}O_{2_{(g)}}, E^0_{\text{cell}} = -2.188\ \text{V}$$

The electrode rinse solution that circulates through compartments 1 and 5 is typically acidic to neutralize the OH ions formed in compartment 1 and prevent precipitation of compounds such as $CaCO_3$ and $Mg(OH)_2$.

The most widely used ion-exchange membranes for electrodialysis, first reported by Juda and McRae [35] in 1950, are: (1) cation-selective membranes containing negatively charged groups fixed to a polymer matrix, and (2) anion-selective membranes containing positively charged groups fixed to a polymer matrix. The former, shown schematically in Figure 14.18, includes fixed anions, mobile cations (called counterions), and mobile anions (called co-ions). The latter are almost completely excluded from the polymer matrix by

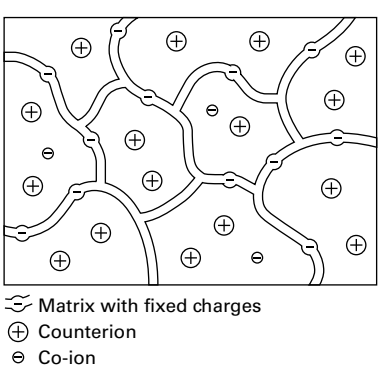

Figure 14.18 Cation-exchange membrane.

[From H. Strathmann, *Sep. and Purif. Methods*, **14** (1), 41–66 (1985) with permission.]

electrical repulsion, called the Donnan effect. For perfect exclusion, only cations are transferred through the membrane. In practice, the exclusion is better than 90%.

A cation-selective membrane may be made of polystyrene cross-linked with divinylbenzene and sulfonated to produce fixed sulfonate, $-SO_3^-$, anion groups. An anion-selective membrane of the same polymer contains quaternary ammonium groups such as $-NH_3^+$. Membranes are 0.2–0.5 mm thick and are reinforced for mechanical stability. The membranes are flat sheets, containing 30 to 50% water and have a network of pores too small to permit water transport.

A cell pair or unit cell contains one cation-selective membrane and one anion-selective membrane. A commercial electrodialysis system consists of a large stack of membranes in a plate-and-frame configuration, which, according to Applegate [2] and the *Membrane Handbook* [6], contains 100 to 600 cell pairs. In a stack, membranes of 0.4 to 1.5 m^2 surface area are separated by 0.5 to 2 mm with spacer gaskets. The total voltage or electrical potential applied across the cell includes: (1) the electrode potentials, (2) overvoltages due to gas formation at the two electrodes, (3) the voltage required to overcome the ohmic resistance of the electrolyte in each compartment, (4) the voltage required to overcome the resistance in each membrane, and (5) the voltage required to overcome concentration-polarization effects in the electrolyte solutions adjacent to the membrane surface. For large stacks, the latter three voltage increments predominate and depend upon the current density (amps flowing through the stack per unit surface area of membranes). A typical voltage drop across a cell pair is 0.5–1.5 V. Current densities are in the range of 5–50 mA/cm^2. Thus, a stack of 400 membranes (200 unit cells) of 1 m^2 surface area each might require 200 V at 100 A. Typically 50 to 90% of brackish water is converted to water, depending on concentrate recycle. As the current density is increased for a given membrane surface area, the concentration-polarization effect increases. Figure 14.19 is a schematic of this effect for a cation-selective membrane, where c_m refers to cation concentration in the membrane, c_b refers to bulk electrolyte cation concentration, and

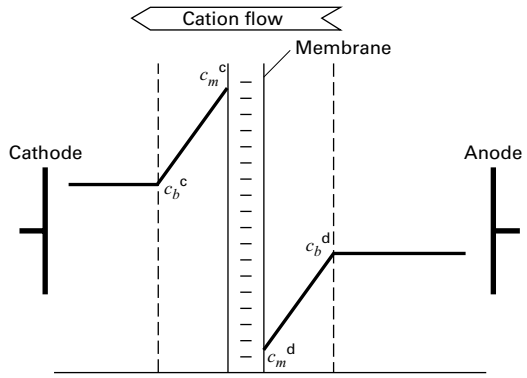

Figure 14.19 Concentration-polarization effects for a cation-exchange membrane.

[From H. Strathmann, *Sep. and Purif. Methods*, **14** (1), 41–66 (1985) with permission.]

superscripts c and d refer to concentrate side and dilute side. The maximum or limiting current density occurs when c_m^d reaches zero. Typically, an electrodialysis cell is operated at 80% of the limiting current density, which is determined by experiment, as is the corresponding cell voltage or resistance.

The gases formed at the electrodes at the ends of the stack are governed by *Faraday's law of electrolysis*. One Faraday (96,520 coulombs) of electricity reduces at the cathode and oxidizes at the anode an equivalent of oxidizing and reducing agent corresponding to the transfer of 6.023×10^{23} (Avogadro's number) electrons through wiring from the anode to the cathode. In general, it takes a large quantity of electricity to form appreciable quantities of gases in an electrodialysis process.

Of importance in design of an electrodialysis process are the membrane area and electrical-energy requirements, as discussed by Applegate [2] and Strathmann [36]. The membrane area is estimated from the current density, rather than from permeability and mass-transfer resistances, by applying Faraday's law:

$$A_M = \frac{FQ\Delta c}{i\xi} \tag{14-82}$$

where A_M = total area of all cell pairs, m^2; F = Faraday's constant (96,520 amp-s/equivalent); Q = volumetric flow rate of the diluate (potable water), m^3/s; Δc = difference between feed and diluate ion concentration in equivalents/m^3; i = current density, amps/m^2 of a cell pair, usually about 80% of i_{max}; and ξ = current efficiency <1.00.

The efficiency accounts for the fact that not all of the current is effective in transporting ions through the membranes. Inefficiencies are caused by a Donnan exclusion of less than 100%, some transfer of water through the membranes, current leakage through manifolds, etc. Power consumption is given by

$$P = IE \tag{14-83}$$

where P = power, W; I = electric current flow through the stack; and E = voltage across the stack. Electrical current is given by a rearrangement of (14-82),

$$I = \frac{FQ\Delta c}{n\xi} \tag{14-84}$$

where n is the number of cell pairs.

The main application of electrodialysis is to the desalinization of brackish water in the salt-concentration range of 500 to 5,000 ppm (mg/L). Below this range, ion exchange is more economical, whereas above this range, to 50,000 ppm, reverse osmosis is preferred. However, electrodialysis cannot produce water with a very low dissolved-solids content because of the high electrical resistance of dilute solutions. Other applications include recovery of nickel and copper from electroplating rinse water; deionization of cheese whey, fruit juices, wine, milk, and sugar molasses; separation of salts, acids, and bases from organic compounds; and recovery of organic compounds from their salts. Bipolar membranes, prepared by laminating a cation-selective membrane and an anion-selective membrane back-to-back, are used to produce H_2SO_4 and NaOH from a Na_2SO_4 solution.

EXAMPLE 14.10 Electrodialysis of Brackish Water.

Estimate membrane area and electrical-energy requirements for an electrodialysis process to reduce the salt (NaCl) content of 24,000 m^3/day of brackish water from 1,500 mg/L to 300 mg/L with a 50% conversion. Assume each membrane has a surface area of 0.5 m^2 and each stack contains 300 cell pairs. A reasonable current density is 5 mA/cm^2, and the current efficiency is 0.8 (80%).

Solution

Use (14-82) to estimate membrane area:

$$F = 96{,}520 \text{ A/equiv}$$

$$Q = (24{,}000)(0.5)/(24)(3{,}600) = 0.139 \text{ m}^3/\text{s}$$

$$\text{MW}_{\text{NaCl}} = 58.5,\ i = 5 \text{ mA/cm}^2 = 50 \text{ A/m}^2$$

$$\Delta c = (1{,}500 - 300)/58.5 = 20.5 \text{ mmol/L or } 20.5 \text{ mol/m}^3$$

$$= 20.5 \text{ equiv/m}^3$$

$$A_M = \frac{(1)(96{,}520)(0.139)(20.5)}{(50)(0.8)} = 6{,}876 \text{ m}^2$$

Each stack contains 300 cell pairs with a total area of 0.5(300) = 150 m^2. Therefore, the number of stacks = 6,876/150 = 46 in parallel. From (14-84), electrical current flow is given by

$$I = \frac{(96{,}500)(0.139)(20.5)}{(300)(0.8)}$$

$$= 1{,}146 \text{ A or } I/\text{stack} = 1{,}146/46 = 25 \text{ A/stack}$$

To obtain the electrical power, the average voltage drop across each cell pair is needed. Assume a value of 1 V. From (93) for 300 cell pairs:

$$P = (1{,}146)(1)(300) = 344{,}000 \text{ W} = 344 \text{ kW}$$

Additional energy is required to pump feed, recycle concentrate, and electrode rinse.

It is instructive to estimate the amount of feed that would be electrolyzed (as water to hydrogen and oxygen gases) at the electrodes. From the half-cell reactions presented earlier, half a molecule of H_2O is electrolyzed for each electron, or 0.5 mol H_2O is electrolyzed for each faraday of electricity.

$$1{,}146 \text{ amps} = 1{,}146 \text{ coulombs/s}$$

$$\text{or } (1{,}146)(3{,}600)(24) = 99{,}010{,}000 \text{ coulombs/day}$$

$$\text{or } 99{,}010{,}000/96{,}520 = 1{,}026 \text{ faradays/day}$$

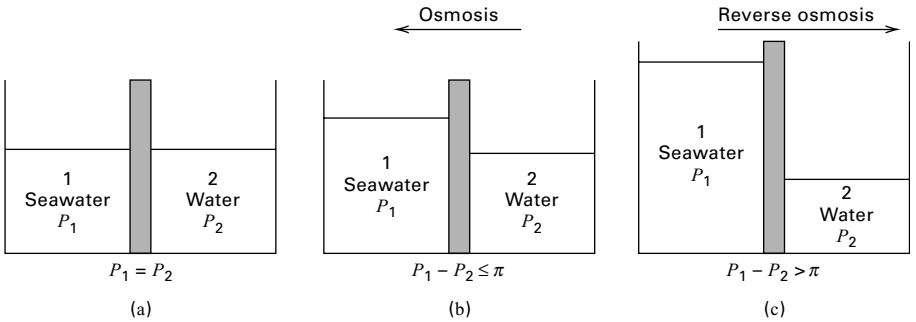

Figure 14.20 Osmosis and reverse-osmosis phenomena. (a) Initial condition. (b) At equilibrium after osmosis. (c) Reverse osmosis.

This electrolyzes (0.5)(1,026) = 513 mol/day of water. The feed rate is 12,000 m^3/day, or

$$\frac{(12{,}000)(10^6)}{18} = 6.7 \times 10^8 \text{ mol/day}$$

Therefore, the amount of water electrolyzed is negligible.

§14.6 REVERSE OSMOSIS

Osmosis, from the Greek word for "push," refers to passage of a solvent, such as water, through a membrane that is much more permeable to solvent (A) than to solute(s) (B) (e.g., inorganic ions). The first recorded account of osmosis was in 1748 by Nollet, whose experiments were conducted with water, an alcohol, and an animal-bladder membrane. Osmosis is illustrated in Figure 14.20, where all solutions are at 25°C. In the initial condition (a), seawater of approximately 3.5 wt% dissolved salts and at 101.3 kPa is in cell 1, while pure water at the same pressure is in cell 2. The dense membrane is permeable to water, but not to dissolved salts. By osmosis, water passes from cell 2 to the seawater in cell 1, causing dilution of the dissolved salts. At equilibrium, the condition of Figure 14.20b is reached, wherein some pure water still resides in cell 2 and seawater, less concentrated in salt, resides in cell 1. Pressure P_1, in cell 1, is now greater than pressure P_2, in cell 2, with the difference, π, referred to as the *osmotic pressure*.

Osmosis is not a useful separation process because the solvent is transferred in the wrong direction, resulting in mixing rather than separation. However, the direction of transport of solvent through the membrane can be reversed, as shown in Figure 14.20c, by applying a pressure, P_1, in cell 1, that is higher than the sum of the osmotic pressure and the pressure, P_2, in cell 2: that is, $P_1 - P_2 > \pi$. Now water in the seawater is transferred to the pure water, and the seawater becomes more concentrated in dissolved salts. This phenomenon, called *reverse osmosis*, is used to partially remove solvent from a solute–solvent mixture. An important factor in developing a reverse-osmosis separation process is the osmotic pressure, π, of the feed mixture, which is proportional to the solute concentration. For pure water, $\pi = 0$.

In reverse osmosis (RO), as shown in Figure 14.21, feed is a liquid at high pressure, P_1, containing solvent (e.g., water) and solubles (e.g., inorganic salts and, perhaps, colloidal matter). No sweep liquid is used, but the other side of the membrane is maintained at a much lower pressure, P_2. A dense membrane such as an acetate or aromatic polyamide, permselective for the solvent, is used. To withstand the large ΔP, the membrane must be thick. Accordingly, asymmetric or thin-wall composite membranes, having a thin, dense skin or layer on a thick, porous support, are needed. The products of reverse osmosis are a permeate of almost pure solvent and a retentate of solvent-depleted feed. A perfect separation between solvent and solute is not achieved, since only a fraction of the solvent is transferred to the permeate.

Reverse osmosis is used to desalinate and purify seawater, brackish water, and wastewater. Prior to 1980, multistage, flash distillation was the primary desalination process, but by 1990 this situation was dramatically reversed, making RO the dominant process for new construction. The dramatic shift from a thermally driven process to a more economical, pressure-driven process was made possible by Loeb and Sourirajan's [7] development of an asymmetric membrane that allows pressurized water to pass through at a high rate, while almost preventing transmembrane flows of dissolved salts, organic compounds, colloids, and microorganisms. Today more than 1,000 RO desalting plants are producing more than 750,000,000 gal/day of potable water.

According to Baker et al. [5], use of RO to desalinize water is accomplished mainly with spiral-wound and

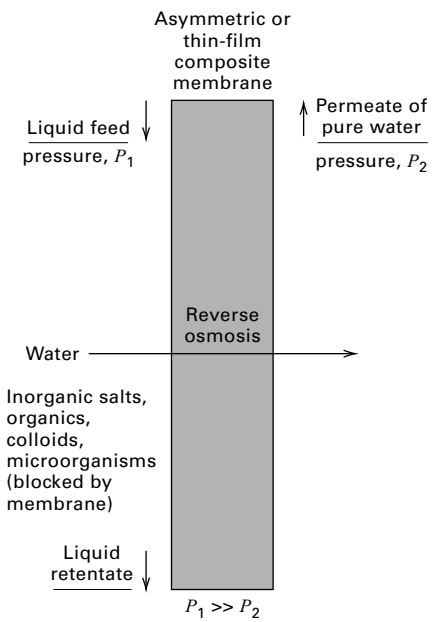

Figure 14.21 Reverse osmosis.

hollow-fiber membrane modules utilizing cellulose triacetate, cellulose diacetate, and aromatic polyamide membrane materials. Cellulose acetates are susceptible to biological attack, and to acidic or basic hydrolysis back to cellulose, making it necessary to chlorinate the feed water and control the pH to within 4.5–7.5. Polyamides are not susceptible to biological attack, and resist hydrolysis in the pH range of 4–11, but are attacked by chlorine.

The preferred membrane for the desalinization of seawater, which contains about 3.5 wt% dissolved salts and has an osmotic pressure of 350 psia, is a spiral-wound, multileaf module of polyamide, thin-film composite operating at a feed pressure of 800 to 1,000 psia. With a transmembrane water flux of 9 gal/ft^2-day (0.365 m^3/m^2-day), this module can recover 45% of the water at a purity of about 99.95 wt%. A typical module is 8 inches in diameter by 40 inches long, containing 365 ft^2 (33.9 m^2) of membrane surface. Such modules resist fouling by colloidal and particulate matter, but seawater must be treated with sodium bisulfate to remove oxygen and/or chlorine.

For desalinization of brackish water containing less than 0.5 wt% dissolved salts, hollow-fiber modules of high packing density, containing fibers of cellulose acetates or aromatic polyamides, are used if fouling is not serious. Because the osmotic pressure is much lower (<50 psi), feed pressures can be <250 psia and transmembrane fluxes may be as high as 20 gal/ft^2-day.

Other uses of reverse osmosis, usually on a smaller scale than the desalinization of water, include: (1) treatment of industrial wastewater to remove heavy-metal ions, nonbiodegradable substances, and other components of possible commercial value; (2) treatment of rinse water from electroplating processes to obtain a metal-ion concentrate and a permeate that can be reused as a rinse; (3) separation of sulfites and bisulfites from effluents in pulp and paper processes; (4) treatment of wastewater in dyeing processes; (5) recovery of constituents having food value from wastewaters in food-processing plants (e.g., lactose, lactic acid, sugars, and starches); (6) treatment of municipal water to remove inorganic salts, low-molecular-weight organic compounds, viruses, and bacteria; (7) dewatering of certain food products such as coffee, soups, tea, milk, orange juice, and tomato juice; and (8) concentration of amino acids and alkaloids. In such applications, membranes must have chemical, mechanical, and thermal stability to be competitive with other processes.

As with all membrane processes where feed is a liquid, three resistances to mass transfer must be considered: the membrane resistance and the two fluid-film or boundary-layer resistances on either side of the membrane. If the permeate is pure solvent, then there is no film resistance on that side of the membrane.

Although the driving force for water transport is the concentration or activity difference in and across the membrane, common practice is to use a driving force based on osmotic pressure. Consider the reverse-osmosis process of Figure 14.20c. At thermodynamic equilibrium, solvent chemical potentials or fugacities on the two sides of the membrane must be equal. Thus,

$$f_A^{(1)} = f_A^{(2)} \tag{14-85}$$

From definitions in Table 2.2, rewrite (14-85) in terms of activities:

$$a_A^{(1)} f_A^0\{T, P_1\} = a_A^{(2)} f_A^0\{T, P_2\} \tag{14-86}$$

For pure solvent, A, $a_A^{(2)} = 1$. For seawater, $a_A^{(1)} = x_A^{(1)}\gamma_A^{(1)}$. Substitution into (14-86) gives

$$f_A^0\{T, P_2\} = x_A^{(1)}\gamma_A^{(1)} f_A^0\{T, P_1\} \tag{14-87}$$

Standard-state, pure-component fugacities f^0 increase with increasing pressure. Thus, if $x_A^{(1)}\gamma_A^{(1)} < 1$, then from (14-87), $P_1 > P_2$. The pressure difference $P_1 - P_2$ is shown as a hydrostatic head in Figure 14.20b. It can be observed experimentally, and is defined as the osmotic pressure, π.

To relate π to solvent or solute concentration, the Poynting correction of (2-28) is applied. For an incompressible liquid of specific volume, υ_A,

$$f_A^0\{T, P_2\} = f_A^0\{T, P_1\} \exp\left[\frac{\upsilon_{A_L}(P_2 - P_1)}{RT}\right] \tag{14-88}$$

Substitution of (14-87) into (14-88) gives

$$\boxed{\pi = P_1 - P_2 = -\frac{RT}{\upsilon_{A_L}} \ln\left(x_A^{(1)}\gamma_A^{(1)}\right)} \tag{14-89}$$

Thus, osmotic pressure replaces activity as a thermodynamic variable.

For a mixture on the feed or retentate side of the membrane that is dilute in the solute, $\gamma_A^{(1)} = 1$. Also, $x_A^{(1)} = 1 - x_B^{(1)}$ and $\ln\left(1 - x_B^{(1)}\right) \approx -x_B^{(1)}$. Substitution into (14-89) gives

$$\pi = P_1 - P_2 = RT\, x_B^{(1)}/\upsilon_{A_L} \tag{14-90}$$

Finally, since $x_B^{(1)} \approx n_B/n_A, n_A\upsilon_{A_L} = V$, and $n_B/V = c_B$, (14-100) becomes

$$\boxed{\pi \approx RTc_B} \tag{14-91}$$

which was used in Exercise 1.8. For seawater, Applegate [2] suggests the approximate expression

$$\pi = 1.12T \sum \bar{m}_i \tag{14-92}$$

where π is in psia, T is in K, and $\sum \bar{m}_i$ is the summation of molarities of dissolved ions and nonionic species in the solution in mol/L. More exact expressions for π are those of Stoughton and Lietzke [38].

In the general case, when there are solutes on each side of the membrane, at equilibrium $(P_1 - \pi_1) = (P_2 - \pi_2)$. Accordingly, as discussed by Merten [37], the driving force for solvent transport through the membrane is $\Delta P - \Delta\pi$, and the rate of mass transport is

$$\boxed{N_{H_2O} = \frac{P_{M_{H_2O}}}{l_M}(\Delta P - \Delta\pi)} \tag{14-93}$$

where ΔP = hydraulic pressure difference across the membrane = $P_{\text{feed}} - P_{\text{permeate}}$, and $\Delta\pi$ = osmotic pressure difference across the membrane = $\pi_{\text{feed}} - \pi_{\text{permeate}}$.

If the permeate is almost pure solvent, $\pi_{\text{permeate}} \approx 0$.

The flux of solute (e.g., salt) is given by (14-49) in terms of membrane concentrations, and is independent of ΔP across the membrane. Accordingly, the higher the ΔP, the

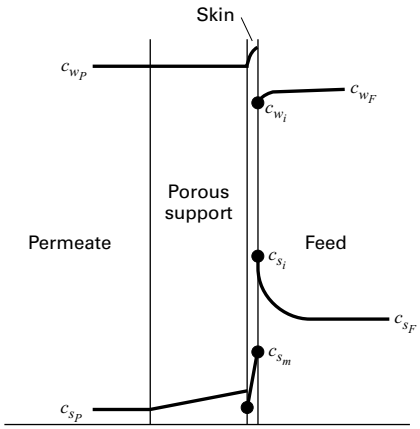

Figure 14.22 Concentration-polarization effects in reverse osmosis.

purer the permeate water. Alternatively, the flux of salt may be conveniently expressed in terms of *salt passage*, *SP*,

$$SP = (c_{\text{salt}})_{\text{permeate}}/(c_{\text{salt}})_{\text{feed}} \qquad (14\text{-}94)$$

Values of *SP* decrease with increasing ΔP. *Salt rejection* is given by $SR = 1 - SP$.

For brackish water of 1,500 mg/L NaCl, at 25°C, (14-92) predicts $\pi = 17.1$ psia. For seawater of 35,000 mg/L NaCl, at 25°C, (14-92) predicts $\pi = 385$ psia, while Stoughton and Lietzke [38] give 368 psia. From (14-93), ΔP must be $> \Delta\pi$ for reverse osmosis to occur. For desalination of brackish water by RO, ΔP is typically 400–600 psi, while for seawater, it is 800–1,000 psi.

The feed water to an RO unit contains potential foulants, which must be removed prior to passage through the membrane unit; otherwise, performance and membrane life are reduced. Suspended solids and particulate matter are removed by screening and filtration. Colloids are flocculated and filtered. Scale-forming salts require acidification or water softening, and biological materials require chlorination or ozonation. Other organic foulants are removed by adsorption or oxidation.

Concentration polarization is important on the feed side of RO membranes and is illustrated in Figure 14.22, where concentrations are shown for water, c_w, and salt, c_s. Because of the high pressure, activity of water on the feed side is somewhat higher than that of near-pure water on the permeate side, thus providing the driving force for water transport through the membrane. The flux of water to the membrane carries with it salt by bulk flow, but because the salt cannot readily penetrate the membrane, salt concentration adjacent to the surface of the membrane, c_{s_i}, is $> c_{s_F}$. This difference causes mass transfer of salt by diffusion from the membrane surface back to the bulk feed. The back rate of salt diffusion depends on the mass-transfer coefficient for the boundary layer (or film) on the feed side. The lower the mass-transfer coefficient, the higher the value of c_{s_i}. The value of c_{s_i} is important because it fixes the osmotic pressure, and influences the driving force for water transport according to (14-93).

Consider steady-state transport of water with back-diffusion of salt. A salt balance at the upstream membrane surface gives

$$N_{\text{H}_2\text{O}} c_{s_F}(SR) = k_s(c_{s_i} - c_{s_F})$$

Solving for c_{s_i} gives

$$c_{s_i} = c_{s_F}\left(1 + \frac{N_{\text{H}_2\text{O}}(SR)}{k_s}\right) \qquad (14\text{-}95)$$

Values of k_s are estimated from (14-78). The concentration-polarization effect is seen to be most significant for high water fluxes and low mass-transfer coefficients.

A quantitative estimate of the importance of concentration polarization is derived by defining the concentration-polarization factor, Γ, by a rearrangement of the previous equation:

$$\Gamma \equiv \frac{c_{s_i} - c_{s_F}}{c_{s_F}} = \frac{N_{\text{H}_2\text{O}}(SR)}{k_s} \qquad (14\text{-}96)$$

Values of *SR* are in the range of 0.97–0.995. If $\Gamma >$, say, 0.2, concentration polarization may be significant, indicating a need for design changes to reduce Γ.

Feed-side pressure drop is also important because it causes a reduction in the driving force for water transport. Because of the complex geometries used for both spiral-wound and hollow-fiber modules, it is best to estimate pressure drops from experimental data. Feed-side pressure drops for spiral-wound modules and hollow-fiber modules range from 43 to 85 and 1.4 to 4.3 psi, respectively [6].

A schematic diagram of a reverse-osmosis process for desalination of water is shown in Figure 14.23. The source of feed water may be a well or surface water, which is pumped

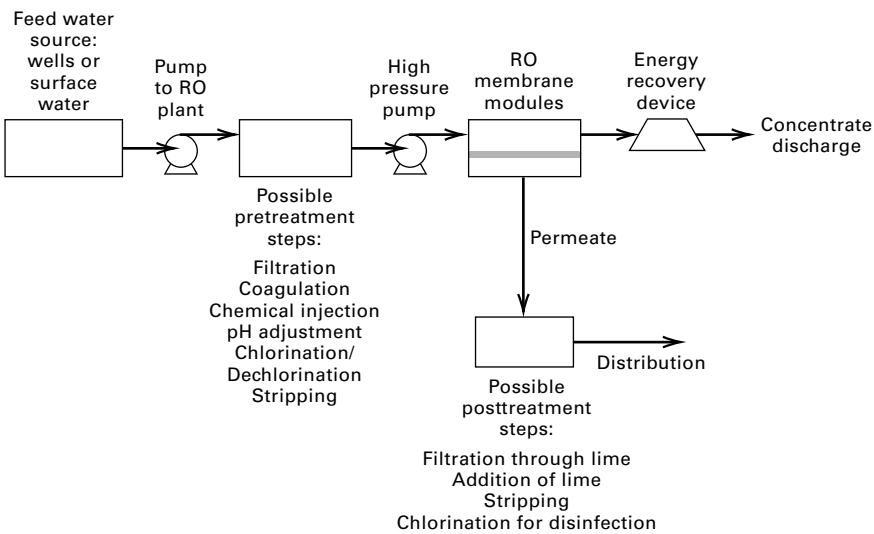

Figure 14.23 Reverse-osmosis process.

through a series of pretreatment steps to ensure a long membrane life. Of particular importance is pH adjustment. The pretreated water is fed by a high-pressure discharge pump to a parallel-and-series network of reverse-osmosis modules. The concentrate, which leaves the membrane system at a high pressure that is 10–15% lower than the inlet pressure, is then routed through a power-recovery turbine, which reduces the net power consumption by 25–40%. The permeate, which may be 99.95 wt% pure water and about 50% of the feed water, is sent to a series of post-treatment steps to make it drinkable.

EXAMPLE 14.11 Polarization Factor in Reverse Osmosis.

At a certain point in a spiral-wound membrane, the bulk conditions on the feed side are 1.8 wt% NaCl, 25°C, and 1,000 psia, while bulk conditions on the permeate side are 0.05 wt% NaCl, 25°C, and 50 psia. For this membrane the permeance values are 1.1×10^{-5} g/cm^2-s-atm for H_2O and 16×10^{-6} cm/s for the salt. If mass-transfer resistances are negligible, calculate the flux of water in gal/ft^2-day and the flux of salt in g/ft^2-day. If $k_s = 0.005$ cm/s, estimate the polarization factor.

Solution

Bulk salt concentrations are

$$c_{S_F} = \frac{1.8(1{,}000)}{58.5(98.2)} = 0.313 \text{ mol/L on feed side}$$

$$c_{S_P} = \frac{0.05(1{,}000)}{58.5(99.95)} = 0.00855 \text{ mol/L on permeate side}$$

For water transport, using (14-92) for osmotic pressure and noting that dissolved NaCl gives 2 ions per molecule:

$$\Delta P = (1{,}000 - 50)/14.7 = 64.6 \text{ atm}$$

$$\pi_{\text{feedside}} = 1.12(298)(2)(0.313) = 209 \text{ psia} = 14.2 \text{ atm}$$

$$\pi_{\text{permeate side}} = 1.12(298)(2)(0.00855) = 5.7 \text{ psia} = 0.4 \text{ atm}$$

$$\Delta P - \Delta\pi = 64.6 - (14.2 - 0.4) = 50.8 \text{ atm}$$

$$P_{M_{H_2O}}/l_M = 1.1 \times 10^{-5} \text{ g/cm}^2\text{-s-atm}$$

From (14-93),

$$N_{H_2O} = \left(1.1 \times 10^{-5}\right)(50.8) = 0.000559 \text{ g/cm}^2\text{-s} \quad \text{or}$$

$$\frac{(0.000559)(3{,}600)(24)}{(454)(8.33)\left(1.076 \times 10^{-3}\right)} = 11.9 \text{ gal/ft}^2\text{-day}$$

For salt transport:

$$\Delta c = 0.313 - 0.00855 = 0.304 \text{ mol/L} \quad \text{or} \quad 0.000304 \text{ mol/cm}^3$$

$$P_{M_{NaCl}}/l_M = 16 \times 10^{-6} \text{ cm/s}$$

From (14-49):

$$\text{or} \quad N_{NaCl} = 16 \times 10^{-6}(0.000304) = 4.86 \times 10^{-9} \text{ mol/cm}^2\text{-s}$$

$$\frac{\left(4.86 \times 10^{-9}\right)(3{,}600)(24)(58.5)}{1.076 \times 10^{-3}} = 22.8 \text{ g/ft}^2\text{-day}$$

The flux of salt is much smaller than the flux of water.

To estimate the concentration-polarization factor, first convert the water flux through the membrane into the same units as the salt mass-transfer coefficient, k_s, i.e., cm/s:

$$N_{H_2O} = \frac{0.000559}{1.00} = 0.000559 \text{ cm/s}$$

From (14-94), the salt passage is

$$SP = 0.00855/0.313 = 0.027$$

Therefore, the salt rejection $= SR = 1 - 0.027 = 0.973$.

From (14-96), the concentration-polarization factor is

$$\Gamma = \frac{0.000559(0.972)}{0.005} = 0.11$$

Here polarization is not particularly significant.

§14.7 GAS PERMEATION

Figure 14.24 shows gas permeation (GP) through a thin film, where feed gas, at high pressure P_1, contains some low-molecular-weight species (MW $<$ 50) to be separated from small amounts of higher-molecular-weight species. Usually a sweep gas is not needed, but the other side of the membrane is maintained at a much lower pressure, P_2, often near-ambient to provide an adequate driving force. The membrane, often dense but sometimes microporous, is permselective for the low-molecular-weight species A. If the membrane is dense, these species are absorbed at the surface and then transported through the membrane by one or more mechanisms. Then, permselectivity depends on both membrane absorption and transport rate. Mechanisms are formulated in terms of a partial-pressure or fugacity driving force using the solution-diffusion model of (14-55). The products are a permeate enriched in A and a retentate enriched in B. A near-perfect separation is generally not achievable. If the membrane is microporous, pore size is extremely important because it is necessary to block the passage of species B. Otherwise, unless molecular weights of A and B differ appreciably, only a very modest separation is achievable, as was discussed in connection with Knudsen diffusion, (14-45).

Since the early 1980s, applications of GP with dense polymeric membranes have increased dramatically. Major applications include: (1) separation of hydrogen from methane; (2) adjustment of H_2-to-CO ratio in synthesis gas; (3) O_2 enrichment of air; (4) N_2 enrichment of air; (5) removal of

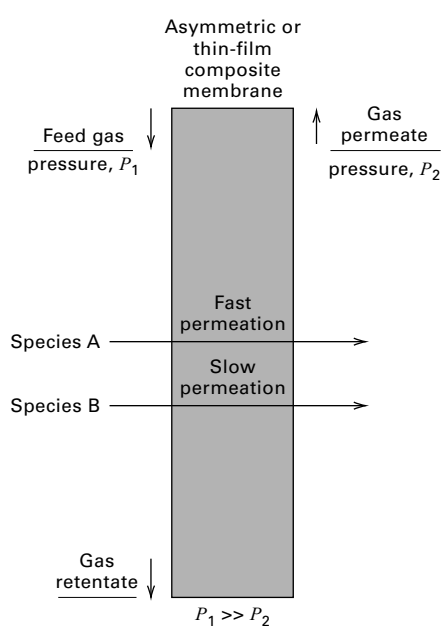

Figure 14.24 Gas permeation.

CO_2; (6) drying of natural gas and air; (7) removal of helium; and (8) removal of organic solvents from air.

Gas permeation competes with absorption, pressure-swing adsorption, and cryogenic distillation. Advantages of gas permeation, as cited by Spillman and Sherwin [39], are low capital investment, ease of installation, ease of operation, absence of rotating parts, high process flexibility, low weight and space requirements, and low environmental impact. In addition, if the feed gas is already high pressure, a gas compressor is not needed, and thus no utilities are required.

Since 1986, the most rapidly developing application for GP has been air separation, for which available membranes have separation factors for O_2 with respect to N_2 of 3 to 7. However, product purities are economically limited to a retentate of 95–99.9% N_2 and a permeate of 30–45% O_2.

Gas permeation also competes favorably for H_2 recovery because of high separation factors. The rate of permeation of H_2 through a dense polymer membrane is more than 30 times that for N_2. GP can achieve a 95% recovery of 90% pure H_2 from a feed gas containing 60% H_2.

Early applications of GP used nonporous membranes of cellulose acetates and polysulfones, which are still predominant, although polyimides, polyamides, polycarbonates, polyetherimides, sulfonated polysulfones, Teflon, polystyrene, and silicone rubber are also finding applications for temperatures to at least 70°C.

Although plate-and-frame and tubular modules can be used for gas permeation, almost all large-scale applications use spiral-wound or hollow-fiber modules because of their higher packing density. Commercial membrane modules for gas permeation are available from many suppliers. Feed-side pressure is typically 300 to 500 psia, but can be as high as 1,650 psia. Typical refinery applications involve feed-gas flow rates of 20 million scfd, but flow rates as large as 300 million scfd have been reported [40]. When the feed contains condensables, it may be necessary to preheat the feed gas to prevent condensation as the retentate becomes richer in the high-molecular-weight species. For high-temperature applications where polymers cannot be used, membranes of glass, carbon, and inorganic oxides are available, but are limited in their selectivity.

For dense membranes, external mass-transfer resistances or concentration-polarization effects are generally negligible, and (14-55) with a partial-pressure driving force can be used to compute the rate of membrane transport. As discussed in §14.3.5 on module flow patterns, the appropriate partial-pressure driving force depends on the flow pattern. Cascades are used to increase degree of separation.

Progress is being made in the prediction of permeability of gases in glassy and rubbery homopolymers, random copolymers, and block copolymers. Teplyakov and Meares [41] present correlations at 25°C for the diffusion coefficient, D, and solubility, S, applied to 23 different gases for 30 different polymers. Predicted values for glassy polyvinyltrimethylsilane (PVTMS) and rubbery polyisoprene are listed in Table 14.10. D and S values agree with data to within ±20% and ±30%, respectively.

Gas-permeation separators are claimed to be relatively insensitive to changes in feed flow rate, feed composition, and loss of membrane surface area [42]. This claim is tested in the following example.

Table 14.10 Predicted Values of Diffusivity and Solubility of Light Gases in a Glassy and a Rubbery Polymer

Permeant	$D \times 10^{11}$, m^2/s	$S \times 10^4$, gmol/m^3-Pa	P_M, barrer
Polyvinyltrimethylsilane (Glassy Polymer)			
He	470	0.18	250
Ne	87	0.26	66
Ar	5.1	1.95	30
Kr	1.5	6.22	29
Xe	0.29	20.6	18
Rn	0.07	69.6	15
H_2	160	0.54	250
O_2	7.6	1.58	37
N_2	3.8	0.84	9
CO_2	4.0	13.6	160
CO	3.7	1.28	14
CH_4	1.9	3.93	22
C_2H_6	0.12	30.2	10
C_3H_8	0.01	98.1	2.8
C_4H_{10}	0.001	347	1.2
C_2H_4	0.23	17.8	12
C_3H_6	0.038	77.6	9
C_4H_8	0.0052	293	4.5
C_2H_2	0.58	16.8	32
C_3H_4 (m)	0.17	138.1	70
C_4H_6 (e)	0.053	318.5	50
C_3H_4 (a)	0.15	186.5	83
C_4H_6 (b)	0.03	226.1	20
Polyisoprene (Rubber-like Polymer)			
He	213	0.06	35
Ne	77.4	0.08	18
Ar	14.6	0.58	25
Kr	7.2	1.78	25
Xe	2.7	5.68	45
Rn	1.2	18.7	64
H_2	109	0.17	54
O_2	18.4	0.47	26
N_2	12.2	0.26	10
CO_2	12.6	3.80	140
CO	12.1	0.38	14
CH_4	8.0	1.14	27
C_2H_6	3.3	8.13	79
C_3H_8	1.6	25.4	123
C_4H_{10}	1.5	86.4	390
C_2H_4	4.3	4.84	62
C_3H_6	2.7	20.3	163
C_4H_8	1.5	73.3	333
C_2H_2	5.7	4.64	80
C_3H_4 (m)	4.1	35.3	433
C_4H_6 (e)	2.9	79.6	690
C_3H_4 (a)	4.5	47.4	640
C_4H_6 (b)	3.4	40.0	410

Note: m, methylacetylene; e, ethylacetylene; a, allene; b, butadiene.

EXAMPLE 14.12 Recovery of H_2 Permeation.

The feed to a membrane separator consists of 500 lbmol/h of a mixture of 90% H_2 (H) and 10% CH_4 (M) at 500 psia. Permeance values based on a partial-pressure driving force are

$$\bar{P}_{M_H} = 3.43 \times 10^{-4} \text{ lbmol/h-ft}^2\text{-psi}$$
$$\bar{P}_{M_M} = 5.55 \times 10^{-5} \text{ lbmol/h-ft}^2\text{-psi}$$

The flow patterns in the separator are such that the permeate side is well mixed and the feed side is in plug flow. The pressure on the permeate side is constant at 20 psia, and there is no feed-retentate pressure drop. (a) Compute the membrane area and permeate purity if 90% of the hydrogen is transferred to the permeate. (b) For the membrane area determined in part (a), calculate the permeate purity and hydrogen recovery if: (1) the feed rate is increased by 10%, (2) the feed composition is reduced to 85% H_2, and (3) 25% of the membrane area becomes inoperative.

Solution

The following independent equations apply to all parts of this example. Component material balances:

$$n_{i_F} = n_{i_R} + n_{i_P}, \quad i = \text{H, M} \qquad (1,2)$$

Dalton's law of partial pressures:

$$P_k = p_{\text{H}_k} + p_{\text{M}_k}, \quad k = F, R, P \qquad (3,4,5)$$

Partial-pressure–mole relations:

$$p_{\text{H}_k} = P_k n_{\text{H}_k}/(n_{\text{H}_k} + n_{\text{M}_k}), \quad k = F, R, P \qquad (6,7,8)$$

Solution-diffusion transport rates are obtained using (14-55), assuming a log-mean partial-pressure driving force based on the exiting permeate partial pressures on the downstream side of the membrane because of the assumption of perfect mixing.

$$n_{i_P} = \bar{P}_{M_i} A_M \left[\frac{p_{i_F} - p_{i_R}}{\ln\left(\dfrac{p_{i_F} - p_{i_P}}{p_{i_R} - p_{i_P}}\right)} \right], \quad i = \text{H, M} \qquad (9,10)$$

Thus, a system of 10 equations has the following 18 variables:

$$\begin{array}{cccccc} A_M & n_{\text{H}_F} & n_{\text{M}_F} & P_F & P_R & P_P \\ \bar{P}_{M_H} & n_{\text{H}_R} & n_{\text{M}_R} & p_{\text{H}_F} & p_{\text{H}_R} & p_{\text{H}_P} \\ \bar{P}_{M_M} & n_{\text{H}_P} & n_{\text{M}_P} & p_{\text{M}_F} & p_{\text{M}_R} & p_{\text{M}_P} \end{array}$$

To solve the equations, eight variables must be fixed. For all parts of this example, the following five variables are fixed:

$\bar{P}_{M_H}$ and P_{M_M} given above

$P_F = 500$ psia $\quad P_R = 500$ psia $\quad P_P = 20$ psia

For each part, three additional variables must be fixed.

(a)

$$n_{\text{H}_F} = 0.9(500) = 450 \text{ lbmol/h}$$
$$n_{\text{M}_F} = 0.1(500) = 50 \text{ lbmol/h}$$
$$n_{\text{H}_P} = 0.9(450) = 405 \text{ lbmol/h}$$

Solving Equations (1)–(10) above, using a program such as MathCad, Matlab, or Polymath,

$A_M = 3.370 \text{ ft}^2$

$n_{\text{M}_P} = 20.0$ lbmol/h $\quad n_{\text{H}_R} = 45.0$ lbmol/h $\quad n_{\text{M}_R} = 30.0$ lbmol/h

$p_{\text{H}_F} = 450$ psia $\quad p_{\text{M}_F} = 50$ psia $\quad p_{\text{H}_R} = 300$ psia

$p_{\text{M}_R} = 200$ psia $\quad p_{\text{H}_P} = 19.06$ psia $\quad p_{\text{M}_P} = 0.94$ psia

(b) Calculations are made in a similar manner using Equations (1)–(10). Results for parts (1), (2), and (3) are:

	Part		
	(1)	(2)	(3)
Fixed:			
n_{H_F}, lbmol/h	495	425	450
n_{M_F}, lbmol/h	55	75	50
A_M, ft^2	3,370	3,370	2,528
Calculated, in lbmol/h:			
n_{H_P}	424.2	369.6	338.4
n_{M_P}	18.2	25.9	11.5
n_{H_R}	70.8	55.4	111.6
n_{M_R}	36.8	49.1	38.5
Calculated, in psia:			
p_{H_F}	450	425	450
p_{M_F}	50	75	50
p_{H_R}	329	265	372
p_{M_R}	171	235	128
p_{H_P}	19.18	18.69	19.34
p_{M_P}	0.82	1.31	0.66

From the above results:

	Part			
	(a)	(b1)	(b2)	(b3)
Mol% H_2 in permeate	95.3	95.9	93.5	96.7
% H_2 recovery in permeate	90	85.7	87.0	75.2

It is seen that when the feed rate is increased by 10% (Part b1), the H_2 recovery drops about 5%, but the permeate purity is maintained. When the feed composition is reduced from 90% to 85% H_2 (Part b2), H_2 recovery decreases by about 3% and permeate purity decreases by about 2%. With 25% of the membrane area inoperative (Part b3), H_2 recovery decreases by about 15%, but the permeate purity is about 1% higher. Overall, percentage changes in H_2 recovery and purity are less than the percentage changes in feed flow rate, feed composition, and membrane area, thus confirming the insensitivity of gas-permeation separators to changes in operating conditions.

§14.8 PERVAPORATION

Figure 14.25 depicts pervaporation (PV), which differs from dialysis, reverse osmosis, and gas permeation in that the phase on one side of the pervaporation membrane is different from that on the other. Feed to the membrane module is a liquid mixture at pressure P_1, which is high enough to maintain a liquid phase as the feed is depleted of species A and B to produce liquid retentate. A composite membrane is used that is selective for species A, but with some finite permeability for species B. The dense, thin-film side of the membrane is in contact with the liquid side. The retentate is enriched in species B. Generally, a sweep fluid is not used on the other

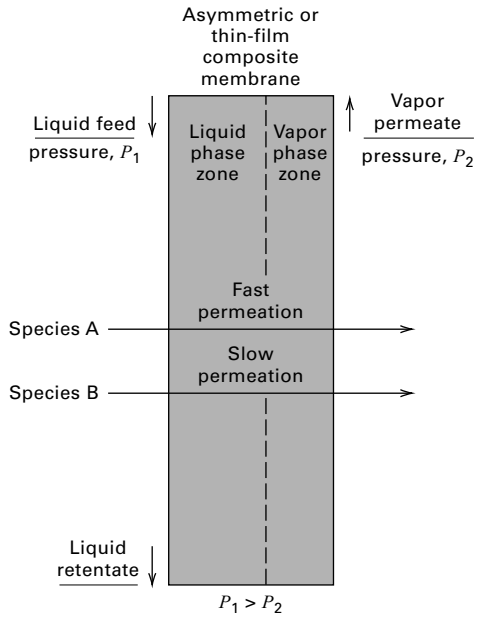

Figure 14.25 Pervaporation.

side of the membrane, but a pressure P_2, which may be a vacuum, is held at or below the dew point of the permeate, making it vapor. Vaporization may occur near the downstream face such that the membrane operates with two zones, a liquid-phase zone and a vapor-phase zone, as shown in Figure 14.25. Alternatively, the vapor phase may exist only on the permeate side of the membrane. The vapor permeate is enriched in species A. Overall permeabilities of species A and B depend on solubilities and diffusion rates. Generally, solubilities cause the membrane to swell.

The term *pervaporation* is a combination of the words "*per*mselective" and "e*vaporation*." It was first reported in 1917 by Kober [43], who studied several experimental techniques for removing water from albumin–toluene solutions. The economic potential of PV was shown by Binning et al. [44] in 1961, but commercial applications were delayed until the mid-1970s, when adequate membrane materials became available. Major commercial applications now include: (1) dehydration of ethanol; (2) dehydration of other organic alcohols, ketones, and esters; and (3) removal of organics from water. The separation of close-boiling organic mixtures like benzene–cyclohexane is receiving much attention.

Pervaporation is favored when the feed solution is dilute in the main permeant because sensible heat of the feed mixture provides the permeant enthalpy of vaporization. If the feed is rich in the main permeant, a number of membrane stages may be needed, with a small amount of permeant produced per stage and reheating of the retentate between stages. Even when only one membrane stage is sufficient, the feed liquid may be preheated.

Many pervaporation schemes have been proposed [6], with three important ones shown in Figure 14.26. A hybrid process for integrating distillation with pervaporation to produce 99.5 wt% ethanol from a feed of 60 wt% ethanol is shown in Figure 14.26a. Feed is sent to a distillation column operating at near-ambient pressure, where a bottoms product of nearly pure water and an ethanol-rich distillate of 95 wt% is produced. The distillate purity is limited by the 95.6 wt% ethanol–water azeotrope. The distillate is sent to a pervaporation unit, where a permeate of 25 wt% alcohol and a retentate of 99.5 wt% ethanol is produced. The permeate vapor is condensed under vacuum and recycled to the distillation column, the vacuum being sustained with a vacuum pump. The dramatic difference in separability by pervaporation as compared to vapor–liquid equilibrium for distillation is shown in Figure 14.27 from Wesslein et al. [45], with a 45° line for reference. For pervaporation, compositions refer to a liquid feed (abscissa) and a vapor permeate (ordinate) at 60°C for a polyvinylalcohol (PVA) membrane and a vacuum of 15 torr. There is no limitation on ethanol purity, and the separation index is high for feeds of > 90 wt% ethanol.

A pervaporation process for dehydrating dichloroethylene (DCE) is shown in Figure 14.26b. The liquid feed, which is DCE saturated with water (0.2 wt%), is preheated to 90°C at 0.7 atm and sent to a PVA membrane system, which produces a retentate of almost pure DCE (<10 ppm H_2O) and a permeate vapor of 50 wt% DCE. Following condensation, the two resulting liquid phases are separated, with the DCE-rich phase recycled and the water-rich phase sent to an air stripper, steam stripper, adsorption unit, or hydrophobic, pervaporation membrane system for residual DCE removal.

For removal of VOCs (e.g., toluene and trichloroethylene) from wastewater, pervaporation with hollow-fiber modules of silicone rubber can be used, as shown in Figure 14.23c. The retentate is almost pure water (<5 ppb of VOCs) and the permeate, after condensation, is (1) a water-rich phase that is recycled to the membrane system and (2) a nearly pure VOC phase.

A pervaporation module may operate with heat transfer or adiabatically, with the enthalpy of vaporization supplied by feed enthalpy. Consider the adiabatic pervaporation of a binary liquid mixture of A and B. Ignore heat of mixing. For an enthalpy datum temperature of T_0, an enthalpy balance—in terms of mass flow rates m, liquid sensible heats C_P, and heats of vaporization ΔH^{vap}—gives

$$\begin{aligned}&(m_{\text{A}_F}C_{P_\text{A}} + m_{\text{B}_F}C_{P_\text{B}})(T_F - T_0)\\ &= [(m_{\text{A}_F} - m_{\text{A}_P})C_{P_\text{A}} + (m_{\text{B}_F} - m_{\text{B}_P})C_{P_\text{B}}](T_R - T_0)\\ &\quad + (m_{\text{A}_P}C_{P_\text{A}} + m_{\text{B}_P}C_{P_\text{B}})(T_P - T_0) + m_{\text{A}_P}\Delta H^{\text{vap}}_{\text{A}}\\ &\quad + m_{\text{B}_P}\Delta H^{\text{vap}}_{\text{B}}\end{aligned} \tag{14-97}$$

where enthalpies of vaporization are evaluated at T_P. After collection of terms, (14-98) reduces to

$$\begin{aligned}&(m_{\text{A}_F}C_{P_\text{A}} + m_{\text{B}_F}C_{P_\text{B}})(T_F - T_R)\\ &= (m_{\text{A}_P}C_{P_\text{A}} + m_{\text{B}_P}C_{P_\text{B}}) \times (T_P - T_R)\\ &\quad + \left(m_{\text{A}_P}\Delta H^{\text{vap}}_{\text{A}} + m_{\text{B}_P}\Delta H^{\text{vap}}_{\text{B}}\right)\end{aligned} \tag{14-98}$$

Permeate temperature, T_P, is the dew point at the permeate vacuum upstream of the condenser. The retentate temperature is computed from (14-98).

Membrane selection is critical in the commercial application of PV. For water permeation, hydrophilic membrane materials are preferred. For example, a three-layer composite

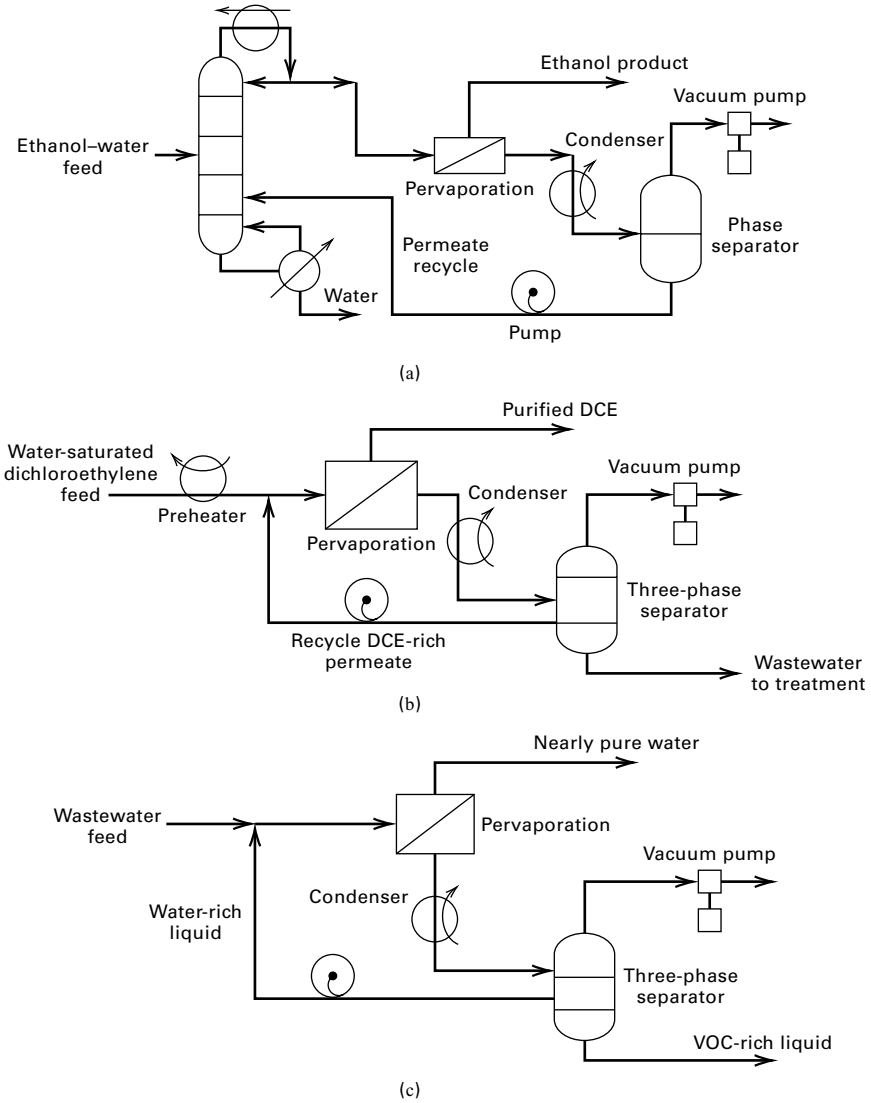

Figure 14.26 Pervaporation processes. (a) Hybrid process for removal of water from ethanol. (b) Dehydration of dichloroethylene. (c) Removal of volatile organic compounds (VOCs) from wastewater.

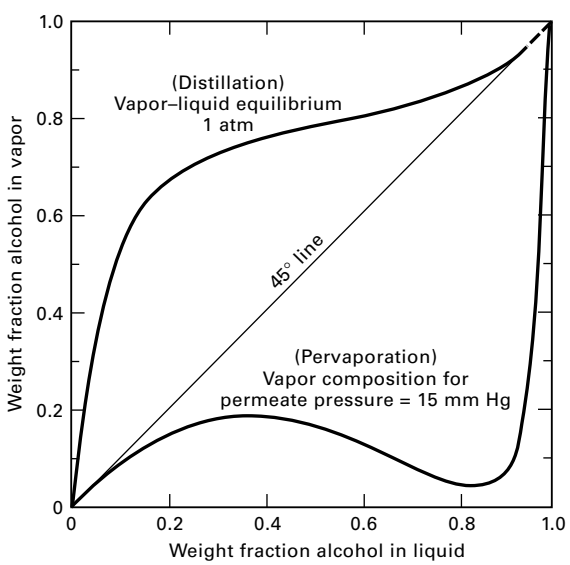

Figure 14.27 Comparison of ethanol–water separabilities. [From M. Wesslein et al., *J. Membrane Sci.*, **51**, 169 (1990).]

membrane is used for the dehydration of ethanol, with water being the main permeating species. The support layer is porous polyester, which is cast on a microporous polyacrylonitrile or polysulfone membrane. The final layer, which provides the separation, is dense PVA of 0.1 μm in thickness. This composite combines chemical and thermal stability with adequate permeability. Hydrophobic membranes, such as silicone rubber and Teflon, are preferred when organics are the permeating species.

Commercial membrane modules for PV are almost exclusively of the plate-and-frame type because of the ease of using gasketing materials that are resistant to organic solvents and the ease of providing heat exchange for vaporization and high-temperature operation. Hollow-fiber modules are used for removal of VOCs from wastewater. Because feeds are generally clean and operation is at low pressure, membrane fouling and damage is minimal, resulting in a useful membrane life of 2–4 years.

Models for transport of permeant through a membrane by pervaporation have been proposed, based on solution-diffusion (§14.3.4). They assume equilibrium between the upstream liquid and the upstream membrane surface, and

between the downstream vapor and its membrane side. Membrane transport follows Fick's law, with a permeant concentration gradient as the driving force. However, because of phase change and nonideal-solution feed, simple equations like (14-79) for dialysis and (14-55) for gas permeation do not apply.

A convenient PV model is that of Wijmans and Baker [46], who express the driving force for permeation in terms of a partial-vapor-pressure difference. Because pressures on both sides of the membrane are low, the gas phase follows the ideal-gas law. Therefore, at the upstream membrane surface (1), permeant activity for component i is

$$a_i^{(1)} = f_i^{(1)}/f_i^{(0)} = p_i^{(1)}/P_i^{s(1)} \tag{14-99}$$

where P_i^s is the vapor pressure at the feed temperature. Liquid on the upstream side of the membrane is generally nonideal. Thus, from Table 2.2:

$$a_i^{(1)} = \gamma_i^{(1)} x_i^{(1)} \tag{14-100}$$

Combining (14-99) and (14-100):

$$p_i^{(1)} = \gamma_i^{(1)} x_i^{(1)} P_i^{s(1)} \tag{14-101}$$

On the vapor side of the membrane (2), partial pressure is

$$p_i^{(2)} = y_i^{(2)} P_P^{(2)} \tag{14-102}$$

Thus, the driving force can be expressed as

$$\left(\gamma_i^{(1)} x_i^{(1)} P_i^{s(1)} - y_i^{(2)} P_P^{(2)}\right)$$

The corresponding permeant flux, after dropping unnecessary superscripts, is

$$\boxed{N_i = \frac{P_{M_i}}{l_M}\left(\gamma_i x_i P_i^s - y_i P_P\right)} \tag{14-103}$$

or

$$\boxed{N_i = \overline{P}_{M_i}\left(\gamma_i x_i P_i^s - y_i P_P\right)} \tag{14-104}$$

where γ_i and x_i refer to feed-side liquid, P_i^s is the vapor pressure at the feed-side temperature, y_i is the mole fraction in the permeant vapor, and P_P is total permeant pressure. Unlike gas permeation, where P_{M_i} depends mainly on permeant, polymer, and temperature, the permeability for pervaporation depends also on the concentrations of permeants in the polymer, which can be large enough to cause swelling and cross-diffusion. It is thus best to back-calculate and correlate permeant flux with feed composition at a given feed temperature and permeate pressure. Because of nonideal effects, selectivity can be a strong function of feed concentration and permeate pressure, causing inversion of selectivity, as illustrated next.

EXAMPLE 14.13 Pervaporation.

Wesslein et al. [45] present the following experimental data for the pervaporation of liquid mixtures of ethanol (1) and water (2) at a feed temperature of 60°C for a permeate pressure of 76 mmHg, using a commercial polyvinylalcohol membrane:

wt% Ethanol		Total Permeation Flux
Feed	Permeate	kg/m^2-h
8.8	10.0	2.48
17.0	16.5	2.43
26.8	21.5	2.18
36.4	23.0	1.73
49.0	22.5	1.46
60.2	17.5	0.92
68.8	13.0	0.58
75.8	9.0	0.40

At 60°C, vapor pressures are 352 and 149 mmHg for ethanol and water, respectively.

Liquid-phase activity coefficients at 60°C for the ethanol (1)–water (2) system are given by the van Laar equations (§2.6.5):

$$\ln \gamma_1 = 1.6276\left[\frac{0.9232x_2}{1.6276x_1 + 0.9232x_2}\right]^2$$

$$\ln \gamma_2 = 0.9232\left[\frac{1.6276x_1}{1.6276x_1 + 0.9232x_2}\right]^2$$

Calculate permeance for water and ethanol from (14-104).

Solution

For the first row of data, mole fractions in the feed (x_i) and permeate (y_i), with $MW_1 = 46.07$ and $MW_2 = 18.02$, are

$$x_1 = \frac{0.088/46.07}{\dfrac{0.088}{46.07} + \dfrac{(1.0 - 0.088)}{18.02}} = 0.0364$$

$$x_2 = 1.0 - 0.0364 = 0.9636$$

$$y_1 = \frac{0.10/46.07}{\dfrac{0.10}{46.07} + \dfrac{0.90}{18.02}} = 0.0416$$

$$y_2 = 1.0 - 0.0416 = 0.9584$$

Activity coefficients for the feed mixture are

$$\gamma_1 = \exp\left\{1.6276\left[\frac{0.9232(0.9636)}{1.6276(0.0364) + 0.9232(0.9636)}\right]^2\right\} = 4.182$$

$$\gamma_2 = \exp\left\{0.9232\left[\frac{1.6276(0.0364)}{1.6276(0.0364) + 0.9232(0.9636)}\right]^2\right\} = 1.004$$

From the total mass flux, component molar fluxes are

$$N_1 = \frac{(2.48)(0.10)}{46.07} = 0.00538\frac{\text{kmol}}{\text{h} - \text{m}^2}$$

$$N_2 = \frac{(2.48)(0.90)}{18.02} = 0.1239\frac{\text{kmol}}{\text{h} - \text{m}^2}$$

From (14-104), permeance values are

$$\bar{P}_{M_1} = \frac{0.00538}{(4.182)(0.0364)(352) - (0.0416)(76)}$$

$$= 0.000107\frac{\text{kmol}}{\text{h} - \text{m}^2 - \text{mmHg}}$$

$$\bar{P}_{M_2} = \frac{0.1239}{(2.004)(1.0 - 0.0364)(149) - (1.0 - 0.0416)(76)}$$

$$= 0.001739\frac{\text{kmol}}{\text{h} - \text{m}^2 - \text{mmHg}}$$

Results for other feed conditions are computed in a similar manner:

wt% Ethanol		Activity Coefficient in Feed		Permeance, kmol/h-m^2-mmHg	
Feed	Permeate	Ethanol	Water	Ethanol	Water
8.8	10.0	4.182	1.004	1.07×10^{-4}	1.74×10^{-3}
17.0	16.5	3.489	1.014	1.02×10^{-4}	1.62×10^{-3}
26.8	21.5	2.823	1.038	8.69×10^{-5}	1.43×10^{-3}
36.4	23.0	2.309	1.077	6.14×10^{-5}	1.17×10^{-3}
49.0	22.5	1.802	1.158	4.31×10^{-5}	1.10×10^{-3}
60.2	17.5	1.477	1.272	1.87×10^{-5}	8.61×10^{-4}
68.8	13.0	1.292	1.399	7.93×10^{-6}	6.98×10^{-4}
75.8	9.0	1.177	1.539	3.47×10^{-6}	6.75×10^{-4}

The PVA membrane is hydrophilic. As concentration of ethanol in the feed liquid increases, sorption of feed liquid by the membrane decreases, reducing polymer swelling. As swelling is reduced, the permeance of ethanol decreases more rapidly than that of water, thus increasing selectivity for water. For example, selectivity for water can be defined as

$$\alpha_{2.1} = \frac{(100 - w_1)_P/(w_1)_P}{(100 - w_1)_F/(w_1)_F}$$

where w_1 = weight fraction of ethanol. For cases of 8.8 and 75.8 wt% ethanol in the feed, the selectivities for water are, respectively, 0.868 (more selective for ethanol) and 31.7 (more selective for water).

§14.9 MEMBRANES IN BIOPROCESSING

Semipermeable membranes are widely used to selectively retain and/or permeate biological species based on relative size or solubility in a membrane phase. Membrane bioseparations are the subject of many reviews [50–54] and textbooks [55, 56]. Operations for bioproducts include reverse osmosis (RO), electrodialysis (ED), pervaporation (PV), microfiltration (MF), ultrafiltration (UF), nanofiltration (NF), and virus filtration (VF). Selection of a well-suited operation is guided by considering: (1) physical features of the biological species to be separated; (2) attributes of its matrix; (3) pore-size distribution and surface properties of the membrane; and (4) transport features of a particular operation. These determine species-specific *selectivity* of a membrane. Table 14.11 illustrates nominal membrane pore sizes and species diameters of some membrane bioprocesses and solutions.

Membrane installation and operating costs relate directly to selectivity, membrane *capacity* (volume of feed processed per unit of *surface area* before regeneration or replacement), and *permeate flux* (volumetric flow rate per unit area). Capacity and flux are optimized by reducing buildup of dissolved solids near the membrane wall (*concentration polarization*, CP) and preventing deposition of dissolved or suspended solutes on or in the membrane (*fouling*) [69].

Surface charges on suspended species, filter surfaces, and filter cake, as well as solution state (pH, ionic strength, temperature), all affect retention and resolution of targeted species. Operation is usually at or near physiological conditions to maintain biological activity. Solutions are buffered to pH 7.2 (37°C). Pressure-driving forces are $5 \leq \Delta P \leq 50$ psi. Temperatures are in the range $4 \leq T \leq 30$°C, with 4°C often selected to minimize protease or nuclease activity and growth of contaminant microorganisms.

Factors affecting selection of a membrane for bioseparation include selectivity, biocompatibility, chemical inertness, mechanical stability, and economics.

1. **Selectivity** (e.g., relative solute rejection). The membrane must retain active species and pass contaminants at targeted specifications. Table 14.12 lists sizes of some common solutes in biological streams.
2. **Biocompatibility.** The membrane should resist inactivation, plugging, and fouling by biological species or solution components. *Hydrophilic* membranes resist protein inactivation and fouling better than hydrophobic membranes. Examples of hydrophilic membranes include cellulose (cellulose acetate, regenerated

Table 14.11 Nominal Size in meters of Membrane Pores and Filtered Species in Membrane Bioprocesses

Size, m	10^{-10} (Å) RO	10^{-9} (nm) UF, NF	10^{-8} UF, VF	10^{-7} MF	10^{-6} (μm) MF	10^{-5} MF
Process water	water, salts, ions: monovalent	ions: divalent	colloids		bacteria	
Whole milk	lactose, salts		proteins	fats		casein micelles
Whole blood	salts	amino acids	peptides, proteins	platelets		erythrocytes
Cell culture broth	salts, glucose, vitamins, antibiotics	amino acids, lipids			bacteria	mammalian cells
Cell lysate			virus, proteins, organic macro molecules	virus	cell debris	

Adapted from [51].

Table 14.12 Sizes of Biological Solutes

	MW (dalton)		Diameter (nm)	
	lower	upper	lower	upper
yeast, fungi	-	-	1000.0	10000.0
human red blood cell	-	-	7000.0	8000.0
bacteria	-	-	300.0	1000.0
virus	-	2×10^8	20.0	300.0
protein, polysaccharide	10000	1×10^6	2.0	12.0
antibiotic	300	1000	0.6	1.2
mono-disaccharide	200	400	0.8	1.0
organic acid	100	500	0.4	0.8
inorganic acid	10	100	0.2	0.4
water	18	-	0.2	-

Adapted from [50].

cellulose, cellulose nitrate), polyamide, polyethersulfones (PES), borosilicate glass, or poly(vinylidene difluoride) (i.e., PVDF or Kynar®). *Hydrophobic* membranes are readily fouled by fatty acids, surfactants, and antifoams. They include polyethylene, polypropylene, polycarbonate, and polysulfones, which adsorb and denature proteins; and nonwetted poly(tetrafluoroethylene) (i.e., PTFE or Teflon®).

3. **Chemical inertness.** The membrane, filter housing, and associated glues, resins, potting agents, and adhesives must tolerate use and validatable cleaning and/or sterilization cycles without causing side reactions (e.g., denaturation) or producing significant leaching or *extractables*. Levels of leachables and extractables during operation and cleaning may be validated to be low (<1–10 μg/mL) by comparing NMR spectra of final bulks to profiles from model process streams. Filters for parenteral solutions (for injection or infusion) must comply with United States Pharmacopeia (USP) limits for extractables.
4. **Mechanical stability.** The membrane, its housing, and affiliated components must be able to withstand pressure and temperature ranges employed during use and validatable cleaning and/or sterilization cycles (including backflushing). Membrane housings typically consist of Type 304, 316, or 316L stainless steel that has been passivated and electropolished to ensure a measured roughness average (RA) < 20.
5. ***Economics.*** The filter operation and membrane consumables must reliably provide adequate filtrate flux (minimal concentration polarization) and capacity (minimal surface-area requirement) at reasonable operating conditions (minimal pressure drop to decrease energy consumption) over its use period when projected capital and consumable costs are compared with acceptable alternatives. This includes validatable cleanability and/or sterilizability and re-use, easy module replacement, rapid implementation and scale-up, and long-term vendor support.

§14.9.1 Membrane Operations in Bioprocess Purification Trains

Economic and reliable recovery of active biological product often employs a series of membrane filter operations to harvest cells, clarify debris, concentrate product, remove impurities, reduce bioburden to provide sterility, and exchange buffers. At each filtration step, purified bioproduct must be recovered and its activity preserved while satisfying current good manufacturing practice (cGMP) requirements. Table 14.13 gives a typical sequence of purification steps with corresponding membrane operations and comparable alternatives. Membrane biofiltration technology closely parallels filtration technology used by the chemical industry, as described in Chapter 19. The differences are that in the chemical industry, particles are much larger, woven cloths or metal screens rather than membranes are used as filters to retain the particles, and the hydrodynamics may be different (tangential flow, for example, is not used).

Initial *harvest* of cells can use MF, UF, or centrifugation to recover and concentrate cells from fermentation broth or culture media. This immediately reduces processing volume and associated costs. After harvest, intracellular bioproducts can be recovered from cells by *disruption* using shear, pressure, temperature, or chemical means. *Clarification* using MF alone, or in conjunction with a filter aid (e.g., diatomaceous earth), retains spent cells, fragments, and protein debris while permeating soluble bioproducts.

Purification by using UF can be used with, or instead of, precipitation or chromatography to concentrate product and remove soluble cellular impurities such as nucleic acids and

Table 14.13 Filtration Steps in Biopurification Trains

Step: Purpose	Filter Type	Alternatives
Harvest: Concentrate cells from broth	MF, UF	Centrifuge
Disrupt: Lyse cells		
Debris Clarification: Remove cell debris	MF, filter aid	Centrifuge; expanded-bed chromatography
Purification: Concentrate product; remove impurity	UF	Crystallization; precipitation; chromatography
Polish	MF, UF	Crystallization; ultracentrifuge; chromatography
Sterile Filtration: Reduce bioburden	0.22 μm MF	
Buffer Exchange	MF, UF	

proteins. *Polishing* with direct-flow (dead-end) MF, described in §14.9.3, may be used in lieu of ultracentrifugation to remove residual insoluble particulate and precipitated impurities. *Sterile filtration* in pharmaceutical operations uses a validatable sterilizing-grade 0.22 μm MF to reduce bioburden in preparation for subsequent formulation. One or more sterile *buffer exchanges* often follow sterile filtration to incorporate excipients or adjuvants into the final bulk product prior to filling vials. Compared to centrifugation, membrane filtration of biological products is energy-efficient and less capital intensive, with less product shear and less severe operating conditions.

§14.9.2 Biofiltration Operating Modes

MF, NF, UF, and VF of bioproducts may be conducted by flowing feed normal to a dead-end membrane surface (referred to as direct flow, normal flow, in-line or *dead-end filtration*, DEF) or tangentially across the surface (called *crossflow* or *tangential-flow filtration*, TFF). Figure 14.28 compares normal- and tangential-flow modes. In DEF, a batch of feed solution is forced under pressure through the membrane, causing retained material to accumulate on and within the membrane. The pressure required to maintain a desired flow rate must increase, or permeate flux will decrease. A combined operation, as described in §14.3.1 and illustrated in Example 14.3, in which constant-flux operation is employed up to a limiting pressure, followed by constant-pressure operation until a minimum flux is reached, is superior to either constant-pressure or constant-flux operation. DEF has lower capital cost, lower complexity, and higher operating cost relative to TFF. DEF is better suited for dilute solutions, while TFF can be employed for concentrated solutions.

In TFF, which is more suitable for large-scale, continuous filtration, feed flows along the surface, with only a fraction of the solvent passing through the membrane, while retained matter is carried out with the retentate fluid. Retentate is usually recycled through the filter at tangential-flow velocities parallel to the membrane surface in the 3–25-ft/s range. TFF gives up to 10-fold-higher flux values than DEF [57].

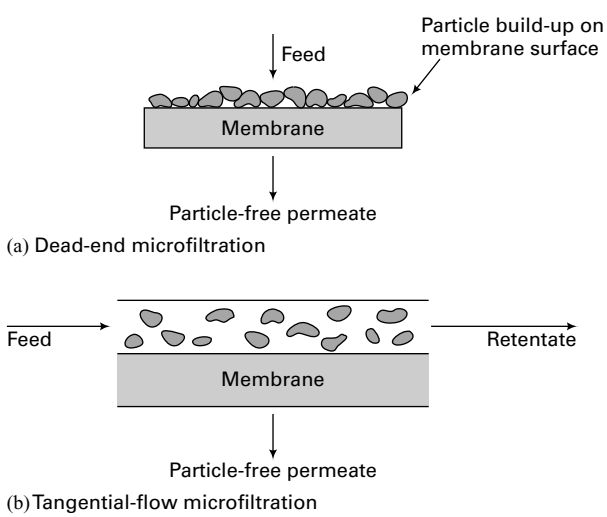

Figure 14.28 Common modes of microfiltration.

The tangential-flow mode is also used, almost exclusively, for RO, as discussed in §14.6, and for UF. Improvements in product yield and throughput in TFF have been demonstrated by operating to maintain flux rather than *transmembrane pressure drop* (TMP). Concentration factors up to 100-fold in single-stage UF systems have been demonstrated using high membrane-packing density and reduced holdup volumes. Maintaining constant retained protein concentration at the membrane surface (c_{wall}) has been shown to enhance product yield and minimize membrane area for large variations in feed quality and membrane properties [58]. Flux data at successively higher TMP values taken at multiple concentrations is fit to stagnant film and osmotic pressure models to estimate values of mass-transfer coefficients, osmotic virial coefficients, and fouled membrane resistance to guide operation to maintain constant c_{wall}, a variable that is not known *a priori*.

High-performance TFF (HPTFF) uses optimal values of buffer pH, ionic strength, and membrane charge to maximize differences in hydrodynamic volume between product and impurity to enhance mass throughput and selectivity as a function of local, pressure-dependent flux [59, 60]. Cocurrent flow on the membrane filtrate side maintains uniform TMP at or below the point at which filtrate flux becomes pressure independent. HPTFF can separate equally sized proteins based on charge differences, monomers from dimers, and single-amino-acid variants in real, dilute feeds, significantly improving yield and purification factors. Scalable UF devices are available that permit 1000-fold volumetric increases with consistent protein yield and permeate flux by increasing channel number in hollow-fiber cassettes or by decreasing channel width in flat-sheet cassettes while maintaining pressure, fluid flow, concentration profile, and channel length [61].

Membrane Geometries for Bioseparations

The most common membrane geometries used in bioprocessing are flat plate, spiral wound, tubular (internal diameter [i.d.] > 0.635 cm), capillary ($0.1 <$ i.d. < 0.635 cm), and hollow fibers ($0.025 <$ i.d. < 0.1 cm), which need clarified feed to avoid clogging. Flat-plate membranes are commonly used in plate-and-frame, filter-leaf, Nutsch, and rotating filter configurations. Plate-and-frame and filter-leaf (pleated) cartridges are typically used for MF. In the latter, the membrane is pleated and then folded around a permeate core. Many module types are inexpensive and disposable. A typical disposable cartridge is 2.5 inches in diameter by 10 inches long, with 3 ft^2 of membrane area. The cartridge may include a prefilter to extend filter life by removing large particles, leaving the microporous membrane to make the required separation. For UF, newer composite-regenerated cellulose membranes that are mechanically strong, easily cleaned, and foul less than synthetic polymers provide better permeability and retention [62, 63]. Covalent surface modification with quaternary amine or sulfonic-acid groups improves membrane selectivity, particularly for HPTFF applications.

Membrane Casting

Polymer membranes used widely in MF, UF, and RO of bioproducts are typically prepared by casting a polymer that has been dissolved in a mixture of solvent and high-boiling nonsolvent as a film of precise thickness on a conveyer in an environmentally controlled chamber [64]. The casting process produces membranes in which pores result from interconnected openings between polyhedral cells formed by progressive evaporation of solvent that causes phase separation. The nonsolvent coalesces into droplets surrounded by a shell of polymer, which gels out of solution and concentrates at phase interfaces. Further solvent evaporation deposits additional polymer that thickens swelling polymer shells, which come into mutual contact as solvent disappears. Area-minimizing forces consolidate the shells into clusters that are distorted into polyhedral cells filled with nonsolvent. Cell edges accumulate polymer, thinning the walls, which rupture and create interconnections between adjacent cells. Metering pores of the membrane consist of the interconnected openings between the polyhedral cells. The concentration of polymer in solution determines intersegmental separation of flexible chain segments that coil and overlap, as opposing electrical attractive and repulsive forces maintain separation of long polymer molecules, increasing pore size at greater dilution.

Membrane Requirements for Biotechnology

Process filters to prepare biopharmaceutical agents described in §1.9—like recombinant proteins or DNA, vaccine antigens, or viral vectors for gene therapy—have the following unique requirements when compared with bioprocess filters used to prepare food and beverages, or to purify other nonpharmacological bioproducts:

1. **Preserve biological activity.** Denaturation, proteolytic cleavage, or misforming of protein projects must be avoided. Immunogenicity of a targeted vaccine antigen, for example, must be maintained.
2. **Satisfy cGMP requirements.** Depending on the application, these may include biocompatibility, sterilizability, and flushout of extractables.
3. **Accommodate modest scales of operation.** Dose sizes of mg or less may be required for vaccine antigens or recombinant proteins. Milligrams to grams of active agents may be recovered from just 10 to 1,000 liters of broth, so process scales are relatively small, particularly for orphan drugs that treat rare diseases.
4. **Include batch operation.** A defined volume of pharmaceutical product undergoes a battery of assays to verify activity, purity, sterility, and other mandates in the Code of Federal Regulations (CFR) to be approveable by the Food and Drug Administration (FDA).

Batch bioprocess volumes are a consequence of the volume of fermentation or cell culture required to produce sufficient active bioproduct to economically satisfy market demands. This batch volume is processed discretely from inception to final release to eliminate carryover contamination that may compromise multiple batches. The batch nature and release criteria of biopharmaceutical operations distinguish them from large-scale, continuous bioprocesses.

Challenges Unique to Filtration in Biotechnology

There are also the following unique challenges to implementing filtration in vaccine bioprocesses in the pharmaceutical industry:

1. **Integrated process.** The process may ‘‘define the product,’’ particularly when complete physicochemical characterization of a biological antigen to satisfy FDA regulatory requirements is not possible. Therefore, filtration cannot be implemented or optimized in isolation, but must be approached as an integral part of the entire series of fermentation, purification, and formulation steps.
2. **Compressed development.** Pressing market need for biotechnology products to prevent or treat public health problems drives accelerated timelines for development. Consequently, as little as weeks to months may be available to select and optimize filters in the lab.
3. **Limited raw materials.** Only mL to L of fermentation or cell culture broth may be initially available for filter selection, characterization, and optimization.
4. **Variable fermentation or cell culture.** Membrane filter operations must accommodate wide variations in cell culture and fermentation composition and productivity while providing consistent yield and purity. Such variability often occurs during scale-up and in campaigns to produce actives for clinical trials.
5. **Operability.** Filter operations that maximize the robustness of process operations must be selected to provide consistent purity and yield, resulting in an economical, validatable process.
6. **Virus removal.** Endogenous virus-like particles in mammalian cells used to manufacture rDNA products and adventitious viruses that contaminate cell cultures (e.g., 20-nm parvovirus) must be reduced to a level of less than one virus particle per 10^6 doses.

Membrane filters provide size-based virus removal in which maximum virus resolution is obtained by optimizing pH, ionic strength, and membrane charge to distinguish proteins (4–12 nm) from virus (12–300 nm) by exploiting charge repulsion. This complements chemical inactivation (chaotropes, low pH, solvents, or detergents), physical inactivation (heat or UV), adsorption (ion-exchange chromatography), or other size-based separations (size-exclusion chromatography).

Membrane bioprocessing can contribute unique benefits to society, as illustrated by membrane filtration of vaccine antigens [65]. Vaccines have virtually eliminated

Table 14.14 Typical Specifications for Nuclepore™ Track-etch Microfiltration Membranes

Specified Pore Size, μm	Pore-size Range, μm	Nominal Pore Density, Pores/cm^2	Nominal Membrane Thickness, μm	Typical Flow Rates at 10 lb/in^2 ΔP, 70°F
				Water, gal/(min)(ft^2)
8.0	6.9–8.0	1×10^5	8.0	144.0
5.0	4.3–5.0	4×10^5	8.6	148.0
3.0	2.5–3.0	2×10^6	11.0	121.0
1.0	0.8–1.0	2×10^7	11.5	67.5
0.8	0.64–0.80	3×10^7	11.6	48.3
0.6	0.48–0.60	3×10^7	11.6	16.3
0.4	0.32–0.40	1×10^8	11.6	17.0
0.2	0.16–0.20	3×10^8	12.0	3.1
0.1	0.08–0.10	3×10^8	5.3	1.9
0.08	0.064–0.080	3×10^8	5.4	0.37
0.05	0.040–0.050	6×10^8	5.4	1.12
0.03	0.024–0.030	6×10^8	5.4	0.006

incidence and associated effects of diseases such as measles, mumps, rubella, polio, diphtheria, and invasive *H. flu*, which once were widespread. Prevention of viral infections that cause Hepatitis A, Hepatitis B, or chicken pox, and bacteria infections from *S. pneumonia* and *B. burgdorferi* (Lyme disease) is now possible. Prophylactic candidates against viral Hepatitis C, HIV, and other agents that cause significant public health issues are under active investigation. Successful clinical investigation of candidate vaccines and manufacture of marketable vaccine products relies on developing consistent, scalable processes to purify bulk vaccine antigen from complex bacterial fermentation and cell culture broths.

§14.9.3 Dead-End Membrane Biofiltration

Dead-end filtration (DEF) is used to recover, concentrate, clarify, and sterilize biological species by depth and surface mechanisms. Microfilters are most commonly employed in the DEF mode. Microfilters have pore sizes ranging from 0.05 to 10 μm, with ~10^{12} pores/m^2. Recovery of ~0.1–20 μm particles like animal cells, yeasts, bacteria, or fungi from large volumes of culture broth by MF provides rapid volume reduction to improve process economics. Clarification of gases, media, intermediate process streams, virus-containing solutions, and beverages like wine, juice, and beer by MF removes insoluble particulate solids. Microfilters rated with 0.1- or 0.2-μm pore sizes are used to sterilize water for injection (WFI), parenteral solutions (for injection or infusion), antibiotics, buffer solutions, and culture media. MF is performed at low TMP, typically less than 50 psi (3.4 bar; 0.35 MPa), to yield high permeate fluxes ranging from 10^{-4} to 10^{-2} m^3 permeate/m^2 membrane areas for unfouled membranes.

Membrane structures for MF include screen filters that collect retained matter on the surface and depth filters that trap particles at constrictions within the membrane. As Porter discusses in Schweitzer [73], depth filters include: (1) thick, high-porosity (80–85%) cast–cellulose–ester membranes having an open, tortuous, sponge-like structure; and (2) thin, low-porosity (nominal 10%) polyester or polycarbonate track-etch membranes of a sieve-like structure with narrow distribution of straight-through, cylindrical pores. The latter have a much sharper cut-off, resulting in enhanced separation factors. For example, a Nuclepore™ Type 2 membrane can separate a male-determining sperm from a female-determining sperm. As shown in Table 14.14, Nuclepore™ membranes come in pore sizes from 0.03 to 8.0 μm, with water permeate fluxes at 70°F and a TMP of 10 psi, ranging from 0.006–144 gal/min-ft^2.

This section discusses scale-up of DEF and its application to several steps in bioproduct purification: harvesting cell lysates using filter aids, virus filtration, sterile filtration of bioproduct solutions, culture media, room air, and nanofiltration.

Scale-Up of DEF

Filter area required for manufacturing-scale DEF may be quantitatively estimated from lab-scale biofiltration data by determining the filter capacity using a model for filter resistance that is consistent with the data. The V_{max} method [74] uses a pore-constriction model to determine filter capacity faster, and with less feed volume, than by measuring the cumulative filtrate volume that reduces Q to ~10% of Q_o (flow-decay method). Pore constriction assumes that the membrane removes sub-pore-sized particles that interact with membrane surfaces inside pore cavities, where they are retained by adsorption [64]. An increase in species retention at lower TMP and/or at a lower challenge level suggests pore constriction is occurring due to adsorptive sequestration rather than sieving of the species by a filter rated for absolute retention at a given particle size.

EXAMPLE 14.14 Normal-Flow (DEF) Microfiltration.

Consider the time (t) versus volume collected (V) data for a 0.18 m^2 normal-flow MF in the following table. Estimate the capacity, V_{max}, of the filter and the initial flow rate, Q_o. Confirm whether the data fit a pore-constriction model for flux decline at constant TMP. Determine the flow rate at any point during filtration.

Normal-Flow Filtration Data

t (min)	V (L)
0	0
0.25	2.3
0.5	4.3
0.75	6.1
1	7.7
1.25	9.1
1.5	10.3
1.75	11.4
2	12.4

Solution

The linearized form for pore constriction at constant pressure in Table 14.5 is

$$\frac{t}{V} = \frac{t}{V_o} + \frac{1}{Q_o} \tag{1}$$

with $a = 1/V_o$ and $b = 1/Q_o$, where V_o corresponds to the initial (maximum) filter volumetric capacity and Q_o is the initial flow rate. Fitting the data to a plot of t/V versus t yields $V_o = 33$ L and $Q_o = 10$ L/minute. Then $V_{max} = 33$ L/0.18 $m^2 = 183$ L/m^2.

A pore-constriction mechanism may be confirmed by fitting Q/Q_o versus V/V_o data to the form

$$\frac{Q}{Q_o} = \left(1 - \frac{V}{V_o}\right)^2 \tag{14-105}$$

Equation (14-105) shows that an initial flow rate Q_o will decay to zero when the feed volume V entirely saturates the initial volumetric capacity, V_o, of a filter. Figure 14.29 shows that the data fit the form of (14-105). The instantaneous flux, Q/A, where A equals filter area, can be predicted from (14-105) for any value of fractional capacity V/V_o.

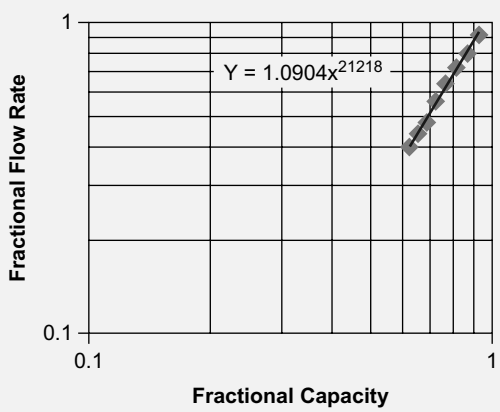

Figure 14.29 Effect of fractional capacity on fractional flow rate to confirm V_{max} filter sizing in Example 14.14.

The V_{max} filter-sizing method is faster and requires less feed volume than the flow-decay method, but may significantly underestimate capacity when pores are interconnected or fouling is not due to pore constriction. Scaling is more reliable by identifying capacity at constant flux in Table 14.5, using the linearized form for intermediate blockage for which $a = P_o^{-1}$ and $b = (P_o V_{max})^{-1}$.

Filter Aids

Adding filter aids (e.g., diatomaceous earth, DE) to clarify lysed bacterial or cultured animal cell feeds by MF can substantially improve throughput, capacity, and clarity. *Diatoms* are million-year-old skeletons of aquatic creatures with diameters of 1–200 μm and pores between 0.1 and 30 μm, resulting in permeabilities of 0.06–30 darcy (1 darcy = 0.9869 μm^2, where 0.9869 is the conversion factor from bar to atm). Calcining adheres diatoms and results in solubilities of approximately 0.1 wt% in dilute acid. Diatomite is 90 wt% silica, with remaining nonsilica elements bound as silicates. Diatomaceous earth clarification of bacterial lysates is attractive relative to centrifugal or membrane clarification in terms of capital cost, fouling, shear, aerosol generation, and scalability.

A typical DE filtration process consists of first layering a 1/16-inch precoat of DE onto a filtration matrix by recirculating a slurry of DE. Then lysate and *body feed* (continuous addition of small amounts of filter aid) are combined at a predetermined rate and pumped onto the precoated matrix at constant flow rate. Solids accumulate with DE on the precoated matrix until back-pressure reaches a preselected target, usually between 30 and 50 psig, at which point pumping is halted, the cake is removed, and the process repeated. Body feed, driving force, and settling times affect permeability, mass recovery, and protein recovery.

Relative to centrifugation or unaided MF, DE filter products have lower turbidities, <20 nephelometric turbidity units (NTU), and at a lower cost ($0.10–$0.30 per lb DE, 0.2–10 lb DE per lb feed) without problems associated with centrifugal shear or limited membrane capacity, although dust is a potential safety issue during handling of bulk DE. There is a $2 billion world market for DE products, including applications in blood fractionation; clarification of beverages including juice, beer, and wine; and processing of oils, pharmaceuticals, chemicals, waste liquids, and sludges [75].

Clarity and Productivity

Use of DE filtration seeks to maximize both clarity and productivity, often leading to competing outcomes that must be balanced. Clarity is optimized by selecting a grade of DE that has an average pore size near the mean particle size of the feed to maximize particle retention. For example, *E. coli* batch fermentations typically yield about 4% by weight with particles > 0.1 μm. Antibiotic fermentation broth is 6 wt% solids, consisting of 1–2 μm particles. To optimize productivity, a ratio of body feed-to-solids content is selected to maximize Darcy permeability. Body feed-to-solids ratios (BF:S) range from 0.25 for rigid particulates to 5 for

gelatinous debris. This results in fluxes from 0.1 to 1.0 gal/ft^2-minute, or flow rates from 30 gpm (sludge) to 10,000 gpm (water). However, a high-permeability DE grade yields high flow rates, whereas a low-permeability DE grade gives high clarity. DE filtration is useful because it can accommodate a range of flow rates and back-pressures, although its performance can be subject to vibration.

Filter-Aided Harvest of Antibiotic Fermentation

Large-scale harvest of mycelial protein from fermentation of antibiotics like penicillin or streptomycin commonly employs continuous rotary filters or rotary vacuum precoat filters [76, 77, 84] described in Chapter 19. Rotation of the drum at a constant rotational velocity, n (rps), exposes a fraction, φ, of the drum-surface area to a reservoir in which mycelia coat the drum. Accumulated mycelia are then washed, dewatered, and finally removed by a string (penicillin) or knife-blade scraper (streptomycin). *Streptomyces* mycelia are more difficult to process than *Penicillium* mycelia and require addition of a filter aid like diatomaceous earth (silica skeletons of algae-like diatoms insoluble in strong acids and alkalis) or perlite (porous aluminum silicate used for rough filtrations). To use diatomaceous earth, a 1/16-inch precoat of filter aid is slurried onto the filter using a vacuum maintained in the drum. Broth mixed with 1% to 5% filter aid or another coagulating agent is suspended in the slurry reservoir. A mixed layer of cells and filter aid adheres to the rotating drum and thickens as it moves toward the wash, dewatering, and final discharge from the drum by a knife blade.

EXAMPLE 14.15 Use of Filter Aid.

Identify a general expression to characterize bulk flow in a filter-aided harvest of bacterial cells for antibiotic recovery. Identify strategies specific for improving filter-aid MF rates for streptomycin and penicillin.

Solution

A variable broth volume of V'/n is filtered with a drum during a time of φ/n corresponding to one revolution of the drum, where $V' =$ filtrate volume per unit time. These variables are substituted into the Ruth equation (14-25) for constant-pressure operation:

$$\left(\frac{V'}{n}\right)^2 + 2\frac{V'}{n}V_o = K\frac{\varphi}{n} \qquad (14\text{-}106)$$

This equation may be rearranged to its straight-line form analogous to (14-26) to estimate average specific cake resistance, from which the compressibility factor may be determined using (14-35).

Filtration rate may be increased by decreasing specific resistance of the cake by five approaches (typical harvest values for particular antibiotics are given in parentheses):

1. Increase filter aid in the slurry (2%–3% filter aid for streptomycin).
2. Decrease pH (pH 3.6 for streptomycin).
3. Extend fermentation time (180 to 200 h for penicillin).
4. Coagulate mycelial protein by heat pretreatment before filtering (30–60 min at $T = 80$–$90°C$ for streptomycin).
5. Minimize cake compression, e.g., by lowering ΔP or raising filter-aid content.

§14.9.4 Sterile Filtration

Solutions

Microporous membranes with pore sizes nominally rated to 0.22 or 0.1 μm are used to sterilize water, nutrient media, buffer formulations, or pharmacological actives during bioprocessing; or to perform sterile fill operations.

Validation of particle removal and retention capacity of 0.22 μm sterile filters is performed using a challenge suspension containing 10^7 cells/cm^2 of *Brevundimonas diminuta* ATCC 12146 bacteria (~0.3 o.d. × 1.0 μm long). The mycoplasma *Acholeplasma laidlawii* is used to validate rated 0.1-μm filters. Base materials for sterile filters include polyether sulphone (PES), polyvinylidene fluoride (PVDF), nylon, polypropylene (PP), and cellulose esters. Asymmetric membranes with a graded pore-size distribution that varies with membrane depth are used to minimize TMP requirements in the standard dead-end configuration. Turbid protein aggregates that result from air–water interfaces during microcavitation in multiple passes through pumps and valves form insoluble particulates that can blind sterile filters and reduce capacity. Particulates may be removed via sieving, depth filtration (e.g., inertial and Brownian impaction), or adsorptive sequestration by adding a depth filter either upstream or as a layer atop the sterile filter (i.e., multilayer) or by casting the sterile filter onto a membrane substrate that has a pore size and/or surface chemistry that removes particulates. Sterile filters are capsulized in self-contained cartridges that are presterilized by gamma irradiation or assembled into a cartridge housing like a Code 7 design, which is available in 10-, 20-, 30-, and 40-inch configurations. Further discussion of cartridge filters is found in Chapter 19.

Integrity Testing

The sterile filter assembly is tested "in-place" using a "bubble-point" or "pressure-hold" (gas-diffusion) method to ensure integrity of the filter and its assembly within the housing. Bubble-point testing measures gas flow through a fully wetted membrane at successively higher pressures [78]. A hydrophilic sterile filter, wetted with water or an aqueous alcohol (isopropanol) solution, is pressurized on its feed side by sterile-filtered, compressed air or N_2. At the bubble point, feed gas overcomes surface tension, σ, of the largest membrane pore and passes through the membrane to appear in the permeate as a stream of bubbles and cause an inflection in a plot of gas flow rate versus pressure. The bubble-point pressure, P_{BP}, required to just displace a liquid from a wetted

membrane pore of diameter d_p is

$$P_{BP} = \frac{4\phi\sigma\cos\theta}{d_p} \qquad (14\text{-}107)$$

where ϕ is the pore-shape correction factor and θ is the contact angle for the wetting fluid in contact with the membrane material. Membrane pore sizes of 0.65–0.1 μm typically yield bubble points of 0.2×10^5 to 8×10^5 Pa (0.2–8 bar). In a pressure hold or ''diffusion test,'' a wetted sterile filter is pressurized at ~80% of its bubble point. Total diffusive flux of sterile-filtered gas through the membrane is measured using an inverted graduated cylinder or flowmeter to meet manufacturer's specification. All connections to and from the assembled filter cartridge must be validated to be sterile.

Scale-Up

The required sterile filtration area depends on the maximum allowable load of organisms possible in the feed solution, dose volume, membrane capacity, and targeted *sterility assurance limit* (SAL). The maximum allowable load is the bioburden or viral load specification in the feed to the sterile filtration. The SAL is the calculated probability of a single unit of product containing a single microorganism (expected to be $<10^{-3}$ for aseptic processes, and designed for at least an extra order of magnitude). Filtration area is then increased, if necessary, to complete sterile filtration within one 8-hour shift to preclude ''grow-through'' (i.e., retained microbes that colonize the filter and grow through to the other side). The sterile filter and any associated depth filters must be compatible with the feed to prevent adsorption of a biologically active ingredient or any excipient, such as a preservative. Validation of pre-use removal of extractables (membrane monomers, storage solutions such as glycerol or ethanol) from the sterile filter assembly prior to use is required.

§14.9.5 Virus Filtration

Removal of endogenous or adventitious contaminating virus to sterilize solutions uses virus filtration membranes intermediate between MF and UF that have 20–70 nm pore sizes. Virus filtration uses composite membranes made from hydrophilic PES (e.g., Millipore's Viresolve® NFR), PVDF (e.g., Millipore's Viresolve® 70, 180, and NFP; Pall's Ultipor® DV50 and DV20), or regenerated cellulose materials to remove ≥ 4-logs of virus per filtration step, which is reported as log reduction value (LRV),

$$\text{LRV} = -\log_{10}\left(\frac{c_{i,P}}{c_{i,b}}\right) \qquad (14\text{-}108)$$

where $c_{i,b}$ and $c_{i,P}$ are concentrations in moles of solute i per volume, e.g., dm^3, of liquid in bulk, b, and permeate, P, solutions, respectively. A *bulk* solution is a reservoir of solute at a uniform concentration that is typically found adjacent to the region of interest (e.g., membrane surface or adsorptive particle surface) and often has a volume that is large relative to that of others (e.g., boundary layers or pore volumes) in a system. A bulk solution can correspond to the *feed* to a membrane system in some circumstances, but it often is *not* the feed, as illustrated in Figures 14.30 and 14.31, where the bulk consists of the *retentate* and the *feed + recycled retentate*, respectively. Using subscript b, rather than F for feed, for the general case clarifies and preserves this distinction. The subscript F may be substituted for b in the appropriate specific cases, but b is more accurate globally and is consistent with widely used references in the field of bioseparations. Removal of both enveloped and non-enveloped viruses is validated by spiking with high titers of model viruses such as animal parvovirus (~22 μm; e.g., minute virus of mice, MVM), poliovirus, SV40, sindbis virus, or reovirus. Parvovirus filters (20 nm pores) like Pall Ultipor® DV20 are designed to remove viruses as small as 20 nm, while retrovirus filters (50–70 nm pores) like Pall Ultipor® DV50 remove viruses ≥ 50 nm. Bacteriophage, more readily obtained at high purity and titer, can be used for initial evaluation of LRV values.

Room air is prepared using high-efficiency particulate air (HEPA) filters, which are large, high-throughput ventilation, depth-type filters made of compacted fibrous glass wool onto which microbes or other airborne particulates are impacted. Such filters reduce particulate load in a room to class 10,000 (airborne particles per m^3) ''acceptable for biotechnology processing'' required for antechamber to sterile work areas, and class 100 (particles per m^3) ''clean or Aseptic'' levels required for sterile filling. Filters are sized according to anticipated flow rate using the pressure differential between one room and an adjacent room or corridor (0.2- to 0.6-inch water) concerning air changes/hour or linear flow rate, usually specified in laminar-flow hoods (5 to 20 ft/s) or aseptic areas. Filters are integrity-tested for 10^3 reduction in aerosol spray of diisoctyl phthalate (DOP). DOP aerosol generators produce ''most penetrating particle'' droplets ~0.3 μm in size, which are less likely to deposit by inertial impaction than larger particles whose trajectory remains constant as fluid veers due to small diffusivities, or than smaller particles that easily traverse adjacent streamlines via Brownian motion due to higher diffusivities [64].

Equipment gases (typically air or N_2) are sterilized by hydrophobic, asymmetric-membrane vent filters rated to 0.2 μm that are installed on all vessels (fermentors, holding tanks, filter canisters) that must be filled or drained to prevent aerosol contamination of, or by, pathogenic batch contents. These filters are sized for area based on maximum anticipated flow rate to allow flow in both directions. Methods for testing them are subject to government mandates, discussed in Chapter 19.

§14.9.6 Nanofiltration

Nanofiltration employs membranes in which nm-sized cylindrical through-pores penetrate the membrane barrier at right angles to its surface [79]. Nanofilter membranes are made primarily from polymer thin films (e.g., porous polycarbonate, polyethylene terephthalate, or polyimide or metal [aluminum] [80]). Pores in thin-film polymer membranes are formed by bombarding (or ''tracking'') the film with high-energy particles, which creates damage tracks that are chemically developed (or ''etched''). Pore dimensions are

controlled by pH, temperature, and time during development, with pore densities ranging from 1 to $\sim 10^6$ pores per cm^2. Track-etch membranes are often thicker and less porous than asymmetric UF membranes.

Alumina membranes are made by electrochemically growing a thin, porous layer of aluminum oxide from aluminum metal in acidic media. Pores of 5–200 nm are arranged in hexagonally packed arrays with densities as high as 10^{11} pores/cm^2. Nanofilters can ''soften'' water by retaining scale-forming, hydrated divalent ions (e.g., Ca^{2+}, Mg^{2+}) while passing smaller hydrated monovalent ions without adding extra Na^+ ions used in ion exchangers [64].

Proteins, nucleic acids, and enantiomers of drugs have been separated in nanotube membranes. The selectivity and flux of species that selectively translocate nanometer-scale pores via free or electrophoresis-assisted diffusion can be controlled by pore characteristics and by incorporating molecular-recognition chemistries (e.g., antibodies, nucleic acids) in nanotube walls. Membranes electrolessly plated with gold and coated with polyethylene glycol (PEG) to give 20- and 45-nm pores selectively pass lysozyme (Lys, MW = 14 kDa) from a solution of Lys and bovine serum albumin (BSA, MW = 67 kDa) based on relative size and diffusivity. Electrophoretic transport due to electrophoretic mobility of proteins based on the Nernst–Planck equation in a transmembrane potential applied using electrodes on feed and permeate sides separates Lys (pI = 11), BSA (pI = 4.9), and hemoglobin (Hb, pI = 7.0, MW = 65 kDa). Coating alumina membranes with antibody Fab fragments distinguishes RS and SR forms of enantiomeric drug 4-[3-(4-fluorophenyl)-2-hydroxy-1-[1,2,4]triazol-1-yl-propyl]-benzonitrile, an inhibitor of aromatase enzyme activity, with selectivities from 2 to 4.5. Selective passage of 18-bp deoxyribonucleic acid (DNA) molecules containing 0 mismatches (perfect complement) versus 1-, and 7-base mismatch DNA gives selectivity coefficients of 3 and 7, respectively, after coating the pores with 30-base DNA hairpin with an 18-base loop, and 1 and 5 after coating the pores with 18-bp linear DNA. Nanotube membrane pores with ligand, voltage, or electromechanical gating can function as ion-channel mimics.

§14.9.7 Tangential-Flow Membrane Biofiltration

Tangential-flow (crossflow) *filtration* (TFF) sweeps a membrane surface with parallel feed flow to enhance flux values relative to direct-flow (dead-end) filtration by reducing cake formation and concentration polarization. *Ultrafiltration* (UF), a term used to identify separations that employ membranes with pore sizes between 0.001 and 0.02 μm, is performed almost exclusively in TFF mode. *Microfiltration* (MF), a term used to identify separations that employ membranes with pore sizes ranging from 0.02 to 10 μm, is also often employed in TFF mode.

UF can selectively retain bioproducts with a molecular-weight range of 300 to 500,000 [81]. Macromolecules like proteins, starches, or DNA and larger species like plasmid DNA [82] and virus-like particles [83] are retained, while smaller solutes like salts, simple sugars, amino acids, and surfactants or replacing buffers are permeated. Ultrafilters have up to $\sim 10^{12}$ pores/cm^2. A UF filter with a molecular weight cut-off (MWCO) of 50,000 retains 90% of globular protein with the corresponding MW. Molecular weights of some widely studied globular proteins are summarized in Table 14.15. Hydrodynamic diameter of a protein is governed by its folding and solution conditions like pH and ionic strength. Therefore, a UF filter is typically selected that has a MWCO value that is 50% of the MW of the retained protein target.

Applications of UF

Cell-concentration factors of 15–50 are reported for harvesting *E. coli*, mycoplasma (for veterinary vaccines), and influenza virus (whole virus vaccine) by UF with a 100,000 MWCO [77]. In addition to cell harvesting, UF is used to process blood and plasma, remove fever-producing (pyrogenic) mucopolysaccharides from medical-grade water, concentrate virus from surface water for assay detection, fractionate immunocomplexes from residual haptens (small molecules that elicit an immune response only when attached to a large carrier such as protein), and concentrate and fractionate other biological species. UF is a large-scale analog of osmotically driven batch dialysis in which unwanted, low-molecular-weight solutes are removed or buffers are exchanged in protein or DNA solutions [85].

Hollow-fiber membranes and flat-sheet membranes configured in plate-and-frame systems are most common for TFF in bioprocessing. Hollow-fiber membranes offer the highest surface area per unit volume and validatable cleanability, whereas plate-and-frame systems incur higher initial capital costs. Recent developments that make UF a mainstay for protein concentration and buffer exchange are: (1) a composite UF membrane consisting of defect-free, low-protein-binding, regenerated cellulose filtration layer bonded atop a mechanically robust polyethylene microporous substrate; (2) simple, effective sanitizing (peroxyacetic acid) and storage (0.1–N NaOH) solutions; (3) linearly scalable module designs.

Process Considerations for TFF

Dead legs (peripheral piping that results in unmixed holdup volumes) should be eliminated. Holdup volume should be minimized during design and fabrication of TFF skids to ensure complete buffer exchange and to minimize holdup losses during recovery of product using: (1) cone-bottomed tanks to minimize final concentrated volume and (2) the return of retentate through the cone bottom using a tee-outlet to aid mixing. To minimize deactivation of proteins during long recirculation times required for TFF: (1) operate at 4°C; (2) eliminate air–water interfaces at which proteins denature, e.g., submerge the retentate return line below the liquid level in the feed tank; and (3) use a large-lobe sanitary lobe pump for recirculation to minimize degradation due to pump shear.

UF or MF operated in TFF mode is often used to harvest *E. coli* or yeast cell suspensions. Harvesting separates a

concentrate of intact cells from cell-free supernatant. MF is more frequently used to sieve species such as bacterial or mammalian cells ranging from 0.1 to 10 μm. MF pore sizes range from 0.02 to 10 μm, though MF is typically categorized by a nominal removal rating that may be unrelated to pore size.

Membrane Selectivity

Species *selectivity* in TFF is related to the solute sieving coefficient, S,

$$S_i = \frac{c_{i,P}}{c_{i,b}} \tag{14-109}$$

where $c_{i,b}$ and $c_{i,P}$ are concentrations (mol/cm^3 of liquid) of solute i in bulk feed, b, and permeate, P, solutions, respectively. Solute passage or rejection by a semipermeable-membrane filter is measured using a rejection coefficient, σ_i, for solute i (also, solute reflection coefficient) from thermodynamics of irreversible processes [81]:

$$\sigma_i = \frac{c_{i,b} - c_{i,P}}{c_{i,b}} = 1 - \frac{c_{i,P}}{c_{i,b}} = 1 - S_i \tag{14-110}$$

Unrestricted passage of solute i through the membrane with the solvent corresponds to $\sigma_i = 0$, while little to no passage of solute i retained by a membrane typically yields $\sigma_i \sim 0.95$–0.98.

The size of a globular macromolecule is denoted by its molecular weight, MW:

$$\text{MW} = \rho N_A \frac{4}{3}\pi a^3 \tag{14-111}$$

where N_A is Avogadro's number, a is macromolecular radius, and ρ is the globular density. Units for MW are usually reported in kDa (1 dalton = 1 g/mol), as illustrated in Table 14.15. There is reasonable agreement between (14-111) and empirical data written in the form $\text{MW} = \alpha a^n$, where values for coefficient α (6.1×10^{22}; 1.46×10^{21}; 3.1×10^{25}) and exponent n (2.17; 2; 2.72) have been obtained experimentally for dextran, polyethylene glycol (PEG), and proteins [54].

The MWCO of a UF membrane represents the MW of a globular protein that exhibits $\sigma_i = 0.9$. Retention, MWCO, and MW may be related [54] by

$$\sigma_i = \left\{1 - \left[1 - \left(\frac{\text{MW}}{\text{MWCO}}\right)^{1/3}\right]^2\right\}^2 \tag{14-112}$$

In practice, the value of σ_i is influenced by membrane characteristics (porosity, chemistry) as well as by external influences (TMP, solute concentration(s) in the feed, temperature, pH, ionic strength) and thus may vary over the course of an operation. Negative zeta potentials (measured across the membrane) are typical for materials such as cellulose acetate or sulphonated polysulphone for pH > 3, as well as for chemically neutral materials such as PVDF or PES due to strong adsorption of anions from the buffer or electrolyte solution. It is common for σ_i to vary from 0 to 1 over a range of solute MW between about 10 to 10^2-fold. Thus, complete separation by UF of biological species that differ in MW by less than about 10-fold is rare, and partial retention to some degree of similar-sized compounds occurs most frequently. For UF membranes, retention-cut-off curves are established experimentally. Figure 14.30 shows two generic curves. A sharp cut-off is desirable, but more typical is the diffuse cut-off curve, because of the difficulty in producing a membrane with a narrow pore-size distribution.

Electrostatic Effects

Decreasing salt concentration from 100 to 1 mM decreases the protein-sieving coefficient ≥ 100-fold [86], an effect attributed to electrostatic and electrokinetic effects.

Table 14.15 Physical Parameters of Some Widely Studied Proteins

Protein	Molecular Weight (kDa)	Stokes Radius (nm)	pI
Urease	480		5.0
Collagen (gelatin)	345		
γ Globulin	170		6.6
β-galactosidase (β-gal) (*Escherichia coli*)	116		
Human tissue plasminogen activator (tPA)	70		
Bovine serum albumin (BSA)	66.2	3.6	4.9
Hemoglobin	68		6.8
Bovine hemoglobin (Hb)	65		7.0
Chicken ovalbumin (OA)	45		
Horseradish peroxidase (*Amoricia rusticana*)	44		
Protein A (*Staphylococcus aureus*)	42		
Egg albumin	33.8–40.5		4.6
Pepsin	34.5		1
Chymotrypsinogen	25		9.5
β-lactoglobulin	18.3		5.2
Human calmodulin	18.2		4.46
Myoglobin	16.7		7.0
Hen egg white lysozyme (HEW)	14.4	2	11
Cytochrome C (Cyt C)	12.4		10.6

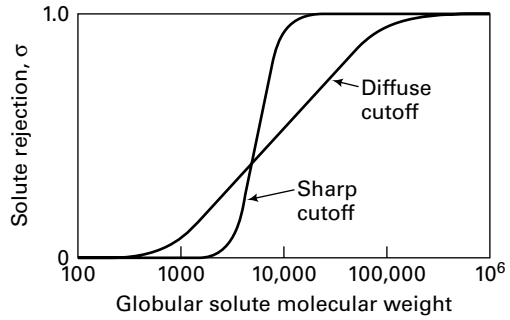

Figure 14.30 Molecular-weight cut-off curves.

Electrostatic interactions between a solute and counterions and co-ions in solution produce a diffuse ion cloud or electrical double layer that increases its effective size. Distortion of this double layer adjacent to pore walls and electrostatic interactions between charged solute and charged membrane surface also affect sieving. Buffer conductivities < 50 mS (millisiemen)/cm (1 siemen $= 1$ ohm^{-1}) enhance permeability and anionic protein selectivity of negatively charged, composite, regenerated cellulose membranes functionalized with sulfonic acid.

Concentration Polarization

Partially or completely retained dissolved or suspended solutes increase in concentration from bulk solution toward the membrane surface during membrane filtration, creating reversible *concentration polarization* (CP), a major factor limiting TFF, MF, and UF. Concentration polarization can reduce solute flux and change solute-rejection characteristics via increasing osmotic resistance to pressure-driving force or inducing solute–solute or solute–surface coagulative interactions that result in aggregration, cake formation, or pore plugging [81]. At steady state, partially rejected solute in a static film of thickness δ adjacent to the membrane surface is transported away from the surface by pore convection and diffusion at a rate equal to its bulk convective flux toward the surface:

$$Jc_{i,P} + D_e \frac{dc_i}{dz} = Jc_i \tag{14-113}$$

where D_e is the effective solute diffusivity in the liquid film (cm^2/s), J is the z-directed volumetric filtration flux of solvent (cm^3/cm^2-s) normal to the surface from (14-4), c_i is the concentration of solute i (mol/cm^3 of liquid), subscript P indicates permeate concentration in an adjacent membrane pore, and subscript b indicates bulk (e.g., feed) concentration. Separating variables in (14-113) and integrating across the mass boundary-layer thickness with boundary conditions $c_i\{z = 0\} = c_{i,b}$ and $c_i\{z = \delta\} = c_{i,w}$ at the membrane wall yields the classical stagnant-film model [87]:

$$J = \frac{D_e}{\delta} \ln \frac{c_{i,w} - c_{i,P}}{c_{i,b} - c_{i,P}} \tag{14-114}$$

Substituting (14-110) for solute rejection into (14-114) gives

$$\frac{c_{i,w}}{c_{i,b}} = \frac{\exp(J\delta/D_e)}{\sigma_i + (1 - \sigma_i)\exp(J\delta/D_e)} \tag{14-115}$$

For a completely rejected species, $\sigma = 1$ and $c_{i,P} = 0$, and (14-114) reduces to

$$J = \frac{D_e}{\delta} \ln \frac{c_{i,w}}{c_{i,b}} \tag{14-116}$$

which shows that permeate flux is proportional to $\ln(c_{i,b})^{-1}$, causing permeate flux to slow as UF concentration of a desired biological product proceeds, until flux attains a maximum pressure-independent value. Maximum $c_{i,w}$ for solid particles is $\sim$74%, corresponding to hexagonal close packing, whereas for deformable particles [e.g., red blood cells (RBC)], it may increase up to 95%. It also shows that species concentration at the wall relative to its bulk value—i.e., the polarization modulus, $c_{i,w}/c_{i,b}$, a measure of the extent of CP—increases in exponential proportion to a dimensionless ratio of bulk convective transport to Brownian diffusive transport in the film given by

$$\frac{J\delta}{D_e} = J/k_c \tag{14-117}$$

where k_c, in dm^3 m^{-2} h^{-1} (LMH) or in m/s, is a diffusive mass-transfer coefficient. High membrane permeability (high J) and/or high MW solutes (small D_e) may produce severe CP with $c_{i,w}/c_{i,b} > 10$, which drives solute–membrane (e.g., adsorptive) or solute–solute (e.g., precipitation) interactions. Eventually, the solubility limit for solute i may be reached, maximizing $c_{i,w}$ and eliminating increases in permeate flux J in (14-116), even with a larger ΔP driving force, which is negated by gel-layer formation. Solvent flux as a function of solute concentration is shown in Figure 14.31 for two protein solutes. Instead of correlating flux with the logarithm of solute concentration, it may be correlated with concentration factor, CF, which is defined in terms of volumetric flow rates of feed and retentate:

$$CF = \frac{Q_F}{Q_R} \tag{14-118}$$

Higher transmembrane velocities and local vortices or eddies induced by obstructions to local flow, macroscopic turbulent flow, or rotation of the sieving surface decrease film thickness, δ, and resistive polarization effects. Concentration polarization may be reduced by:

1. **Module design.** Introducing features like tangential flow, mixing, or turbulence promoters to disrupt CP; membrane protrusions such as dimples, or corrugation.

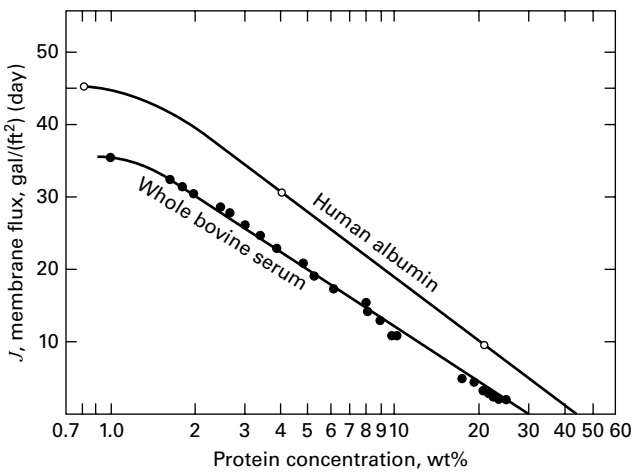

Figure 14.31 Effect of solute concentration on membrane flux.

2. **Hydrodynamic flow management.** Increasing tangential-flow rate, decreasing convective flux below the critical flux for fouling to reduce CP buildup rate, pulsing or reversing feed flow to disrupt CP.
3. **Treatment of feed.** Adding dynamic, solid particles to feed to scour the CP.
4. **Membrane treatment.** Modifying electrostatics to minimize coagulative solute–membrane and solute–solute interactions.
5. **Periodic membrane cleaning.** Including in-line procedures such as back-pulsing, intermittently spiking filtrate pressure to induce temporary back-flow of filtrate into the static film and disrupt the CP layer.

Fouling

Solute interactions in biofiltration may result in membrane fouling, the primary factor limiting microfiltration permeate flux. Fouling results from kinetic adsorption or flow-induced deposition onto, or intrusion into, the membrane by macromolecules (e.g., proteins), colloids, and particles with low diffusion coefficients. Aggregates generated by microcavitation at the pump or by shear at the membrane surface in the case of proteins, or by velocity gradients imparted by an impeller, pump, or flow in a duct in the case of colloids, contribute to fouling. Fouling phenomena constrict, and may eventually blind (block), membrane pores. A sequence of four periods usually produces fouling in MF [88]:

1. **Macromolecular sorption.** Dissolved macromolecules introduced in the feed adsorb rapidly to membrane surfaces, decreasing permeate rate in proportion to coverage, until a pseudo–steady state is reached.
2. **Particle deposition.** The first sublayer builds as colloids, like suspended cells, slowly deposit, decreasing permeate flux as monolayer coverage is approached.
3. **Sublayer rearrangement.** Additional sublayers build, reducing the cross section for axial flow, which increases the wall shear rate and axial pressure gradient. More shear increases Brownian and shear-induced back-diffusion of solids and inertial lift while higher TMP grows and compresses the sublayers, reducing the flux.
4. **Non-Newtonian viscous effects.** Densification of sublayers increases bulk concentration until it increases rapidly and bulk viscosity becomes sharply non-Newtonian, precipitously dropping permeate flux. Concentrated particle suspensions exhibit a concentration-dependent effective shear viscosity that can be correlated by Euler's equation [89]:

$$\mu\{\phi\} = \mu_o\left(1 + \frac{\frac{1}{2}[\mu]\phi}{1 - \phi/\phi_{max}}\right) \qquad (14\text{-}119)$$

where fitted parameters $[\mu]$ and ϕ_{max} are intrinsic velocity and maximum particle volume fraction with best-fit values of 3.0 and 0.58, respectively, at low shear rates. Equation (14-119) shows that $\mu/\mu_o = 1.5$, 2.0, 2.9, and 5.4 for $\phi =$ 0.2, 0.3, 0.4, and 0.5, respectively.

Fouling lowers permeate flux and alters membrane selectivity. Protein fouling may be minimized by various chemical, physical, and hydrodynamic means. Chemically, selecting sorption-minimizing hydrophilic membrane materials (PVDF, for example), and reducing nominal pore size of the skin below the MW of suspended proteins, decreases CP and fouling. As an example, bovine serum albumin (BSA, 69,000 Da), which forms full and partial monolayers in the ultra-thin skin of asymmetric membranes of sizes $\geq$ 300,000 and 100,000 MWCO, respectively, exhibits no measurable skin adsorption on 50,000 MWCO membranes [90]. Physically, the membrane may be back-flushed using pressure or electrical driving forces, or seed particles added to drag macromolecules away from the membrane. Hydrodynamically, fluid shear rate at the membrane surface may be increased via turbulence, inserts, or rotating disks. Fouling or CP may be disrupted by inducing flow instabilities via surface roughness, pulsation, or flow reversal, or by creating secondary flows using vortices [91]. Taylor vortices are created via Couette flow in annuli of cylindrical devices. Dean vortices arise from flow in a helically coiled channel. Simultaneous application of more than one hydrodynamic method yields flux improvements ranging from 2.5- to 9-fold [88], which are offset by increased energy requirement, equipment complexity, and difficulty in membrane replacement.

Cleaning

It is good practice to measure the clean water flux, J_{H_2O}, of a TFF membrane prior to its initial use at anticipated operating conditions (T, ΔP, J, pH). Between batches, when J_{H_2O} has decreased to an unacceptably low value, say, 50% of J_{H_2O}, the membrane may be cleaned using hydraulic or chemical methods to restore J_{H_2O}. Hydraulic cleaning generally uses 45 L of clean, 40–50°C water/m^2 of membrane area at a crossflow velocity $\geq$ 1.5 m/s to dislodge and wash away gross soil. Pulsed reversal of permeate flow (backflushing) at a TMP that is a fraction of that in forward flow may assist in disrupting plugs or cake. One or more chemical cleaning agents such as alkalis (0.1 to 1.0-M NaOH, pH of 10–14); enzymes (proteases, amylases, 0.2% Terg-A-zyme®, pH 10); disinfectants (300 ppm sodium hypochlorite, pH 10; hydrogen peroxide); or nonionic alkaline detergents [0.1% sodium dodecyl sulfate (SDS) or Tween 80, pH 5–8] to remove organic deposits, or agents like acids (0.1–N H_3PO_4, pH 1) or complexing agents [e.g., EDTA] to remove inorganics are often alternated between clean-water flushes to remove soils. Manufacturers will typically recommend cleaning agents at concentrations compatible with a particular membrane. Membranes are usually stored in 0.1-M NaOH to prevent microbial growth between batches. An irreversible decline in J_{H_2O} usually results from a series of periodic use and cleaning cycles and ultimately requires membrane replacement.

Predicting Permeate Flux from Boundary-Layer Mass Transport

The film mass-transfer coefficient, $k_c = D_e/\delta$ in (14-117), may be obtained from Sherwood-number correlations for

laminar flow and turbulent flow using $N_{Sh} = k_c d_H / D_e$, where d_H is the hydraulic diameter

$$d_H = \frac{4(\text{cross-sectional area for flow})}{\text{wetted perimeter of flow channel}} \tag{14-120}$$

In §3.4, N_{Sh} was evaluated in laminar flow using the general Graetz solution for fully developed flow in a straight circular tube of diameter $D = d_H$ between limiting values of $N_{Sh} = 3.656$ for large distances, x, down the flow channel, and

$$N_{Sh} = \alpha \left(\frac{N_{Re} N_{Sc}}{x/D} \right)^{1/3} \tag{14-121}$$

for small x, where $\alpha = 1.077$ for $100 < N_{Re} N_{Sc} d_H / L < 5000$, as derived by Leveque [93]. In the latter regime, permeate flux, J, from TFF increases in proportion to the 1/3 power of average axial velocity. Values of N_{Sh} for a range of geometries and flow conditions may be obtained using a generalized form of (14-121) [32],

$$N_{Sh} = \alpha \left(\frac{d_H}{L} \right)^a \left(\frac{\rho d_H u_L}{\mu} \right)^b \left(\frac{\mu}{\rho D_e} \right)^c \tag{14-122}$$

where L is the length of the flow channel, u_L is the average axial velocity of the feed, and a, b, and c are coefficients. Values of b are often obtained empirically, whereas values of a and c are usually derived theoretically. Table 14.16 lists values of these coefficients for UF and MF in laminar and turbulent flow for tubes and channels. For example, in turbulent flow, flux (theoretically) increases in proportion to the 0.875 power of average axial velocity.

For UF in which laminar flow is fully developed, the Porter equation relates $k_c = D_e / \delta$ to a geometry-dependent shear rate, γ [93]:

$$k_c = 0.816 \left(\frac{\gamma}{L} D^2 \right)^{0.33} \tag{14-123}$$

where $\gamma = 8u_L / d_H$ for tubes and $\gamma = 6u_L / d_H$ for rectangular channels of height h.

Thus, flow may be increased, albeit to the power of 1/3, by raising channel velocity or decreasing channel height. Experimental data confirm application of (14-113)–(14-123) for a large number of macromolecular solutions including proteins as well as suspensions of colloidal particles such as latex beads [81].

Table 14.16 Coefficients of Sherwood Number for Mass Transport in TFF

	α	a	b	c
Laminar:				
UF, empirical	[93]	0	0.5	1/3
MF of cells, empirical	[93]	0	0.8	1/3
Tube, theoretical [93]	1.62	1/3	1/3	1/3
Channel, theoretical	1.86	1/3	1/3	1/3
Turbulent:				
UF	0.023	0	0.083 to 1.0	1/3
MF of cells	0.023	0	1.3	1/3
Theoretical	0.023	0	0.875	1/4

Shear-Induced Diffusion

TFF of particles above ~1 μm in size yields experimental flux values 1 to 2 logs higher than (14-117) evaluated with (14-121) [88]. This flux enhancement has been attributed to *shear-induced diffusion* of particles with diameters from about 1–30 μm and inertial lift of larger particles. Interactions (“collisions”) between particles concentrated on neighboring streamlines in shear flow cause transient displacements perpendicular to streamlines, which increase in proportion to shear rate and to the square of particle size. Each particle rotates in shear flow, producing rotational flow in nearby fluid that exerts drag forces on neighboring particles.

Effects of shear-induced diffusion may be examined by replacing Brownian diffusivity in (14-121) with a random-walk type of shear-induced hydrodynamic diffusivity D_s given by [94]:

$$D_s = \alpha \gamma_w a^2 \tag{14-124}$$

for small particles of radius a that constitute volume fraction $0.2 < \phi_b < 0.45$ in the bulk, where γ_w is the fluid shear at the membrane surface. The empirical α is reported to be ~0.025 for 1.6-mm disks and spheres. A value of 0.03 was applied to analyze shear-induced diffusion in UF [95].

EXAMPLE 14.16 Shear-Induced Diffusivity.

Compare hydrodynamic and shear-induced diffusivity values for a 1-μm particle at a shear rate of 1,000 s^{-1} [88].

Solution

From (14-124), shear-induced diffusivity is 3×10^{-7} cm^2/s. From (3-38), hydrodynamic diffusivity is 2×10^{-9} cm^2/s. Shear-induced diffusivity is about 150 times larger.

Substituting (14-124) and (14-123) into (14-121) shows that shear-induced diffusion enhances mass transport of 1–40-μm particles by a factor of $2.4 u_L a^2 / D_e D$. Using (14-116) gives a steady length-averaged transmembrane flux [53],

$$\langle J \rangle = \alpha \gamma_w \left(\frac{a^4}{L} \right)^{1/3} \ln \left(\frac{c_{i,w}}{c_{i,b}} \right) \tag{14-125}$$

where the coefficient α ranges from 0.126 for constant-viscosity fluids to 0.072 for fluids with a concentration-dependent viscosity [96]. The term $\ln(c_w / c_b)$ may be replaced by $(\phi_w / \phi_b)^{1/3}$ [88].

EXAMPLE 14.17 Membrane Flux for Fluid Shear.

Estimate the flux for a membrane module with $L = 30$ cm, in which particles of radius $a = 0.5$ μm at a relative concentration of $c_w / c_b = 10^3$ are separated using a fluid velocity that produces a typical shear rate of $\gamma_w = 4000$ s^{-1}.

Table 14.17 Predicted MF Flux Dependence on Brownian and Shear-Induced Diffusion and Inertial-Lift Transport Mechanisms [51]

Dominant Mechanism	Exponent	Brownian Diffusion	Shear-Induced Diffusion	Inertial Lift
Shear rate		Low	Intermediate	High
Particle size, a (μm)		<1	0.5–~40	>~30
Shear rate, γ_w	n	0.33	1	2
Particle size, a	m	−0.67	1.33	3
Volume fraction, ϕ_b	p	−0.33	−0.33	0
Filter length, L	q	−0.33	−0.33	0
Suspension viscosity, μ	r	−1	−0.33	−1

Solution

Using (14-125),

$$\langle J\rangle = 0.126\left(4\times10^3\right)\left[\frac{\left(5\times10^{-7}\right)^4}{0.3}\right]^{1/3}\ln\left(10^3\right)(3600)(1000)$$

$$= \text{a stable operating flux of } 74\ \text{L/m}^2\text{-h}.$$

Inertial Lift

Nonlinear hydrodynamic interactions arising from streamline distortions in the gap between particles greater than about 20 μm in diameter and the flow boundary of the surrounding flow field result in inertial lift, which carries dilute suspensions away from membrane walls with thin fouling layers. Inertial lift results in steady transmembrane flux in fast laminar flow of [97]:

$$J = \frac{0.036\,\rho a^3\gamma_w^2}{\mu} \tag{14-126}$$

for permeate with viscosity μ and density ρ [88].

A general form for steady permeate flux shown in (14-125) and (14-126) may be written as

$$J = c\gamma_w^n a^m \phi_b^p L^q \mu^r \tag{14-127}$$

where c is a model-specific constant and theoretical values of exponents n, m, p, q, and r are summarized in Table 14.17 for the three mechanisms. In each case, flux increases with γ_w and decreases with μ to varying degrees. Higher values of volume fraction and filter length decrease flux in the diffusion models but have no anticipated effect on inertial lift.

Table 14.18 Experimental Permeate Flux Dependence on Shear Rate for Laminar Flow [51]

Suspension	Shear-Rate Dependence, n
Styrene–butadiene latex polymers (5–50% solids by weight) [93]	0.5–0.85
Whole plasma [93]	0.33
Whole blood [93]	0.6
Bacteria (1% solids by weight) [98]	0.5–0.8
Colloidal impurities (5–10 μm) [99]	0.49–0.86
Yeast [100, 101]	0.4–0.7, 1.1
Bovine blood [102]	0.9

Flux decreases with particle size in Brownian diffusion, but increases with size in shear-induced diffusion and inertial lift. Experimental values for n from intermediate-sized particles in Table 14.18 are in a range consistent with the shear-induced diffusion model.

A larger net charge on a protein increases its diffusivity so that mass-transfer coefficients increase as |pH − pI| increases and as buffer conductivity decreases. For example, mass-transfer coefficients for a monoclonal antibody increase from 49 to 73 L/m^2-h as conductivity decreases from 20 to 1 mS/cm [53].

EXAMPLE 14.18 Membrane Flux Mechanisms.

Compare the steady-state flux in cm/s for typical conditions of $\gamma_w = 10^3\ \text{s}^{-1}$, $T = 293$ K, $\mu = 0.01$ g/cm-s, $\rho = 1.0$ g/cm^3, $\phi_w = 0.6$, $\phi_b = 0.01$, $L = 10$ cm, and $h = 0.1$ cm, for 1- and 50-μm particles using models for Brownian diffusion, shear-induced diffusion, and inertial lift [51].

Solution

Values for steady-state flux for each of the particles are summarized in Table 14.19. Shear-induced diffusion provides the largest flux for both particles. Inertial lift provides flux comparable to shear-induced diffusion for the 50-μm particles. For the 1-μm particles, diffusion provides a flux that is ~fourfold lower.

Table 14.19 Predicted Flux from Different Transport Mechanisms

Predicted flux (cm/s)	Brownian Diffusion	Shear-Induced Diffusion	Inertial Lift
$a = 1$ μm	6.3×10^{-5}	2.4×10^{-4}	4.5×10^{-7}
$a = 50$ μm	4.6×10^{-6}	4.4×10^{-2}	5.6×10^{-2}

Permeate Flux

An average value of permeate flux for a TFF system in (14-116) may be obtained from (14-4) by calculating an average value of TMP, ΔP_M, the driving force for TFF across a tangential-flow filter,

$$\Delta P_M = \frac{P_i + P_o}{2} - P_f \tag{14-128}$$

Table 14.20 Typical Values of TMP in TFF

	TMP (psi)
MF	<15
UF	15–150
RO	450–1200

where subscript i represents inlet or feed, o represents outlet or retentate, and f is filtrate, whose pressure is often atmospheric pressure. Typical TMP values for TFF are summarized in Table 14.20.

Increasing ΔP_M eventually raises $c_{i,w}$ in (14-114)–(14-116) to a limiting solubility point at which accumulated solute forms a semisolid gel [103]. Further increases in ΔP_M beyond gel formation increase the thickness of the gel layer and decrease solvent flux. From (14-4) and (14-128), the flux corresponds to

$$J = \frac{\Delta P_M - R_i \Delta\pi}{\mu(R_g + R_M)} \tag{14-129}$$

where $\Delta\pi$ is the osmotic pressure of the polarized solute, defined in (14-90) to (14-93), which resists the superimposed ΔP_M driving force; R_g is the resistance due to the gel formed by CP, which varies with solute composition, concentration, and tangential velocity across the membrane; and R_M is the membrane resistance. Osmotic pressure of a 20°C solution of 50 kg/m^3 sucrose (MW 342) is 0.356 MPa (51.6 psi), whereas it is 1.22×10^{-5} MPa (1.77×10^{-3} psi) for a large colloid (~20 nm; MW = 10^7) at the same concentration and temperature. Permeate flux is maximized in practice by identifying optimal values of transmembrane velocity and ΔP_M, below which filtration rate increases linearly with TMP and above which filtration rate decreases due to reduced velocity.

Economics

The cost of installing a fully automated sanitary-filter system, complete with pumps, piping, tanks, and membrane, is summarized in Table 14.21 for five different membrane systems [105]. Also shown is the cost for periodic replacement of membrane modules. Permeate flux varies with the chosen configuration, which impacts the total installed and consumables cost per unit volume of feed.

Table 14.21 Costs of Sanitary-Filter System Installation and Membrane Replacement [105]

	Cost ($/m^2)	
Membrane System	System Installation Capital	Consumable Replacement
Spiral-wound	150–600	30–80
Tubular	1000–1500	100–200
Hollow-fiber	1500–2000	110–160
Plate-and-frame	1500–5000	300–700
Ceramic	5000–15,000	2000–2500

To estimate cost of energy consumed and process fluid heating, the pump power, P_o, in kW required to achieve a tangential-flow rate Q in m^3/h for a given pressure increase across the pump ΔP_{pump} in psi may be estimated as

$$P_o = \frac{Q \Delta P_{\text{pump}}}{522\eta} \tag{14-130}$$

where the pump and motor fractional efficiency, η, has typical values ranging from 0.85 for positive displacement pumps to 0.65 for centrifugal pumps.

Process Configurations

Four configurations or combinations thereof are used for TFF: (1) batch TFF, (2) continuous bleed-and-feed TFF, (3) batch diafiltration, and (4) continuous bleed-and-feed diafiltration. Each of these configurations is next discussed in detail and illustrated by examples.

Batch TFF

Figure 14.32 shows a batch configuration where the membrane unit consists of cartridges in parallel. Initially, the feed tank is filled with a batch, V_F, of feed with solute concentration c_F. The solution is pumped through the cartridges, where permeate is continuously removed but retentate is recycled, usually at a high volumetric flow rate, Q, to minimize fouling. As solvent selectively passes through the membrane, the retained volume of solution in the system, $V\{t\}$, decreases and its retentate solute concentration, $c_R\{t\}$, increases. Operation is terminated when the desired solute retentate concentration, c_R, is reached. At that point, the feed tank and associated equipment contain the final retentate, V_R, which can be drained to another tank. After cleaning, another batch is processed. The required time for batch processing depends on the membrane area, A, and permeate flux J, which decreases with time due to increasing solute concentration on the upstream side, as evidenced in Figure 14.31.

Assume the feed contains completely rejected solutes and only partially rejected solutes, and that the flux is a linear function of the logarithm of the concentration factor, CF,

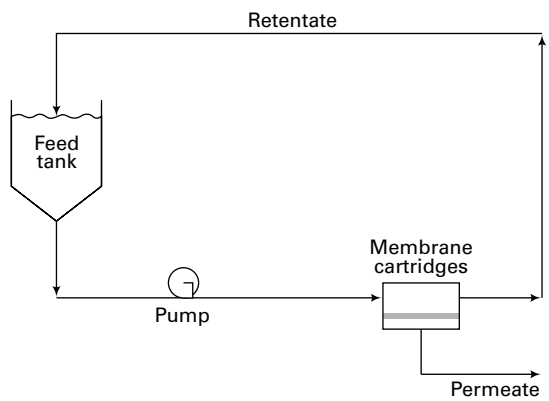

Figure 14.32 Batch TFF.

where for the batch process of Figure 14.32, CF as a function of time is

$$CF = \frac{V_F}{\text{retained } V\{t\}} \tag{14-131}$$

Then, it can shown that the average flux, J_{avg}, for the batch process is approximately

$$J_{avg} = J\{c_F\} - 0.33[J\{c_F\} - J\{c_R\}] \tag{14-132}$$

where values of $J\{c_F\}$ and $J\{c_R\}$ are from experimental data like that in Figure 14.31. The required membrane area as a function of batch processing time, t, becomes

$$A = \frac{V_P}{t\,J_{avg}} = \frac{V_F - V_R}{t\,J_{avg}} \tag{14-133}$$

To obtain a solute material balance, note that solute concentration in the retained volume is a function of both the reduction in retained volume and the amount of solute that passes through the membrane. A solute, i, material balance for a differential volume passing through the membrane is, by analogy to (14-69) for gas permeation,

$$\frac{dV}{V} = \frac{dc_{i_R}}{c_{i_P} - c_{i_R}} \tag{14-134}$$

Combining with (14-117) for the definition of rejection, σ_i,

$$\frac{dV}{V} = \frac{dc_{i_R}}{\sigma_i c_{i_R}} \tag{14-135}$$

Integrating this equation from initial feed to final retentate gives an equation for retentate solute concentration as a function of retained volume, where if the retained volume is the final volume, its solute concentration is c_{i_F}.

$$c_{i_R} = c_{i_F}\left(\frac{V_F}{V_R}\right)^{\sigma_i} = c_{i_F}(CF)^{\sigma_i} \tag{14-136}$$

The yield, Y_i, of solute i, defined as the amount of feed solute that is retained in the retentate, is obtained from (14-136):

$$Y_i = \frac{c_{i_R}V_R}{c_{i_F}V_F} = \left(\frac{V_F}{V_R}\right)^{\sigma_i}\left(\frac{V_R}{V_F}\right) = \left(\frac{V_F}{V_R}\right)^{\sigma_i - 1} = CF^{\sigma_i - 1} \tag{14-137}$$

Application of (14-131) to (14-137) is illustrated in the following analysis of ultrafiltration using batch TFF.

EXAMPLE 14.19 Batch UF of an Aqueous Feed.

An aqueous feed of 1,000 L is to undergo batch UF with a polysulfone membrane. Solute concentrations and their measured rejection values are:

Solute	Type Molecule	MW	Concentration, c, g/L	Rejection, σ
Albumin	Globular	67,000	10	1.00
Cytochrome C	Globular	13,000	10	0.70
Polydextran	Linear	100,000	10	0.05

Polydextran has the highest MW, but the lowest rejection because it is a linear rather than a globular molecule. The volume of the final retentate is to be 200 L, which is achieved in a 4-hour batch-processing time. Thus, from (14-118), $CF = 1{,}000/200 = 5$. From experimental measurements, the flux values are 30 L/m^2-h at $CF = 1$ and 10 L/m^2-h at $CF = 5$. Calculate the solute concentration in the final retentate, the yield of each solute, and the membrane area. Neglect changes in solution density.

Solution

From (14-132), the average flux $= 30 - 0.33(30 - 10) = 23.4$ L/m^2-h. The total permeate volume $= 1{,}000 - 200 = 800$ L. From (14–133), for $t = 4$ h,

$$A = \frac{800}{4(23.4)} = 8.55\ \text{m}^2$$

Using (14-137) and (14-136), the yield and concentration of each solute in the final retentate are

Solute	Concentration in Final Retentate, g/L	% Yield
Albumin	50.0	100.0
Cytochrome C	30.9	61.7
Polydextran	10.8	21.7

Note that although polydextran has a very low rejection, value neither the final concentration in the retentate nor the % yield approaches zero.

Batch TFF may damage proteins or cells due to retentate recycle, or allow bacterial growth if residence times are too long. In such circumstances, continuous UF, which is widely used for large-scale processes, is preferred.

Continuous Feed-and-Bleed TFF

Although, as shown in Figure 14.20, continuous reverse osmosis usually operates in a single-pass mode, continuous TFF operates in a multipass mode, called single-stage *feed-and-bleed*, as shown in Figure 14.33. This is achieved by recycling, at steady state, a large fraction of the retentate. In effect, membrane feed is the sum of fresh feed and recycle retentate. The bleed is that portion of the retentate not recycled, but withdrawn as product retentate.

At startup the entire retentate is recycled until the desired retentate concentration is achieved, at which time bleed is initiated. The advantages and disadvantages of feed-and-bleed operation are considered by Cheryan [106] and Zeman and Zydney [56]. The single-pass mode is usually unsuitable

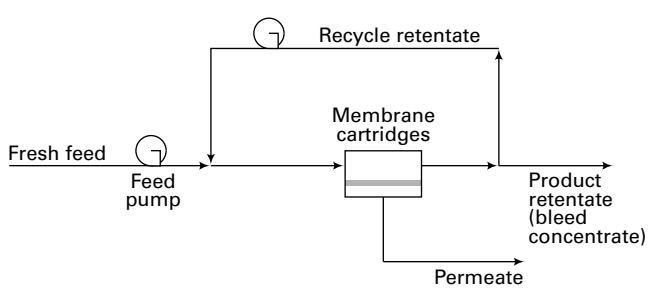

Figure 14.33 Single-stage continuous feed-and-bleed ultrafiltration.

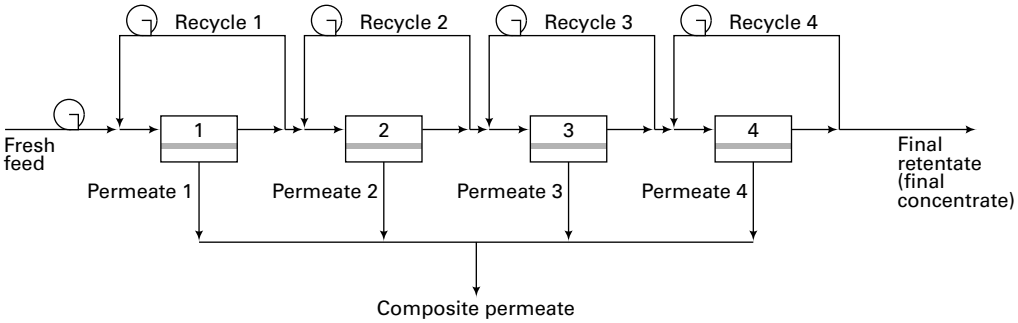

Figure 14.34 Multistage, continuous feed-and-bleed TFF.

for TFF because the main product is the concentrate rather than permeate (as in reverse osmosis), and high yields of permeate are required to adequately concentrate retentate solutes. Typically, the concentration factor, CF, defined by (14-118), has a value of 10. As a result, a single-pass TFF requires a long membrane path or a very large area. A disadvantage of the feed-and-bleed mode, however, is that with the high recycle ratio, the concentration of solutes on the retentate side is highest, resulting, as shown in Figure 14.31, in the lowest flux, with a resulting membrane area larger than that for the batch mode. To counter this, the feed-and-bleed mode is often conducted with four stages, as in Figure 14.34, where the retentate (bleed) from each stage is sent to the next stage, while the permeates from the stages are collected into a final composite permeate. Solute concentrations increase incrementally as the retentates pass through the system. The final and highest concentration is present only in the final stage. As a result, retentate concentrations are lower and fluxes higher than for a single-stage, bleed-and-feed system, for all but the final stage; thus, the total membrane area is smaller. In practice, three to four stages are optimal.

For a single-stage, continuous bleed-and-feed TFF, the material-balance equations in terms of volumetric flow rates and concentrations are:

Total balance: $$Q_F = Q_R + Q_P \tag{14-138}$$

Solute total balance: $$c_{i_F} Q_F = c_{i_R} Q_R + c_{i_P} Q_P \tag{14-139}$$

If the recycle rate is sufficiently high, concentration of the stream flowing on the upstream side of the membrane will be the retentate. Then, if (14-138) and (14-139) are combined with (14-110) and (14-118), rejection in the stage and CF are constant and based on retentate, such that the equation for computing the solute retentate concentration becomes:

$$c_{i_R} = c_{i_F}\left[\frac{CF}{CF(1-\sigma_i)+\sigma_i}\right] \tag{14-140}$$

Area is given by (14-133) in continuous-process form as

$$A = \frac{Q_P}{J\{\text{at } CF\}} \tag{14-141}$$

Solute yield in continuous-process form is given by combining (14-137) with (14-118) and (14-140):

$$Y_i = \frac{c_{i_R} Q_R}{c_{i_F} Q_F} = \frac{1}{CF(1-\sigma_i)+\sigma_i} \tag{14-142}$$

For the four-stage, continuous feed-and-bleed TFF system in Figure 14.34, (14-138) to (14-142) are applied to each stage. It is assumed that the most desirable multistage system is one in which all stages have the same membrane area, to reduce cost of maintenance. The calculations, as described below in Example 14.20, are iterative in nature, using an outer loop in which membrane area per stage is assumed, and an inner loop in which an overall concentration parameter is assumed.

Diafiltration

As seen in Figure 14.31, when a high degree of separation is desired, the flux drops to a low value. To overcome this when it is necessary to continue removing permeable solutes from solutes of little or no permeability, diafiltration, which involves the addition of solvent (usually water) to the retentate, followed by filtration, can be employed. Additional solvent dilutes the retentate to increase the flux in order to achieve a defined solute concentration. The final retentate is not as concentrated in retained solutes, but contains a smaller fraction of permeable solutes.

Diafiltration is conducted in the same modes as UF, i.e., batch or continuous feed-and-bleed, including multistage systems. The added amount of solvent is a variable whose value, for preliminary calculations, may be set equal to the amount of permeate.

Consider a batch diafiltration in which retentate from the previous step is added to the feed tank and recycled, without permeate withdrawal from the membrane unit during startup. Dilution solvent is then added at a continuous rate to the feed tank, under perfect-mixing conditions, with permeate withdrawal at a rate equal to the solvent-addition rate. This operation is sometimes referred to as *fed-batch* or semicontinuous. If the recycle rate is very high, the concentrations of solutes in the membrane unit will be uniform on each side of the membrane; thus rejection in the membrane at any instant is given by (14-110), where both concentrations change with time. Let c_i = the instantaneous solute concentration in the recycle retentate. Initially, before solvent is added, its value is that of the feed, c_{i_F}. If c_{i_P} = the instantaneous permeate solute concentration leaving the membrane unit, (14-110) becomes

$$\sigma_i = 1 - \frac{c_{i_P}}{c_i} \tag{14-143}$$

With a constant volume, V_F, in the feed tank before solvent is added, an instantaneous solute material balance equates the decrease in the amount of solute in the feed tank to the amount of solute appearing in the permeate. But permeate flow rate, Q_P, is equal to the solvent addition rate, $Q_S = dV_S/dt$, giving

for a solute material balance

$$-V_F \frac{dc_i}{dt} = c_{i_P} Q_P = c_{i_P} \frac{dV_S}{dt} \tag{14-144}$$

Combining (14-143) and (14-144) to eliminate c_{i_P} gives, in integral form over time for diafiltration to the final retentate concentration,

$$\int_{c_{i_F}}^{c_{i_R}} \frac{dc_i}{c_i} = -\frac{(1-\sigma_i)}{V_F} \int_0^{V_{S_{\text{total}}}} dV_S \tag{14-145}$$

Integration gives an equation for computing the final retentate concentration:

$$c_{i_R} = c_{i_F} \exp\left[-\frac{V_{S_{\text{total}}}}{V_F}(1-\sigma_i)\right] \tag{14-146}$$

Continuous diafiltration design is similar to continuous ultrafiltration design, as will be illustrated in Example 14.20.

A major industrial application of UF is in processes for manufacturing protein concentrates from skim milk. The milk is coagulated to render two products: (1) a thick precipitate called curd, rich in a phosphoprotein called casein, which is used to make cheese, plastics, paints, and adhesives; and (2) whey (or cheese whey), a watery, residual liquid. One hundred pounds of skim milk yields approximately 10 pounds of curd and 90 pounds of whey. Typically, whey consists, on a mass basis, of 93.35% water; 0.6% true protein (TP) of molecular weight ranging from 10,000 to 200,000; 0.3% nonprotein nitrogen compounds (NPN); 4.9% lactose (a sugar of empirical formula $C_{12}H_{22}O_{11}$ and MW of 342, which has an ambient solubility in water of about 10 wt%); 0.2% lactic acid ($C_3H_6O_3$) of molecular weight 90, which is very soluble in water; 0.6% ash (salts of calcium, sodium, phosphorus, and potassium) of MW from 20 to 100; and 0.05% butter fat.

Proteins are macromolecules consisting of sequences of amino acids, which contain both amino and carboxylic-acid functional groups. When digested, proteins become sources of amino acids, which are classified as nutritionally essential or nonessential. The *nonessential amino acids* are synthesized by a healthy body from metabolized food. *Essential amino acids* cannot be synthesized by the body, but must be ingested. Amino acids are building blocks for health that repair body cells, build and repair muscles and bones, regulate metabolic processes, and provide energy.

Proteins in whey, on a mass basis, are betalactoglobulin (50–55%), alpha-lactalbumin (20–25%), immunoglobulins (10–15%), bovine serum albumin (5–10%), and smaller amounts of glycomacropeptide, lactoferrin, lactoperoxidase, and lysozyme. The first five of these eight proteins provide an excellent source of all eight essential amino acids: isoleucine, leucine, lysine, methionine, phenylalanine, threonine, tryptophan, and valine. Approximately 35 wt% of proteins in whey provide amino acids. The nonprotein nitrogen compounds include ammonia, creatine, creatinine, urea, and uric acid, with MW of 17–168.

To obtain dry protein concentrate from whey requires a number of processes. Most involve UF, separating by size exclusion based on MW and shape. For separation purposes, the compounds in whey consist of five groups: (1) true protein and butter fat, (2) nonprotein nitrogen, (3) lactose, (4) lactic acid and ash, and (5) water. A typical process is shown in Figure 14.35. Whey is pumped to UF Section I, where the exiting retentate (concentrate) contains all of the protein. The other whey-feed components leave in the exiting permeate. The retentate is further concentrated in an evaporator and then spray-dried to produce a *whey-protein concentrate*. Permeate is pumped to UF Section II, where all remaining lactose is retained and sent to a second spray dryer to produce *lactose-rich concentrate*, while the permeate is sent to wastewater treatment. Whey-protein concentrate produced by this process contains too high a lactose content for the millions of individuals who are "lactose intolerant" because of susceptibility to digestive disorders. To produce so-called *whey-protein isolate* of 90–97 wt% protein and almost no lactose or fat, the process of Figure 14.35 is modified by additional ultrafiltration. The following example, based on information in the 2001 AIChE National Student Design Competition, involves an ultrafiltration section for producing a protein concentrate.

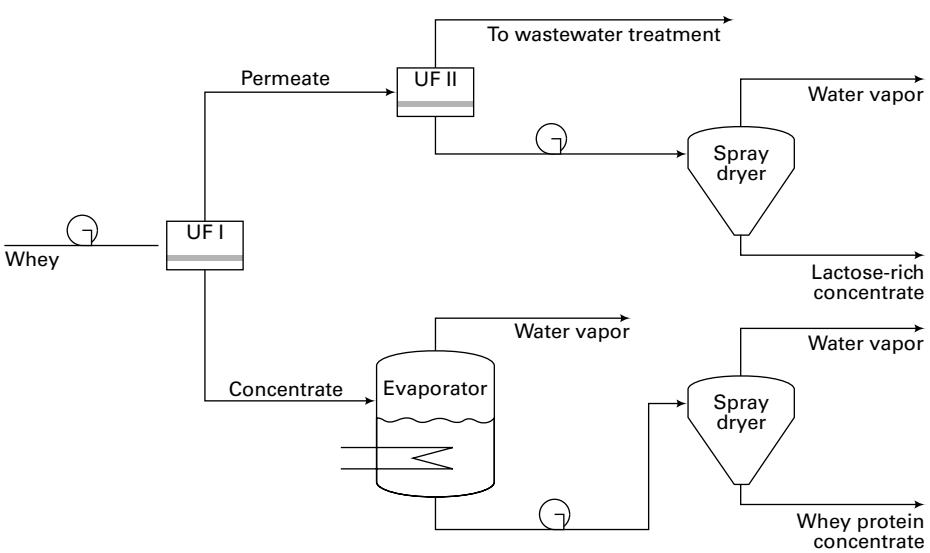

Figure 14.35 Whey process to produce protein and lactose concentrates.

EXAMPLE 14.20 Ultrafiltration Process for Whey.

A cheese plant produces a byproduct stream of 1,000,000 lb/day of whey, to be further processed to obtain a dry powder containing 85 wt% combined TP (true protein) and NPN (nonprotein nitrogen compounds). The process includes three sections: (1) four stages of continuous bleed-and-feed ultrafiltration to reach 55 wt% (dry basis), followed by (2) four stages of continuous diafiltration to reach 75 wt% (dry basis), followed by (3) one stage of batch diafiltration to reach the final 85 wt% (dry basis), with a batch-time limit of 4 hours. Diafiltration must be used above 55 wt% because the retentate from UF becomes too viscous. Each section will use PM 10 ultrafiltration hollow-fiber membrane cartridges from Koch Membrane Systems, which are 3 inches in diameter by 40 inches long, with 26.5 ft^2 of membrane area, at a cost of $200.00 each. For each cartridge, the recirculation (recycle) rate is 23 gpm. The number of cartridges is to be the same in each stage for Sections 1 and 2. The inlet pressure to each is 30 psig, with a crossflow pressure drop of 15 psi and a permeate pressure of 5 psig. For these conditions, the membrane flux has been measured for the whey and correlated as a function of the concentration factor, *CF*, by:

$$\text{membrane flux, gal/ft}^2\text{-day} = 27.9 - 5.3\ln(CF) \qquad (1)$$

where *CF*, for any stage *n*, is defined by reference to the fresh feed to Section 1, as

$$CF_n = F_{\text{Section 1}}/R_n$$

Whey composition and membrane–solute rejections, σ, are:

Component	Wt% in Whey	Flow Rate in Whey, lb/day	Solute Rejection, σ
Water	93.35	933,500	—
True protein, TP	0.6	6,000	0.970
Nonprotein nitrogen, NPN	0.3	3,000	0.320
Lactose	4.9	49,000	0.085
Ash	0.8	8,000	0.115
Butter fat	0.05	500	1.000

Based on σ values, the membrane increases the concentration of TP while selectively removing the low-MW solutes of lactose and ash. Whey and all retentate and permeate streams have a density of 8.5 lb/gal. The continuous sections of the process will operate 20 hr/day, leaving 4 hr/day to remove accumulated membrane foulants and sterilize equipment. For each section, calculate: (1) component material balances in lb/day of operation, including dilution water for diafiltration; (2) percent recovery from whey of TP and NPN in the intermediate and final 85 wt% concentrate; and (3) number of membrane cartridges. Also, for Section 1, make calculations for a single continuous stage, compare results to those for four stages, and discuss advantages and disadvantages of four stages versus one stage.

Solution

The flow diagram for the ultrafiltration–diafiltration process is shown in Figure 14.36.

Single Continuous UF Stage for Section 1 to Reach 55 wt% TP + NPN

First compute results for Section 1 using the single-stage continuous bleed-and-feed UF shown in Figure 14.33. Assume $CF = 10$ and

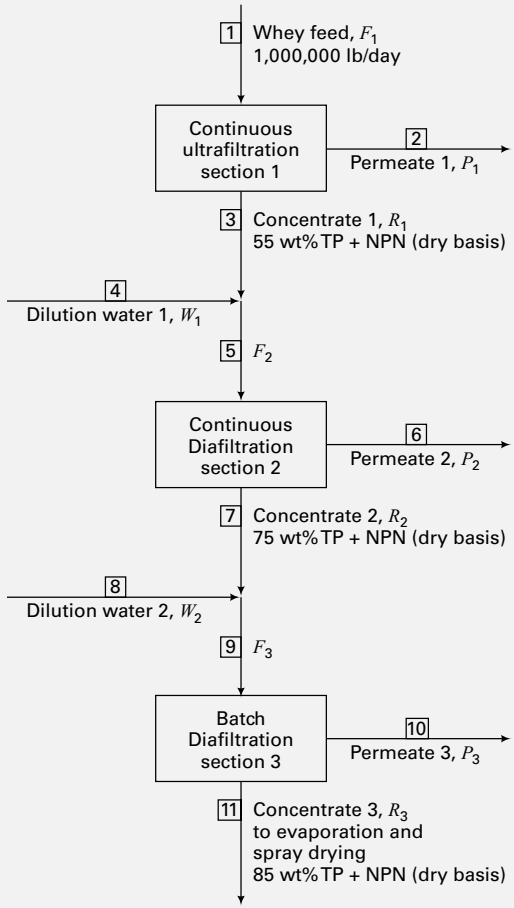

Figure 14.36 Process for Example 14.20.

compute by material balance from the whey-feed rate—F_1 = 1,000,000 lb/day—flow rates of retentate (concentrate) R_1, and permeate P_1. By definition of *CF* for this type of ultrafiltration, $R_1 = F_1/CF = 1{,}000{,}000/10 = 100{,}000$. Therefore, $P_1 = F_1 - R_1 = 1{,}000{,}000 - 100{,}000 = 900{,}000$ lb/day. Next, use a mass flow rate form of the yield equation, (14-142), to compute each solute flow rate in the concentrate. For TP,

$$(m_{\text{TP}})_{R_1} = \frac{(m_{\text{TP}})_{F_1}}{[CF(1-\sigma)+\sigma]} = \frac{6000}{[10(1-0.97)+0.97]} = 4724 \text{ lb/day}$$

Similarly, flow rates of other solutes in the concentrate R_1 are computed as follows, where the water rate is by difference:

Concentrate for a Single Stage of Continuous Ultrafiltration in Section 1, for an Assumed $CF = 10$

Component	Wt% in Concentrate, C_1	Flow Rate in Concentrate, C_1, lb/day
Water	88.157	88,157
True protein, TP	4.724	4,724
Nonprotein nitrogen, NPN	0.421	421
Lactose	5.306	5,306
Ash	0.892	892
Butter fat	0.500	500
Total	100.000	100,000

From this table, the wt% TP + NPN in the concentrate on a dry basis is (4,724 + 421)/(100,000 − 88,157) = 0.4344 or 43.44 wt% (dry basis), which is less than the 55-wt% target. Therefore, the assumed $CF = 10$ is too low. Using a spreadsheet, the Solver function finds $CF = 24.955$, which meets the 55-wt% target. This result gives the following concentrate:

Concentrate for a Single Stage of Continuous Ultrafiltration in Section 1, for the Correct $CF = 24.955$

Component	Wt% in Concentrate, C_1, lb/day	Flow Rate in Concentrate, C_1, lb/day
Water	83.372	33,409
True protein, TP	8.713	3,491
Nonprotein nitrogen, NPN	0.433	174
Lactose	5.335	2,138
Ash	0.899	360
Butter fat	1.248	500
Total	100.000	40,072

The wt% TP + NPN in the concentrate is now (3,491 + 174)/(40,072 − 33,409) = 0.5500 or 55.00%, the specified value.

It is also of interest to compute the % yield of TP + NPN:

$$(3491 + 174)/(6000 + 3000) = 0.4072 \text{ or } 40.72\%$$

Membrane area for this single stage is computed from (14-141). The permeate rate is $P_1 = F_1 - R_1 = 1{,}000{,}000 - 40{,}072 = 959{,}928$ lb/day or 959,928/8.5 = 112,933 gal/day. For 20-h/day operation, the volumetric permeate rate = 112,933/20 = 5,647 gal/h. From (1), for the computed CF,

$$\text{membrane flux} = 27.9 - 5.3\ln(CF) = 27.9 - 5.3\ln(24.955)$$
$$= 10.85 \text{ gal/ft-day or } 10.85/24 = 0.452 \text{ gal/ft}^2\text{-h}$$

Therefore, from (14-141), the membrane area = 5,647/0.452 = 12,490 ft^2. Each cartridge has an area of 26.5 ft^2; therefore, 12,490/26.5 = 471 parallel cartridges are needed. Total fresh feed rate based on 20 hr of operation is

$$\frac{1.000{,}000}{8.5(20)} = 5,882 \text{ gal/h}$$

Fresh feed rate to each cartridge is

$$\frac{5{,}882}{60(471)} = 0.208 \text{ gal/min/cartridge}$$

The combined flow rate (fresh plus recycle) to each cartridge is 0.208 + 23 = 23.208 gal/min, which is a desirable recycle ratio.

To increase the % yield and decrease the number of cartridges, a multistage section is needed. In the problem statement, four stages in series are specified. These are computed next.

Four Continuous UF Stages for Section 1 to Reach 55 wt% TP + NPN

Calculations are based on an equal membrane area for the four stages in Figure 14.34. They are made by a double "trial-and-error" (nested-iteration) procedure, which is best carried out using a spreadsheet with a Solver function. Assume a membrane area per stage. Because the single-stage calculation resulted in an area of 12,500 ft^2, and there are four stages, the total area for four stages will be smaller. First, assume a total area of 8,000 ft^2 or 2,000 ft^2 per stage = A. Next, find, by iteration, the overall concentration factor, $\overline{CF}$, that gives the fresh feed rate to the first stage, as calculated above, of 5,882 gal/h. This is done with a spreadsheet starting from Stage 4 and working backward to Stage 1, using the following equations, where J_n = hourly membrane flux = (1)/24 of Eq. (1), based on a CF using F_1 and R_n. For Stage 4, CF_4 = the assumed $\overline{CF}$ and $R_4 = F_1/CF_4$. Then, for the calculations back to Stage 1:

$$P_n = AJ_n; \quad R_{n-1} = P_n + R_n; \quad CF_{n-1} = F_1/R_{n-1}$$

When Stage 1 is reached by calculation of P_1, the fresh feed rate is computed from $F_1 = P_1 + R_1$. If F_1 is not 5,882 gal/h, new values of $\overline{CF}$ are assumed until the correct value of F_1 is obtained. This iteration can be done with the spreadsheet Solver function. If $\overline{CF} = 20$ and $A = 2{,}000$ ft^2 are assumed, the results are as follows, where all flows are in gal/h:

$\overline{CF}$	R_4	P_4	R_3	P_3	R_2	P_2	R_1	P_1	F_1
20	294	1002	1296	1657	2953	2021	4974	2250	7224
61.2	96.2	508	604	1320	1924	1831	3755	2127	5882

The tabulation shows $F_1 = 7{,}224$ gal/h, which is too high. Using the Solver function, $\overline{CF} = 61.2$ gives the correct F_1, with the corresponding computed values of CF_n and J_n:

$\overline{CF}$	CF_4	J_4	CF_3	J_3	CF_2	J_2	CF_1	J_1
61.2	61.2	0.254	9.735	0.660	3.057	0.916	1.566	1.063

However, the assumed membrane area per stage may not be correct. To check this, calculations similar to those above are carried out with a spreadsheet, starting with Stage 1 and proceeding stage-by-stage to Stage 4. Pertinent results for $A = 2{,}000$ ft^2 per stage and $\overline{CF} = 61.2$ are:

Stage	1	2	3	4
Wt% TP + NPN in retentate from stage (dry basis)	17.47	25.46	44.96	74.16

Because TP + NPN in the retentate from Stage 4 is 74.16 wt% (dry basis), which is higher than the specified 55 wt%, calculations must be repeated for other values of membrane area per stage. For each assumed membrane area, a new value of $\overline{CF}$ that gives the correct fresh feed rate must be found. The following spreadsheet results are obtained when iterating on A and $\overline{CF}$:

A, Membrane Area per Stage, ft^2	$\overline{CF}$ for Correct Fresh Feed Rate	Wt% TP + NPN in Final Retentate (dry basis)
2,000	61.2	74.16
1,750	26.9	63.22
1,700	22.5	60.26
1,650	18.8	57.14
1,600	15.7	53.95
1,617	16.65	55.00

For a continuous, four-stage UF system, with equal membrane area per stage, the desired value of 55 wt% (dry basis) for TP + NPN in

the retentate (concentrate) from Stage 4 corresponds to $A = 1{,}617$ ft^2 per stage and an overall concentration factor, $\overline{CF}$, of 16.65. From these results, the material balance—which includes the combined permeate from four UF stages and the computed retentate (concentrate) of 55 wt% that leaves Stage 4 and becomes feed to the continuous diafiltration section to increase TP + NPN to 75 wt% (dry basis)—is as presented in the following table:

Concentrate and Combined Permeate from a Four-Stage Continuous UF in Section 1, for a $\overline{CF}$ of 16.65 and $A = 1{,}617$ ft^2/Stage, which Meets the 55 wt% Specification

Component	Flow Rate of Whey, lb/day	Flow Rate of Concentrate, lb/day	Flow Rate of Combined Permeate, lb/day
Water	933,500	49,897	883,603
True protein, TP	6,000	5,245	755
Nonprotein nitrogen, NPN	3,000	353	2,647
Lactose	49,000	3,476	45,524
Ash	8,000	603	7,397
Butter fat	500	500	0
Total	1,000,000	60,074	939,926

For Section 1, the number of ultrafiltration cartridges required is $1{,}617/26.5 = 61$ cartridges per stage or a total of 244 cartridges for four stages. The % yield of TP + NPN in the concentrate is $(5{,}245 + 353)/(6{,}000 + 3{,}000) \times 100\% = 62.20\%$. These results compare to 471 cartridges and a % yield of 40.72% for a single stage in Section 1. On both counts, the four-stage system is preferred. However, a definitive economic analysis would include additional piping and instrumentation costs for a four-module system.

Four Continuous Diafiltration Stages for Section 2 to Reach 75 wt% TP + NPN

The following procedure is based on equal membrane areas for the four stages, based on a flow diagram similar to Figure 14.34, differing only in the addition of water to the feed to each stage. Calculations for a continuous, multistage diafiltration system require iteration on a single variable, the added water rate, to achieve the specified 75 wt% TP + NPN. This is done with a spreadsheet using the Solver function.

For each diafiltration stage, the added water rate, W_n, is the same and is equal to W. The permeate rate, P_n, for each stage is set equal to the added water rate. Therefore, the feed rates to the stages, F_1 for the first stage and R_{n-1} for the succeeding three stages (i.e., before the added water and the recycle), are all equal to the retentate (concentrate) rate, R_n, sent to the next stage, and all retentate rates are the same, i.e., $F_1 = R_n$. These simplifications result in the same concentration factor, $\overline{CF}$, for every stage:

$$\overline{CF} = \frac{W + F_1}{F_1} \tag{2}$$

For a continuous diafiltration system of n stages, with solute i, flow rates in the concentrate from the final stage are given by an equation, obtained by applying (14-142) successively to each stage, that sets the solute flow rate in the feed to Stages 2, 3, and 4 equal to the flow rate in the retentate from the preceding stage:

$$(m_i)_{R_n} = (m_i)_{F_1}\left[\frac{1}{\overline{CF}(1-\sigma_i)+\sigma_i}\right]^n \tag{3}$$

Using a spreadsheet, (2) and (3) are solved, where values of $(m_i)_{F_1}$ are solute component flow rates in the concentrate leaving Section 1, as given in the table above. Solute rejections, σ_i, are given in the problem statement. A value is assumed for the added water rate to each stage, W, and $\overline{CF}$ is computed from (2). From (3), values of $(m_i)_{R_n}$ are computed for each solute. The wt% TP + NPN (dry basis) is then calculated, and if it is not the specified 75 wt%, a new value of W is chosen. Assume W at half the feed rate F_1, or $60{,}074/2 = 30{,}037$ lb/day. From (1), $\overline{CF} = (30{,}037 + 60{,}074)/60{,}074 = 1.50$. For TP, from (3),

$$(m_{TP})_{R_4} = 5{,}245\left[\frac{1}{1.50(1-0.97)+0.97}\right]^4 = 4{,}942 \text{ lb/day}$$

The calculations are repeated for other components, and the water rate in the concentrate from Stage 4 of Section 2 is determined so that the total concentrate flow rate equals that of the feed, 60,074 lb/day. The wt% TP + NPN in the concentrate is then calculated, with a result of 78.2 wt%, which is higher than the specified 75 wt%. Using the Solver function, the correct water rate for each stage is found to be 23,332 lb/day or a total of 93,328 lb/day for the four stages, with a corresponding $\overline{CF} = 1.388$. The resulting material balance—which includes the combined permeate and the computed retentate (concentrate) of 75 wt% that leaves Stage 4 to become the feed to the batch diafiltration section to increase the wt% TP + NPN to 85% (dry basis)—is as presented in the next table.

Concentrate and Combined Permeate from a Four-Stage Continuous Diafiltration in Section 2, and an Added Water Rate of 23,332 lb/day per Stage, which Meets the 75 wt% Specification

Component	Flow Rate in Feed to Section 2, lb/day	Flow Rate in Concentrate, lb/day	Flow Rate in Combined Permeate, lb/day
Water	49,897	53,214	90,011
True protein, TP	5,245	5,007	238
Nonprotein nitrogen, NPN	353	138	215
Lactose	3,476	1,030	2,446
Ash	603	185	418
Butter fat	500	500	0
Total	60,074	60,074	93,328

From these results, the yield of TP + NPN from diafiltration is $(5{,}007 + 138)/(5{,}245 + 353) \times 100\% = 91.91\%$ for an overall yield, to this point, of $(0.9191)(0.6220) \times 100\% = 57.17\%$. The membrane flux for each stage is obtained from (1). However, the CF used in that equation is the ratio of the whey feed for the process to the retentate rate from the stage, which for the four stages of diafiltration is the same as that for the last stage of the ultrafiltration in Section 1. A value of $CF = 1{,}000{,}000/60{,}074 = 16.65$ applies, which results in a membrane flux of 0.5415 gal/h-ft^2. The volumetric permeate flow rate per stage $= 93{,}328/[(20)(4)(8.5)] = 137$ gal/h. The membrane area required per stage $= 137/0.5415 = 253$ ft^2. The number of cartridges per stage $= 253/26.5 = 9.5 \approx 10$ cartridges per diafiltration stage, for a total of 40 diafiltration cartridges.

These results for four stages of diafiltration may be compared to the results obtained with just a single continuous diafiltration stage, which gives an added water rate of 167,200 gal/day (compared to 93,328 for four stages) and an overall TP + NPN yield of 55% (compared to 57% for four stages).

A Single Batch Diafiltration Stage for Section 3 to Reach 85 wt% TP + NPN

The final membrane section is a single batch diafiltration with maximum batch time of 4 hr. A feed tank is filled with concentrate from Section 2, and water is added continuously over the 4-hr period to maintain the liquid level in the tank. With a high recycle ratio, the concentration of solutes in the retentate is maintained constant, with solute i, and flow rates in the concentrate feed are given by (14-146) in mass flow form:

$$(m_i)_R = (m_i)_F \exp\left[-\frac{W}{F}(1-\sigma_i)\right] \tag{4}$$

where W and F are amounts of additional water and feed processed during the 4-hr period. To reach 85 wt%, it is important to remove the lactose from the feed. For example, suppose the daily amount of added water is equal to the daily amount of feed from Section 2. Then, $W/F = 1$. From the preceding table, that feed contains 1,030 lb/day of lactose, which has the rejection $\sigma = 0.085$. Substitution into (71) gives

$$(m_{\text{lactose}})_R = 1{,}030 \exp[-1(1-0.085)] = 413 \text{ lb/day}$$

Flows of other solutes in the concentrate from Section 3 are computed similarly and the wt% TP + NPN (dry basis) is obtained. The spreadsheet Solver function determined that the added water needed to achieve 85 wt% is 80,520 lb/day.

The following material balance includes permeate from the batch diafiltration stage and computed retentate (concentrate) of 85 wt% (dry basis) from Section 3.

Concentrate and Permeate from a Single-Stage Batch Diafiltration in Section 3, for an Added Water Rate of 80,520 lb/day, to Meet the 85 wt% Specification

Component	Flow Rate of Feed to Section 3, lb/day	Flow Rate of Concentrate, lb/day	Flow Rate of Permeate, lb/day
Water	53,214	54,351	79,383
True protein, TP	5,007	4,810	197
Nonprotein nitrogen, NPN	138	55	83
Lactose	1,030	302	728
Ash	185	56	129
Butter fat	500	500	0
Total	60,074	60,074	80,520

The % yield of TP + NPN in Section 3 is $(4{,}810 + 55)/(5{,}007 + 138) \times 100\% = 94.56\%$. The overall yield of TP + NPN from the whey feed is $(4{,}810 + 55)/(9{,}000) \times 100\% = 54.06\%$.

The membrane flux is 0.5415 gal/h-ft^2, as in Section 2. The volumetric permeate flow rate over a 4-hour batch operation = 80,520/[(4)(8.5)] = 2,368 gal/h. Therefore, the membrane area required = 2,368/0.5415 = 4,373 ft^2. The number of cartridges needed in Section 3 is 4,373/26.5 = 165.

SUMMARY

1. The separation of liquid and gas mixtures with membranes is an emerging separation operation. Applications began accelerating in the 1980s. The products of separation are retentate and permeate.
2. The key to an efficient and economical membrane-separation process is the membrane. It must have good permeability, high selectivity, solute compatibility, high capacity, stability, freedom from fouling, and a long life.
3. Commercialized membrane-separation processes include dialysis, electrodialysis, reverse osmosis, gas permeation, pervaporation, ultrafiltration, and microfiltration.
4. Most membranes for commercial separation processes are natural or synthetic, or glassy or rubbery polymers cast as a film from a solvent mixture. However, for high-temperature (>200°C) operations with chemically reactive mixtures, ceramics, metals, and carbon find applications.
5. To achieve high permeability and selectivity, dense, nonporous membranes are preferred. For mechanical integrity, membranes 0.1–1.0 mm thick are incorporated as a surface layer or film onto or as part of a thicker asymmetric or composite membrane.
6. To achieve a high surface area per unit volume, membranes are fabricated into spiral-wound or hollow-fiber modules. Less surface is available in plate-and-frame, tubular, and monolithic modules.
7. Permeation through a membrane occurs by many mechanisms. For a microporous membrane, mechanisms include bulk flow (no selectivity), liquid and gas diffusion, Knudsen diffusion, restrictive diffusion, sieving, and surface diffusion. For a nonporous membrane, a solution-diffusion mechanism applies.
8. Flow patterns in membrane modules have a profound effect on overall permeation rates. Idealized flow patterns for which theory has been developed include perfect mixing, countercurrent flow, cocurrent flow, and crossflow. To overcome separation limits of a single membrane module stage, modules can be arranged in series and/or parallel cascades.
9. In gas permeation, boundary-layer or film mass-transfer resistances on either side of the membrane are usually negligible compared to the membrane resistance. For separation of liquid mixtures, external mass-transfer effects and concentration polarization can be significant.

10. For most membrane separators, the component mass-transfer fluxes through the membrane can be formulated as the product of two terms: concentration, partial pressure, fugacity, or activity-driving force; and a permeance $\bar{P}_{M_i}$, which is the ratio of the permeability, P_{M_i}, to the membrane thickness, l_M.

11. In the dialysis of a liquid mixture, small solutes of type A are separated from the solvent and larger solutes of type B with a microporous membrane. The driving force is the concentration difference across the membrane. Transport of solvent can be minimized by adjusting pressure differences across the membrane to equal osmotic pressure.

12. In electrodialysis, a series of alternating cation- and anion-selective membranes are used with a direct-current voltage across an outer anode and an outer cathode to concentrate an electrolyte.

13. In reverse osmosis, the solvent of a liquid mixture is selectively transported through a dense membrane. By this means, seawater can be desalinized. The driving force for solvent transport is fugacity difference, which is commonly expressed in terms of $\Delta P - \Delta\pi$, where π is the osmotic pressure.

14. In gas permeation, mixtures of gases are separated by differences in permeation rates through dense membranes. The driving force for each component is its partial pressure difference, Δp_i, across the membrane. Both permeance and permeability depend on membrane absorptivity for the particular gas species and species diffusivity. Thus, $P_{M_i} = H_i D_i$.

15. In pervaporation, a liquid mixture is separated with a dense membrane by pulling a vacuum on the permeate side of the membrane so as to evaporate the permeate. The driving force may be approximated as a fugacity difference expressed by $\left(\gamma_i x_i P_i^s - y_i P_P\right)$. Permeability can vary with concentration because of membrane swelling.

16. Polymer membranes cast from solvent mixtures are used for harvest, clarification, purification, polishing, sterile filtration, and buffer exchange in bioprocessing. Selection of a membrane for biofiltration is guided by its solute selectivity, capacity, and flux, which are impacted by concentration polarization and fouling.

17. Microfiltration, ultrafiltration, and virus filtration are pressure-driven operations that selectively retain species in aqueous solutions based on their size, charge, and composition. They may be operated in normal-flow (dead-end) or tangential-flow modes. To be used in bioseparations, these membranes must preserve biological activity, satisfy cGMP requirements, and allow batch processing.

18. Bulk transport in biofiltration is modeled by Darcy's law using resistances for membrane and solute that is retained as a cake to restrict or completely block pores. Constant-flux and constant-pressure equations allow identification of the appropriate model for resistance.

19. Normal-flow operation is used primarily to clarify debris or remove infectious agents from solutions, gases, and parenteral drug suspensions. Filter aids increase capacity of debris removal. Capacity, throughput, and scale-up of normal-flow filters can be characterized using $V_{\max}$ models.

20. Tangential-flow operation is used primarily for cell harvest, species concentration, and purification, or buffer exchange. Selectivity in tangential-flow filtration is determined by solute size, charge, and composition.

21. Permeate flux in tangential-flow filtration is predicted using mass-transfer models for concentration polarization, boundary-layer mass transport, shear-induced diffusion, and inertial lift. Mass-transport coefficients in tangential-flow filtration are functions of species size and charge, solution composition, system geometry, and hydrodynamic shear and viscosity.

22. Tangential-flow filtration may be configured in four ways: batch, feed-and-bleed, batch diafiltration, and continuous feed-and-bleed diafiltration.

REFERENCES

1. Lonsdale, H.K., *J. Membrane Sci.*, **10**, 81 (1982).

2. Applegate, L.E., *Chem. Eng.*, **91**(12), 64–89 (1984).

3. Havens, G.G., and D.B. Guy, *Chem. Eng. Progress Symp. Series*, **64** (90), 299 (1968).

4. Bollinger, W.A., D.L. MacLean,and R.S. Narayan, *Chem. Eng. Progress*, **78**(10), 27–32 (1982).

5. Baker, R.W., E.L. Cussler, W. Eykamp, W.J. Koros, R.L. Riley, and H. Strathmann, *Membrane Separation Systems—A Research and Development Needs Assessment*, Report DE 90-011770, Department of Commerce, NTIS, Springfield, VA (1990).

6. Ho, W.S.W., and K.K. Sirkar, Eds., *Membrane Handbook*, Van Nostrand Reinhold, New York (1992).

7. Loeb, S., and S. Sourirajan, *Advances in Chemistry Series*, Vol. **38**, *Saline Water Conversion II* (1963).

8. Henis, J.M.S., and M.K. Tripodi, U.S. Patent 4,230,463 (1980).

9. Wrasidlo, W.J., U.S. Patent 3,951,815 (1977).

10. Barrer, R.M., *J. Chem. Soc.*, 378–386 (1934).

11. Barrer, R.M., *Diffusion in and through Solids*, Cambridge Press, London (1951).

12. Mahon, H.I., U.S. Patent 3,228,876 (1966).

13. Mahon, H.I., U.S. Patent 3,228,877 (1966).

14. Hsieh, H.P., R.R. Bhave, and H.L. Fleming, *J. Membrane Sci.*, **39**, 221–241 (1988).

15. Bird, R.B., W.E. Stewart, and E.N. Lightfoot, *Transport Phenomena*, John Wiley & Sons, New York, pp. 42–47 (1960).

16. Ergun, S., *Chem. Eng. Progress*, **48**, 89–94 (1952).

17. Beck, R.E., and J.S. Schultz, *Science*, **170**, 1302–1305 (1970).

18. Beck, R.E., and J.S. Schultz, *Biochim. Biophys. Acta*, **255**, 273 (1972).

19. Brandrup, J., and E.H. Immergut, Eds., *Polymer Handbook*, 3rd ed., John Wiley & Sons, New York (1989).

20. Lonsdale, H.K., U. Merten, and R.L. Riley, *J. Applied Polym. Sci.*, **9**, 1341–1362 (1965).

21. Motamedian, S., W. Pusch, G. Sendelbach, T.-M. Tak, and T. Tanioka, *Proceedings of the 1990 International Congress on Membranes and Membrane Processes*, Chicago, Vol. **II**, pp. 841–843.

22. Barrer, R.M., J.A. Barrie, and J. Slater, *J. Polym. Sci.*, **23**, 315–329 (1957).

23. Barrer, R.M., and J.A. Barrie, *J. Polym. Sci.*, **23**, 331–344 (1957).

24. Barrer, R.M., J.A. Barrie, and J. Slater, *J. Polym. Sci.*, **27**, 177–197 (1958).

25. Koros, W.J., and D.R. Paul, *J. Polym. Sci., Polym. Physics Edition*, **16**, 1947–1963 (1978).

26. Barrer, R.M., *J. Membrane Sci.*, **18**, 25–35 (1984).

27. Walawender, W.P., and S.A. Stern, *Separation Sci.*, **7**, 553–584 (1972).

28. Naylor, R.W., and P.O. Backer, *AIChE J.*, **1**, 95–99 (1955).

29. Stern, S.A., T.F. Sinclair, P.J. Gareis, N.P. Vahldieck, and P.H. Mohr, *Ind. Eng. Chem.*, **57**(2), 49–60 (1965).

30. Hwang, S.-T., and K.L. Kammermeyer, *Membranes in Separations*, Wiley-Interscience, New York, pp. 324–338 (1975).

31. Spillman, R.W., *Chem. Eng. Progress*, **85**(1), 41–62 (1989).

32. Strathmann, H., "Membrane and Membrane Separation Processes," in *Ullmann's Encyclopedia of Industrial Chemistry*, VCH, FRG, Vol. **A16**, p. 237 (1990).

33. Chamberlin, N.S., and B.H. Vromen, *Chem. Engr.*, **66**(9), 117–122 (1959).

34. Graham, T., *Phil. Trans. Roy. Soc. London*, **151**, 183–224 (1861).

35. Juda, W., and W.A. McRae, *J. Amer. Chem. Soc.*, **72**, 1044 (1950).

36. Strathmann, H., *Sep. and Purif. Methods*, **14**(1), 41–66 (1985).

37. Merten, U., *Ind. Eng. Chem. Fundamentals*, **2**, 229–232 (1963).

38. Stoughton, R.W., and M.H. Lietzke, *J. Chem. Eng. Data*, **10**, 254–260 (1965).

39. Spillman, R.W., and M.B. Sherwin, *Chemtech*, 378–384 (June 1990).

40. Schell, W.J., and C.D. Houston, *Chem. Eng. Progress*, **78**(10), 33–37 (1982).

41. Teplyakov, V., and P. Meares, *Gas Sep. and Purif.*, **4**, 66–74 (1990).

42. Rosenzweig, M.D., *Chem. Eng.*, **88**(24), 62–66 (1981).

43. Kober, P.A., *J. Am. Chem. Soc.*, **39**, 944–948 (1917).

44. Binning, R.C., R.J. Lee, J.F. Jennings, and E.C. Martin, *Ind. Eng. Chem.*, **53**, 45–50 (1961).

45. Wesslein, M., A. Heintz, and R.N. Lichtenthaler, *J. Membrane Sci.*, **51**, 169 (1990).

46. Wijmans, J.G., and R.W. Baker, *J. Membrane Sci.*, **79**, 101–113 (1993).

47. Rautenbach, R., and R. Albrecht, *Membrane Processes*, John Wiley & Sons, New York (1989).

48. Rao, M.B., and S. Sircar, *J. Membrane Sci.*, **85**, 253–264 (1993).

49. Baker, R., *Membrane Technology and Applications*, 2nd ed., John Wiley & Sons, New York (2004).

50. Chisti, Y., "Principles of Membrane Separation Processes," in G. Subramanian, Ed., *Bioseparation and Bioprocessing*, Wiley-VCH Verlag GmbH & Co. KGaA, Weinheim (2007).

51. Belfort, G., R.H. Davis, and A.J. Zydney, *J. Membrane Science.*, **96**, 1–58 (1994).

52. Van Reis, R., and A.L. Zydney, *Curr. Opinion Biotechnol.*, **12**, 208–211 (2001).

53. Van Reis, R., and A.L. Zydney, *J. Membr. Sci.*, **297**(1), 16–50 (2007).

54. Aimar, P., *Membranes in Bioprocessing*, 113–139 (1993).

55. McGregor, W.C., Ed., *Membrane Separations in Biotechnology*, Marcel Dekker, Inc., New York (1986).

56. Zeman, L.J., and A.L. Zydney, *Microfiltration and Ultrafiltration: Principles and Applications*, Marcel Dekker, New York (1996).

57. Porter, M.C., *Ind. Eng. Chem. Prod. Res. Dev.*, **11**, 234 (1972).

58. Van Reis, R., E.M. Goodrich, C.L. Yson, L.N. Frautschy, R. Whitely, and A.L. Zydney, *J Membr. Sci.*, **130**, 123–140 (1997).

59. Van Reis, R., J.M. Brake, J. Charkoudian, D.B. Burns, and A.L. Zydney, *J Membr. Sci.*, **159**, 133–143 (1999).

60. Zeman, L.J., and A.L. Zydney, *Microfiltration and Ultrafiltration, Principles and Applications*, Marcel Dekker, Inc., New York (1996).

61. Van Reis, R., E.M. Goodrich, C.L. Yson, L.M. Frautschy, S. Dzengeleski, and H. Lutz, *Biotechnol Bioeng*, **55**, 737–746 (1997).

62. Tucceli, R., and P.V. McGrath, Cellulosic ultrafiltration membrane. U.S. Patent 5,736,051 (1996).

63. Van Reis, R., and A.L. Zydney, "Protein Ultrafiltration," in M.C. Flickinger and S.W. Drew, Eds., *Encyclopedia of Bioprocess Technology: Fermentation, Biocatalysis and Bioseparation*, John Wiley & Sons, New York, pp. 2197–2214 (1999).

64. Meltzer, T.H., "Modus of Filtration," in *Adv, Biochem. Engin./Biotechnol.*, Springer-Verlag, Heidelberg, Vol. **9**, pp. 27–71 (2006).

65. Roper, D.K., A. Johnson, A. Lee, J. Taylor, C. Trimor, and E. Wen, *First International Conference on Membrane and Filtration Technology in Biopurification*, Cambridge, U.K., April 7–9, 1999.

66. Harrison, R.G., P. Todd, S.R. Rudge, and D.P. Petrides, *Bioseparations Science and Engineering*. Oxford University Press, New York (2003).

67. Grace, H.P., *Chem. Eng. Progr.*, **49**, 303 (1953).

68. Ruth, B.F., G.H. Montillon, and R.E. Montanna, *Ind. Eng. Chem.* **25**, 76–82 (1933).

69. Hermia, J., *Trans. Inst. Chem. Eng. –Lond.* **60**, 183 (1982).

70. Ho C.-C. and A.L. Zydney, *J Colloid Interface Sci.*, **232**, 389 (2000).

71. Ho C.-C. and A.L. Zydney, *Ind. Eng. Chem. Res.*, **40**, 1412 (2001).

72. Zydney, A.L.and C.-C. Ho, *Biotech. Bioeng.*, **83**, 537 (2001).

73. Schweitzer, P. A., *Handbook of Separation Techniques for Chemical Engineers*, 2nd ed., Section 2.1 by M.C. Porter, McGraw-Hill Book Co., New York (1988).

74. Badmington, G., M. Payne, R. Wilkins, and E. Honig, *Pharmaceut. Tech.*, **19**, 64 (1995).

75. Meltzer, T.H., and M.W. Jornitz, *Filtration in the Biopharmaceutical Industry*, Marcel Dekker, Inc., New York (1998).

76. Shuler, M.L., and F. Kargi, *Bioprocess Engineering*, 2nd ed., Prentice Hall PTR, Upper Saddle River, NJ (2002).

77. Bailey, J.E., and D.F. Ollis, *Biochemical Engineering Fundamentals*, 2nd ed., McGraw-Hill, New York (1986).

78. Emory, S., *Pharm. Technol.*, **13**, 68 (1980).

79. Baker, L.A., and C.R. Martin, *Nanotechnology in Biology and Medicine: Methods, Devices and Applications*, Vol. 9, pp. 1–24 (2007).

80. Baker, L.A., T. Choi, and C.R. Martin, *Current Nanoscience*, **2**(3), 243–255 (2006).

81. Belfort, G., "Membrane Separation Technology: An Overview," in H.R. Bungay and G. Belfort, Eds., *Advanced Biochemical Engineering*, John Wiley & Sons, New York, p. 253 (1987).

82. Kahn, D.W., M.D. Butler, G.M. Cohen, J.W. Kahn, and M.E. Winkler, *Biotechnol. Bioeng.*, **69**, 101–106 (2000).

83. Cruz, P.E., C.C. Peixoto, K. Devos, J.L. Moreira, E. Saman, and M.J. T. Carrondo, *Enzyme Microb. Technol.*, **26**, 61–70 (2000).

84. Ladisch, M.R., *Biseparations Engineering*, Wiley-Interscience, New York (2001).

85. Scopes, R.K., *Protein Purification*, 2nd ed., Springer-Verlag, New York (1987).

86. Pujar, N.S., and A.L. Zydney, *Ind. Eng. Chem. Res.*, **22**, 2473 (1994).

87. Blatt, W.F., A. Dravid, A.S. Michaels, and L. Nelson, "Solute Polarization and Cake Formation in Membrane Ultrafiltration: Causes Consequences, and Control Techniques," in J.E. Flinn, Ed., *Membrane Science and Technology*, Plenum Press, New York, pp. 47–97 (1970).

88. Belfort, G., R.H. Davis, and A.J. Zydney, *J. Membrane Sci.*, **96**, 1–58 (1994).

89. Leighton, D.T., and A. Acrivos, *J. Fluid Mech.*, **181**, 415–439 (1987).

90. Robertson, B.C., and A.L. Zydney, *J. Colloid Interface Sci.*, **134**, 563 (1990).

91. Winzeler, H.B., and G. Belfort, *J Membrane Sci.*, **80**, 157–185 (1993).

92. Sandler, S.I., *Chemical, Biochemical, and Engineering Thermodynamics*, 4th ed., John Wiley & Sons, New York (2006).

93. Porter, M.C., *Ind. Eng. Chem. Prod. Res. Dev.*, **11**, 234 (1972).

94. Eckstein, E.C., P.G. Bailey, and A.H. Shapiro, *J. Fluid Mech.*, **7**, 191 (1977).

95. Zydney, A.L., and C.K. Colton, *Chem. Eng. Commun.*, **47**, 1 (1986).

96. Davis, R.H., and J.D. Sherwood, *Chem. Eng. Sci.*, **45**, 3204–3209 (1990).

97. Drew, D.A., J.A. Schonber, and G. Belfort, *Chem. Eng. Sci.*, **46**, 3219–3224 (1991).

98. Henry, J.D., "Cross Flow Filtration," in N.N. Li, Ed., *Recent Developments in Separation Science*, CRC Press, Cleveland, OH, Vol. **2**, pp. 205–225 (1972).

99. Belfort, G., P. Chin, and D.M. Dziewulski, "A New Gel-Polarization Model Incorporating Lateral Migration for Membrane Fouling," *Proc. World Filtration Congress III*, Philadelphia, PA, p. 91 (1982).

100. Taddei, C., P. Aimar, J.A. Howell, and J.A. Scott, *J. Chem. Technol. Biotechnol.*, **47**, 365–376 (1990).

101. Le, M.S., *J. Chem. Technol. Biotechnol.*, **37**, 59–66 (1987).

102. Sakai, K., K. Ozawa, K. Ohashi, R. Yoshida, and H. Sakarai, *Ind. Eng. Chem. Res.*, **28**, 57–64 (1989).

103. Geankoplis, C.J., *Transport Processes and Separation Process Principles*, 4th ed., Prentice Hall PTR, New Jersey (2003).

104. Nielsen, W.K., Ed., *Membrane Filtration and Related Molecular Separation Technologies*, International Dairy Books, Aarhus, Denmark (2000).

105. Cheryan, M., *Ultrafiltration Handbook*, Technomic Publishing Co., Lancaster, PA (1986).

STUDY QUESTIONS

14.1. What are the two products from a membrane separation called? What is a sweep?

14.2. What kinds of materials are membranes made from? Can a membrane be porous or nonporous? What forms pores in polymer membranes?

14.3. What is the basic equation for computing the rate of mass transfer through a membrane? Explain each of the four factors in the equation and how they can be exploited to obtain high rates of mass transfer.

14.4. What is the difference between permeability and permeance? How are they analogous to diffusivity and the mass-transfer coefficient?

14.5. For a membrane separation, is it usually possible to achieve both a high permeability and a large separation factor?

14.6. What are the three mechanisms for mass transfer through a porous membrane? Which are the best mechanisms for making a separation? Why?

14.7. What is the mechanism for mass transfer through a dense (nonporous) membrane? Why is it called solution-diffusion? Does this mechanism work if the polymer is completely crystalline? Explain.

14.8. How do the solution-diffusion equations differ for liquid transport and gas transport? How is Henry's law used for solution-diffusion for gas transport? Why are the film resistances to mass transfer on either side of the membrane for gas permeation often negligible?

14.9. What are the four idealized flow patterns in membrane modules? Which is the most effective? Which is the most difficult to calculate?

14.10. What is osmosis? Can it be used to separate a liquid mixture? How does it differ from reverse osmosis? For what type of mixtures is it well suited?

14.11. Can a near-perfect separation be made with gas permeation? If not, why not?

14.12. What is pervaporation?

14.13. How do microfiltration and ultrafiltration differ from reverse osmosis with respect to pore size, pressure drop, and the nature of the permeate?

14.14. What is the evidence that concentration polarization and fouling are occurring during biofiltrations, and what steps are taken to minimize these effects?

14.15. What are the four common configurations for ultrafiltration?

14.16. What is continuous feed-and-bleed ultrafiltration? What are its limitations?

14.17. What is diafiltration? How does it differ from continuous feed-and-bleed ultrafiltration? Under what conditions is diafiltration used in conjunction with continuous feed-and-bleed ultrafiltration?

14.18. In microfiltration, why is an operation that combines constant-flux and constant-pressure operations used?

EXERCISES

Section 14.1

14.1. Differences between membrane separations and other separations.

Explain, as completely as you can, how membrane separations differ from: (a) absorption and stripping; (b) distillation; (c) liquid–liquid extraction; (d) extractive distillation.

14.2. Barrer units for permeabilities.

For the commercial application of membrane separators discussed at the beginning of this chapter, calculate the permeabilities of hydrogen and methane in barrer units.

14.3. Membrane separation of N_2 from CH_4.

A new asymmetric, polyimide polymer membrane has been developed for the separation of N_2 from CH_4. At 30°C, permeance values are 50,000 and 10,000 barrer/cm for N_2 and CH_4, respectively. If this new membrane is used to perform the separation in Figure 14.37, determine the membrane surface area in m^2, and the kmol/h of CH_4 in the permeate. Base the driving force for diffusion on the arithmetic average of the partial pressures of the entering feed and the exiting retentate, with the permeate-side partial pressures at the exit condition.

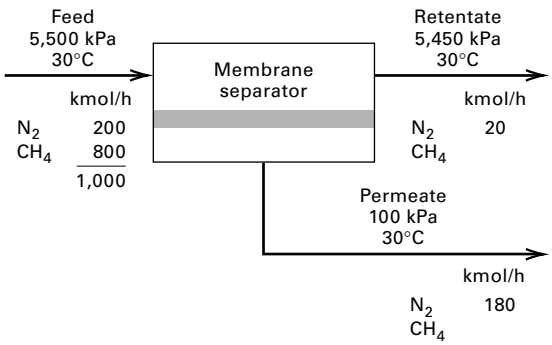

Figure 14.37 Data for Exercise 14.3.

Section 14.2

14.4. Characteristics of a hollow-fiber module.

A hollow-fiber module has 4,000 ft^2 of membrane surface area based on the size of the fibers, which are 42 μm i.d. × 85 μm o.d. × 1.2 m long each. Determine the: (a) number of hollow fibers in the module; (b) diameter of the module, assuming the fibers are on a square spacing of 120 μm center-to-center; and (c) membrane surface area per unit volume of module (packing density) m^2/m^3. Compare your result with that in Table 14.4.

14.5. Geometry of a membrane module.

A spiral-wound module made from a flat sheet of membrane material is 0.3 m in diameter and 3 m long. If the packing density (membrane surface area/unit module volume) is 500 m^2/m^3, what is the center-to-center spacing of the membrane in the spiral, assuming a collection tube 1 cm in diameter?

14.6. Characteristics of a monolithic element.

A monolithic membrane element of the type shown in Figure 14.4d contains 19 flow channels of 0.5 cm in inside diameter by 0.85 m long. If 9 of these elements are in a cylindrical module of the type in Figure 14.5, determine values for: (a) module volume in m^3; and (b) packing density in m^2/m^3. Compare your value with values for other membrane modules given in Table 14.4.

Section 14.3

14.7. Porous membrane with pressure differential.

Water at 70°C is passed through a polyethylene membrane of 25% porosity with an average pore diameter of 0.3 μm and an average tortuosity of 1.3. The pressures on the downstream and upstream sides of the membrane are 125 and 500 kPa, respectively. Estimate the flux of water in m^3/m^2-day.

14.8. Knudsen flow in a membrane.

A porous-glass membrane, with an average pore diameter of 40 Å, is used to separate light gases at 25°C when Knudsen flow may be dominant. The pressures are 15 psia downstream and not > 120 psia upstream. The membrane has been calibrated with pure helium gas, giving a constant permeability of 117,000 barrer. Experiments with pure CO_2 give a permeability of 68,000 barrer. Assuming that helium is in Knudsen flow, predict the permeability of CO_2. Is it in agreement with the experimental value? If not, suggest an explanation. Reference: Kammermeyer, K., and L.O. Rutz, *C.E.P. Symp. Ser.*, **55** (24), 163–169 (1959).

14.9. Partial condensation and surface diffusion.

Two mechanisms for the transport of gas through a porous membrane not discussed in §14.3 or illustrated in Figure 14.6 are (1) partial condensation in the pores by some components of the gas mixture to the exclusion of other components, and subsequent transport of the condensed molecules through the pore, and (2) selective adsorption on pore surfaces of some components and subsequent surface diffusion across the pores. In particular, Rao and Sircar [48] have found that the latter mechanism provides a potentially attractive means for separating hydrocarbons from hydrogen for low-pressure gas streams. In porous-carbon membranes with continuous pores 4–15 Å in diameter, little pore void space is available for Knudsen diffusion of hydrogen when the hydrocarbons are selectively adsorbed.

Typically, the membranes are not more than 5 μm in thickness. Measurements at 295.1 K of permeabilities for five pure components and a mixture of the five components are as follows:

	Permeability, barrer		
Component	As a Pure Gas	In the Mixture	mol% in the Mixture
H_2	130	1.2	41.0
CH_4	660	1.3	20.2
C_2H_6	850	7.7	9.5
C_3H_8	290	25.4	9.4
nC_4H_{10}	155	112.3	19.9
			100.0

A refinery waste gas mixture of the preceding composition is to be processed through such a porous-carbon membrane. If the pressure of the gas is 1.2 atm and an inert sweep gas is used on the permeate side such that partial pressures of feed-gas components on that side are close to zero, determine the permeate composition on a sweep-gas-free basis when the composition on the upstream pressure side of the membrane is that of the feed gas. Explain why the component permeabilities differ so much between pure gas and the gas mixture.

14.10. Module flow pattern and membrane area.

A mixture of 60 mol% propylene and 40 mol% propane at a flow rate of 100 lbmol/h and at 25°C and 300 psia is to be separated with a polyvinyltrimethylsilane polymer (see Table 14.10 for permeabilities). The membrane skin is 0.1 μm thick, and spiral-wound modules are used with a pressure of 15 psia on the permeate side. Calculate the material balance and membrane area in m^2 as a function of the cut (fraction of feed permeated) for: (a) perfect-mixing flow pattern and (b) crossflow pattern.

14.11. Membrane area for gas permeation.

Repeat part (a) of Exercise 14.10 for a two-stage stripping cascade and a two-stage enriching cascade, as shown in Figure 14.14. However, select just one set of reasonable cuts for the two stages of each case so as to produce 40 lbmol/h of final retentate.

14.12. Dead-end microfiltration of skim milk.

Using the membrane and feed conditions of and values for R_m and K_2 determined in Example 14.3 for DE microfiltration,

compute and plot the permeate flux and cumulative permeate volume as a function of time. Assume a combined operation with Stage 1 at a constant permeate rate of 10 mL/minute to an upper-limit pressure drop of 25 psi, followed by Stage 2 at this pressure drop until the permeate rate drops to a lower limit of 5 mL/minute.

14.13. Concentration polarization in dialysis.

Repeat Example 14.8 with the following changes: tube-side Reynolds number = 25,000; tube inside diameter = 0.4 cm; permeate-side mass-transfer coefficient = 0.06 cm/s. How important is concentration polarization?

Section 14.4

14.14. Dialysis to separate Na_2SO_4.

An aqueous process stream of 100 gal/h at 20°C contains 8 wt% Na_2SO_4 and 6 wt% of a high-molecular-weight substance (A). This stream is processed in a continuous countercurrent-flow dialyzer using a pure water sweep of the same flow rate. The membrane is a microporous cellophane with pore volume = 50%, wet thickness = 0.0051 cm, tortuosity = 4.1, and pore diameter = 31Å. The molecules to be separated have the following properties:

	Na_2SO_4	A
Molecular weight	142	1,000
Molecular diameter, Å	5.5	15.0
Diffusivity, $cm^2/s \times 10^5$	0.77	0.25

Calculate the membrane area in m^2 for only a 10% transfer of A through the membrane, assuming no transfer of water. What is the % recovery of the Na_2SO_4 in the diffusate? Use log-mean concentration-driving forces and assume the mass-transfer resistances on each side of the membrane are each 25% of the total mass-transfer resistances for Na_2SO_4 and A.

14.15. Removal of HCl by dialysis.

A dialyzer is to be used to separate 300 L/h of an aqueous solution containing 0.1-M NaCl and 0.2-M HCl. Laboratory experiments with the microporous membrane to be used give the following values for the overall mass-transfer coefficient K_i in (14-79) for a log-mean concentration-driving force:

	K_i, cm/min
Water	0.0025
NaCl	0.021
HCl	0.055

Determine the membrane area in m^2 for 90, 95, and 98% transfer of HCl to the diffusate. For each case, determine the complete material balance in kmol/h for a sweep of 300 L/h.

Section 14.5

14.16. Desalinization by electrodialysis.

A total of 86,000 gal/day of an aqueous solution of 3,000 ppm of NaCl is to be desalinized to 400 ppm by electrodialysis, with a 40% conversion. The process will be conducted in four stages, with three stacks of 150 cell pairs in each stage. The fractional desalinization will be the same in each stage and the expected current efficiency is 90%. The applied voltage for the first stage is 220 V. Each cell pair has an area of 1,160 cm^2. Calculate the current density in mA/cm^2, the current in A, and the power in kW for the first stage. Reference: Mason, E.A., and T.A. Kirkham, *C.E.P. Symp. Ser.*, **55** (24), 173–189 (1959).

Section 14.5

14.17. Reverse osmosis of seawater.

A reverse-osmosis plant is used to treat 30,000,000 gal/day of seawater at 20°C containing 3.5 wt% dissolved solids to produce 10,000,000 gal/day of potable water, with 500 ppm of dissolved solids and the balance as brine containing 5.25 wt% dissolved solids. The feed-side pressure is 2,000 psia, while the permeate pressure is 50 psia. A single stage of spiral-wound membranes is used that approximates crossflow. If the total membrane area is 2,000,000 ft^2, estimate the permeance for water and the salt passage.

14.18. Reverse osmosis with multiple stages.

A reverse-osmosis process is to be designed to handle a feed flow rate of 100 gpm. Three designs have been proposed, differing in the % recovery of potable water from the feed:

Design 1: A single stage consisting of four units in parallel to obtain a 50% recovery

Design 2: Two stages in series with respect to the retentate (four units in parallel followed by two units in parallel)

Design 3: Three stages in series with respect to the retentate (four units in parallel followed by two units in parallel followed by a single unit)

Draw the three designs and determine the percent recovery of potable water for Designs 2 and 3.

14.19. Concentration of Kraft black liquor by two-stage reverse osmosis.

Production of paper requires a pulping step to break down wood chips into cellulose and lignin. In the Kraft process, an aqueous solution known as white liquor and consisting of dissolved inorganic chemicals such as Na_2S and NaOH is used. Following removal of the pulp (primarily cellulose), a solution known as weak Kraft black liquor (KBL) is left, which is regenerated to recover white liquor for recycle. In this process, a 15 wt% (dissolved solids) KBL is concentrated to 45 to 70 wt % by multieffect evaporation. It has been suggested that reverse osmosis be used to perform an initial concentration to perhaps 25 wt%. Higher concentrations may not be feasible because of the high osmotic pressure, which at 180°F and 25 wt% solids is 1,700 psia. Osmotic pressure for other conditions can be scaled with (14-102) using wt% instead of molality.

A two-stage RO process, shown in Figure 14.38, has been proposed to carry out this initial concentration for a feed rate of 1,000 lb/h at 180°F. A feed pressure of 1,756 psia is to be used for the first stage to yield a permeate of 0.4 wt% solids. The feed pressure to the second stage is 518 psia to produce water of 300 ppm dissolved solids and a retentate of 2.6 wt% solids. Permeate-side pressure for both stages is 15 psia. Equation (14-93) can be used to estimate membrane area, where the permeance for water can be taken as 0.0134 lb/ft^2-hr-psi in conjunction with an arithmetic mean osmotic pressure for plug flow on the feed side. Complete the material balance for the process and estimate the required membrane areas for each stage. Reference: Gottschlich, D.E., and D.L. Roberts. Final Report DE91004710, SRI International, Menlo Park, CA, Sept. 28, 1990.

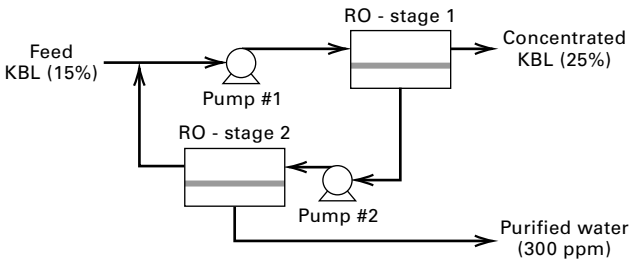

Figure 14.38 Data for Exercise 14.19.

Section 14.7

14.20. Recovery of VOCs by gas permeation.

Gas permeation can be used to recover VOCs (volatile organic compounds) from air at low pressures using a highly selective membrane. In a typical application, 1,500 scfm (0°C, 1 atm) of air containing 0.5 mol% acetone (A) is fed to a spiral-wound membrane module at 40°C and 1.2 atm. A liquid-ring vacuum pump on the permeate side establishes a pressure of 4 cmHg. A silicone-rubber, thin-composite membrane with a 2-μm-thick skin gives permeabilities of 4 barrer for air and 20,000 barrer for acetone.

If the retentate is to contain 0.05 mol% acetone and the permeate is to contain 5 mol% acetone, determine the membrane area required in m^2, assuming crossflow. References: (1) Peinemann, K.-V., J.M. Mohr, and R.W. Baker, *C.E.P. Symp. Series*, **82** (250), 19–26 (1986); (2) Baker, R.W., N. Yoshioka, J.M. Mohr, and A.J. Khan, *J. Membrane Sci.*, **31**, 259–271 (1987).

14.21. Separation of air by gas permeation.

Separation of air into N_2 and O_2 is widely practiced. Cryogenic distillation is most economical for processing 100 to 5,000 tons of air per day, while pressure-swing adsorption is favorable for 20 to 50 tons/day. For small-volume users requiring less than 10 tons/day, gas permeation finds applications where for a single stage, either an oxygen-enriched air (40 mol% O_2) or 98 mol% N_2 can be produced. It is desired to produce a permeate of 5 tons/day (2,000 lb/ton) of 40 mol% oxygen and a retentate of nitrogen, ideally of 90 mol% purity, by gas permeation. Assume pressures of 500 psia (feed side) and 20 psia (permeate). Two companies who can supply the membrane modules have provided the following data:

	Company A	Company B
Module type	Hollow-fiber	Spiral-wound
$\bar{P}_M$ for O_2, barrer/μm	15	35
$\bar{P}_{M_{O_2}}/\bar{P}_{M_{N_2}}$	3.5	1.9

Determine the required membrane area in m^2 for each company. Assume that both module types approximate crossflow.

14.22. Removal of CO_2 and H_2S by permeation.

A joint venture has been underway for several years to develop a membrane process to separate CO_2 and H_2S from high-pressure, sour natural gas. Typical feed and product conditions are:

	Feed Gas	Pipeline Gas
Pressure, psia	1,000	980
Composition, mol%:		
CH_4	70	97.96
H_2S	10	0.04
CO_2	20	2.00

To meet these conditions, the following hollow-fiber membrane material targets have been established:

	Selectivity
CO_2–CH_4	50
H_2S–CH_4	50

where selectivity is the ratio of permeabilities. $P_{M_{CO_2}} = 13.3$ barrer, and membrane skin thickness is expected to be 0.5 μm. Make calculations to show whether the targets can realistically meet the pipeline-gas conditions in a single stage with a reasonable membrane area. Assume a feed-gas flow rate of 10×10^3 scfm (0°C, 1 atm) with crossflow. Reference: Stam, H., in L. Cecille and J.-C. Toussaint, Eds., *Future Industrial Prospects of Membrane Processes*, Elsevier Applied Science, London, pp. 135–152 (1989).

Section 14.8

14.23. Separation by pervaporation.

Pervaporation is to be used to separate ethyl acetate (EA) from water. The feed rate is 100,000 gal/day of water containing 2.0 wt% EA at 30°C and 20 psia. The membrane is dense polydimethylsiloxane with a 1-μm-thick skin in a spiral-wound module that approximates crossflow. The permeate pressure is 3 cmHg. The total measured membrane flux at these conditions is 1.0 L/m^2-h with a separation factor given by (14-59) of 100 for EA with respect to water. A retentate of 0.2 wt% EA is desired for a permeate of 45.7 wt% EA. Determine the required membrane area in m^2 and the feed temperature drop. Reference: Blume, I., J.G. Wijans, and R.W. Baker, *J. Membrane Sci.*, **49**, 253–286 (1990).

14.24. Permeances for pervaporation.

For a temperature of 60°C and a permeate pressure of 15.2 mmHg, Wesslein et al. [45] measured a total permeation flux of 1.6 kg/m^2-h for a 17.0 wt% ethanol-in-water feed, giving a permeate of 12 wt% ethanol. Otherwise, conditions were those of Example 14.13. Calculate the permeances of ethyl alcohol and water for these conditions. Also, calculate the selectivity for water.

14.25. Second stage of a pervaporation process.

The separation of benzene (B) from cyclohexane (C) by distillation at 1 atm is impossible because of a minimum-boiling-point azeotrope at 54.5 mol% benzene. However, extractive distillation with furfural is feasible. For an equimolar feed, cyclohexane and benzene products of 98 and 99 mol%, respectively, can be produced. Alternatively, the use of a three-stage pervaporation process, with selectivity for benzene using a polyethylene membrane, has received attention, as discussed by Rautenbach and Albrecht [47]. Consider the second stage of this process, where the feed is 9,905 kg/h of 57.5 wt% B at 75°C. The retentate is 16.4 wt% benzene at 67.5°C and the permeate is 88.2 wt% benzene at 27.5°C. The total permeate mass flux is 1.43 kg/m^2-h and selectivity for benzene is 8. Calculate flow rates of retentate and permeate in kg/h and membrane surface area in m^2.

Section 14.9

14.26. Permeability of a nanofiltration membrane.

Obtain general expressions for hydraulic membrane permeability, L_p, and membrane resistance, R_m, for laminar flow through a nanofiltration membrane of thickness L that is permeated by right-cylindrical pores of radius r in terms of surface porosity σ, the total area of pore mouths per m^2.

14.27. Constant-pressure cake filtration.

Beginning with the Ruth equation (14-24), obtain general expressions for time-dependent permeate volume, $V\{t\}$, and time-dependent flux, $J\{t\}$, in terms of operating parameters and characteristics of the cake for constant-pressure cake filtration.

14.28. Pore-constriction model.

Derive a general expression for the total filtration time necessary to filter a given feed volume V using the pore-constriction model. From this expression, predict the average volumetric flux during a filtration and the volumetric capacity necessary to achieve a given filtration time, based on laboratory-scale results.

14.29. Minimum filter area for sterile filtration.

Derive a general expression for the minimum filter area requirement per a sterility assurance limit (SAL) in terms of (a) concentration of microorganisms in the feed; (b) volume per unit parenteral dose; (c) sterility assurance limit; and (d) filter capacity.

14.30. Cheese whey ultrafiltration process.

Based on the problem statement of Example 14.20, calculate for just Section 1 the component material balance in pounds per day of operation, the percent recovery (yield) from the whey of the TP and NPN in the final concentrate, and the number of cartridges required if two stages are used instead of four.

14.31. Four-stage diafiltration section.

Based on the problem statement of Example 14.20, design a four-stage diafiltration section to take the 55 wt% concentrate from Section 1 and achieve the desired 85 wt% concentrate, thus eliminating Section 3.